

**Structure-Function Analysis of the Inosine/Guanosine
Transporter from *Leishmania donovani* using Reverse
and Forward genetics**

**by
Shirin Arastu-Kapur
A Dissertation**

**Presented to the Department of
Biochemistry and Molecular Biology
and
The Oregon Health & Science University
School of Medicine**

**In partial fulfillment of the requirements for the degree
of
Doctor of Philosophy**

May 5, 2004

School of Medicine
Oregon Health & Science University

CERTIFICATE OF APPROVAL

This is to certify that the Ph.D. thesis of

Shirin Arastu

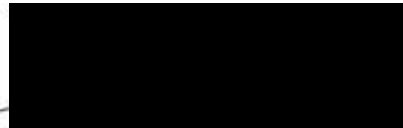
has been approved



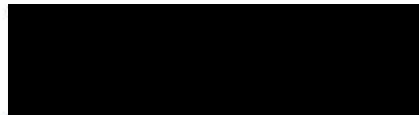
Professor in charge of thesis – Dr. Buddy Ullman




Thesis Committee Chair – Dr. Thomas Shearer



Thesis Committee Member – Dr. Svetlana Lutsenko



Thesis Committee Member – Dr. Scott Landfear



ACKNOWLEDGEMENTS

I would like to thank my advisor, Buddy Ullman. I met him when I was struggling with my decision to be a scientist. His belief in my abilities was pivotal for my conscious choice to become a scientist. He was also very patient during my “disappearing acts” as I tried to manage a long distance marriage.

I would like to thank my thesis advisory committee, Svetlana Lutsenko, Scott Landfear, and Thomas Shearer for their support and guidance. I would also like to thank the administrative staff, particularly Tina Purat and Kathleen Alexander, of the Biochemistry Department for their support.

My thesis would not have been possible without Nicola S. Carter. She mentored me in the laboratory through the past four years. Her insight, patience, and example have been invaluable.

Many of my lab members have contributed to my intellectual growth and optimistic attitude in the lab. Jan taught me tenacity by her example. Nicole taught me protein expression analysis and the importance of identifying one's source of happiness. Casey taught me about yeast and critically read my writing. Armando always encouraged excellence. Francy taught me *Leishmania* tissue culture. Sarah has been very helpful. Sigrid is a role model of someone who manages family and career. Johanna, Eric, Wei, and Judith for their friendships. Jonathan imparts a level headedness to the lab. Also, other lab members who made my scientific world a better place and have touched my life in different

ways: Marie-Pierre, Kate, Kleigman, Sabih, Bronwen, Coral, Mike, Caleb, and Chi.

The friends I made during my graduate career have shown kindness and optimism through the lonely times - Ezhil, Lara, Mihail, Courtney, Mariana, and Joel. Tasso was supportive when I was contemplating a change in labs. Asra and Meenakshi have always been warm and supportive. Ameenah and Rifat for their kindness even when I got busy with labwork. Manbina, Jyoti, and Rahela for constant friendship through my life. Finally, Michelle and Jennifer for support when I immigrated to the US.

I have had many teachers who enforced a positive learning experience. Miss Shanta taught me the concept of a good lab book. Miss Ohlinger introduced me to Penn. Jr. Academy of Science where I won my 1st science award. Dr. Lowe-Krentz gave me the 1st opportunity to do research at a university. Dr. Kurtz introduced me to molecular biology and mutant protein analysis. Dr. Salter introduced me to computational chemistry.

I would also like to thank my in-laws. Al and Dade, my husband's godparents, have been a voice of neutral reasoning in the last few years. It was always nice to talk to my father-in-law, Prakash, about the perils of getting a PhD. A special thanks goes to my mother-in-law, Rama, who has always tried to give me support and understanding. My brother-in-law, Reuben, has tried to keep his relationship with me unbiased. A special thanks also goes to my sister-in-law, Ashima, for her support. A loving thanks to my niece, Simryn, whose unjaded "hi chachi" is something that always brought a smile.

My extended family is incredible, since both my parents are one of twelve children! I am blessed to have a personal relationship with almost all of them – I WISH I could name everyone because they are no less than my nuclear family to me! They are the most comforting of crowds and provide a world of unchanging affection. I wish my children will know the warmth that I grew up with. I never knew my maternal grandfather, but I would like to thank my late maternal and paternal grandmothers and late paternal grandfather for blessing my parents. Also, for always showing unbiased love to their children and grandchildren, and through their example teaching us the importance of a family. A special thanks to my late paternal grandmother, Zaibunnissa Ali, for her unconditional love until her last breath. I would like to thank my aunts and uncles, who have taught me the importance of patience, generosity, excellence, and unconditional love through their examples. I would like to thank all my cousins for their existence, optimism and acceptance, which is enough to wash away the loneliness in life.

I have been blessed with the two most beautiful people for parents, Alamdar and Salma, whose sacrifices and example have brought me to this day. Both of them have taught me to dream and pursue those dreams. Their optimism, self-reliance, and faith are a continuing inspiration in my life. My father planted the seed of hard work in 5th grade when he would wake up at 5 AM to tutor me in math and assure that I got nothing less than full marks. My mother taught me to be resourceful and always keep the fire alive. Even though she is an artist, she made sure I had a laboratory to do my science fair project in at a university while I was still in the eighth grade. Finally, I would like to thank them

for their unconditional and self-less love. It is only because of their strength that I have survived the emotional trials during the last few years. This thesis is dedicated to my parents.

I would like to thank my brother, Samad, for his love through the years. From him I have learnt that every difficulty in life has a solution and you just have to keep trekking through it. I was so happy when he was born.

Finally, I would like to thank one of the most important people in my life, my husband Pawan. He encouraged me to do my 1st research project at Lehigh University. He helped me format this thesis. Most importantly, if he had not entered my life, I would not have done a PhD. His encouragement, inspiration, optimism, love, and sacrifices have brought me to this day.

PREFACE

"In nature's book of secrecy a little shall I read." William Shakespeare

A parasite is one who dines at the table of another. Thus, by slowly pilfering the host of its essential nutrients the parasite survives while its host perishes. Protozoan parasites, such as *Leishmania*, fit right into this definition as they are incapable of *de novo* synthesis of various nutrients, and therefore salvage these essential molecules from their host. Perhaps one of the best ways to combat the parasite's uninvited presence is to exploit the complete dependence of the parasite on the host for essential nutrients. One such class of nutrients is purines. Fortunately, the human host is capable of purine biosynthesis and thus an attempt to intercept the supply of purines to the parasite should leave the host unaffected. The first step in the purine salvage pathway is the uptake of the purine into the parasite by a transporter. Understanding the function of these transporters may be crucial in the design of small molecules to either inhibit the uptake of the nutrients or to deliver a toxic compound to the parasite.

ABSTRACT

Nucleoside transporters from *Leishmania donovani*, LdNT1 and LdNT2, are members of the equilibrative nucleoside transporter family that accommodates 19 conserved residues located mainly in membrane-spanning domains. Two of these conserved residues are charged and occur within predicted transmembrane domain 8. To assess the role of these 'signature' residues in transporter function, the Asp³⁸⁹ and Arg³⁹³ residues within the LdNT2 nucleoside transporter were mutated and the resultant phenotypes evaluated after transfection into Δ *ldnt2* parasites. Whereas an R393K mutant retained transporter activity similar to that of wild type LdNT2, the R393L, D389E, and D389N mutations resulted in dramatic losses of transport capability. Tagging the wild type and mutant *ldnt2* proteins with green fluorescent protein demonstrated that the D389N and D389E mutants targeted properly to the parasite cell surface and flagellum, whereas the localization of R393L at the cell surface was profoundly compromised.

To test whether Asp³⁸⁹ and Arg³⁹³ interact, a series of mutants was generated, D389R/R393, D389/R393D, and D389R/R393D, within the green fluorescent protein-tagged LdNT2 construct. Although all of these *ldnt2* mutants were transport deficient, D389R/R393D localized properly to the plasma membrane, while neither D389R/R393 nor D389/R393D could be detected. Moreover, a transport-incompetent D389N/R393N double *ldnt2* mutant also localized to the parasite membrane, whereas a D389L/R393L *ldnt2* mutant did

not, suggesting that an interaction between residues 389 and 393 may be involved in LdNT2 membrane targeting. These studies establish genetically that Asp³⁸⁹ is critical for optimal transporter function and that a positively charged or polar residue at Arg³⁹³ is essential for proper localization of LdNT2 at the plasma membrane.

LdNT2 from *Leishmania donovani* is a member of the equilibrative nucleoside transporter (ENT) family, which contains 19 conserved residues located mainly in membrane-spanning domains. One of these conserved residues, Asp³⁸⁹ within LdNT2, was previously shown to be important for transporter function without affecting ligand affinity or plasma membrane targeting. To further delineate the role of Asp³⁸⁹ in LdNT2 function, second-site suppressors of the *ldnt2*-D389N mutation were selected in a strain of *Saccharomyces cerevisiae*, which is deficient in purine nucleoside transport and purine biosynthesis. A library of random mutants within the *ldnt2*-D389N background was screened in yeast for restoration of growth on inosine. Twelve independent clones were obtained, each containing secondary site mutations throughout the transporter sequence and capable of inosine transport. One mutation, N175I, was prevalent in the clones obtained and significantly augmented inosine transport capability compared to LdNT2 in yeast.

N175I was subsequently introduced into a *ldnt2*-D389N construct tagged at the NH₂-terminus with green fluorescent protein and transfected into a Δ *ldnt1*/ Δ *ldnt2* *L. donovani* knockout. GFP-N175I/D389N significantly suppressed the D389N phenotype in the knockout and targeted properly to the plasma

membrane and flagellum. Interestingly, N175I decreased inosine affinity by 10-fold within the D389N background relative to wild type GFP-LdNT2. Additional substitutions at Asn¹⁷⁵ established that only large, nonpolar amino acids were capable of suppressing the D389N phenotype, suggesting that the suppression at D389N has a specific size and charge requirement at position 175.

Furthermore, since multiple second-site suppressor mutations were uncovered that alleviate the constraint imparted by the D389N mutation, these data suggest that Asp³⁸⁹ is a conformationally sensitive residue.

To impart spatial orientation to the clustering of second-site mutations, a 3-dimensional model was based on members of the major facilitator superfamily using threading analysis. The model is consistent with previous genetic and biochemical data on ENTs, and indicates that Asn¹⁷⁵ and Asp³⁸⁹ lie in close proximity, and that all of the second-site suppressor mutations cluster to one region of the transporter, supporting the idea that these mutations act to alleviate the conformational constraint imposed by the crippling D389N mutation.

CONTENTS

CHAPTER 1	1
INTRODUCTION	1
1.1. LEISHMANIASIS	1
1.1.1. THE DISEASE: PREVALENCE AND PATHOLOGY	1
1.1.2. THE CAUSATIVE AGENT: LIFE CYCLE AND PARASITE SURVIVAL	3
1.1.2.a Taxonomy and Morphology	3
1.1.2.b. Sandfly Vector: Survival and Attachment	6
1.1.2.c. Human Host: Phagocytosis and Defiance of the Immune System	9
1.2. THERAPIES	14
1.2.1. CURRENT THERAPIES	14
1.2.2. THERAPIES UNDER DEVELOPMENT	16
1.2.3. NEW AVENUES FOR THERAPY DEVELOPMENT	18
1.2.3.a. Differences between the Host and Parasite	18
1.2.3.b. Purine Salvage	19
1.3. NUCLEOSIDE TRANSPORTERS	24
1.3.1. TRANSPORT PROCESSES: OVERVIEW	24
1.3.2. EQUILBRATIVE NUCLEOSIDE TRANSPORTERS (ENT):	27
1.3.2.a. General Characteristics: Human and <i>Leishmania</i> ENTs	27

1.3.2.b. Structure-Function of ENTs	31
1.3.2.c. Contribution of this thesis	36
1.4. FIGURES	39
1.5. REFERENCES	59
CHAPTER 2	77
<hr/>	
MANUSCRIPT 1	77
2.1 ABSTRACT	78
2.2 INTRODUCTION	79
2.3 EXPERIMENTAL PROCEDURES	82
2.4 RESULTS	88
2.5 DISCUSSION	96
2.6 FIGURES	103
2.7 TABLES	117
2.8 REFERENCES	119
CHAPTER 3	124
<hr/>	
MANUSCRIPT 2	124
3.1 ABSTRACT	125
3.2 INTRODUCTION	126
3.3 EXPERIMENTAL PROCEDURES	129

3.4 RESULTS	136
3.5 DISCUSSION	141
3.6 FIGURES	150
3.7 TABLES	166
3.8 REFERENCES	169
CHAPTER 4	176
<hr/>	
MANUSCRIPT 3	176
4.1 ABSTRACT	177
4.2 INTRODUCTION	178
4.3 EXPERIMENTAL PROCEDURES	179
4.4 RESULTS	181
4.5 DISCUSSION	183
4.6 FIGURES	185
4.7 REFERENCES	191
CHAPTER 5	194
<hr/>	
DISCUSSION	194
5.1 ASP³⁸⁹: INSIGHTS INTO FUNCTION OF LDNT2	194
5.2 ARG³⁹³: INSIGHTS INTO FUNCTION AND TARGETING OF LDNT2	197
5.3 TERTIARY TOPOLOGY MODEL	201

5.4 CONCLUDING REMARKS

204

5.5 REFERENCES

206

LIST OF FIGURES

FIG. 1.1. Leishmaniasis distribution and pathology	39
FIG. 1.2. Leishmania life-cycle and Promastigote Cell Biology	41
FIG. 1.3. Structures of Leishmania surface glycoconjugates.	43
FIG. 1.4. Chemical structures of chemotherapy agents for leishmaniasis	45
FIG. 1.5. Leishmania purine salvage pathway	47
FIG. 1.6. Pyrazolopyrimidine metabolism in Leishmania and humans.	49
FIG. 1.7. Chemical structures of purines.	51
FIG. 1.8. Predicted topology and conserved residues (labeled) of the equilibrative nucleoside transporter (ENT) family.	53
FIG 1.9. Substrate and inhibitor specificity of hENT1 and hENT2.	55
FIG 1.10. Schematic of the main findings of the structure function of the ENT	57
FIG. 2.1. Multiple sequence alignment of predicted TM8 of ENT family members.	103
FIG. 2.2. Functional characterization of Asp ³⁸⁹ and Arg ³⁹³ Ldnt2 mutants.	105
FIG. 2.3. Asp ³⁸⁹ and Arg ³⁹³ mutant transporter kinetics.	107
FIG. 2.4. Deconvolution microscopy of Δ Ldnt2 transfectants.	109
FIG. 2.5. Cell surface expression of wild type and mutant Ldnt2 in Δ Ldnt2 transfectants.	111
FIG. 2.6. Characterization of D389R/R ³⁹³ , D ³⁸⁹ /R393D, D389R/R393D GFP-Ldnt2 mutants.	113
FIG. 2.7. Topology of the NH ₂ -Terminus of GFP-LdNT2.	115

<i>FIG. 3.1. Distribution of residues mutated in the second-site suppressor clones.</i>	150
<i>FIG. 3.2. Functional characterization of second-site suppressor clones.</i>	152
<i>FIG. 3.3. Functional characterization of Asn¹⁷⁵ Idnt2 mutants.</i>	154
<i>FIG. 3.4. Deconvolution microscopy of ΔIdnt1/ΔIdnt2 transfectants.</i>	156
<i>FIG. 3.5. Cell surface expression of wild type and mutant Idnt2 in ΔIdnt2 transfectants.</i>	158
<i>FIG. 3.6. Asn¹⁷⁵ mutant transporter kinetics.</i>	160
<i>FIG. 3.7. Multiple sequence alignment of predicted TM4 – TM5 region of ENT family members.</i>	162
<i>FIG. 3.8 Tertiary topology prediction.</i>	164
<i>FIG. 4.1. Restriction Fragment Length Polymorphism at Trp³⁷⁶ locus.</i>	185
<i>FIG. 4.2. Functional characterization of W376X-Idnt2 mutant.</i>	187
<i>FIG. 4.3. Expression of W376X-Idnt2 in ΔIdnt1 /ΔIdnt2 transfectants.</i>	189

Chapter 1

INTRODUCTION

1.1. Leishmaniasis

1.1.1. The Disease: Prevalence and Pathology

Leishmaniasis is a disease endemic in 88 countries on 4 continents (1) with a prevalence of 12 million cases and a worldwide annual incidence of 2 million cases (2,3). It is caused by a single celled protozoan eukaryote, *Leishmania*. Economic development, environmental changes, and an increased number of worldwide travelers have led to the increased incidence of the disease (2,3). In recent years there has been a growing interest in leishmaniasis in the United States due to the increasing number of overseas travelers and U.S. Gulf War veterans (4). Furthermore, coinfection of the human immunodeficiency virus

Chapter 1: INTRODUCTION

(HIV) and *Leishmania* is of significance since both pathogens reside in macrophages within the host, and a species of *Leishmania* (*L. infantum*) was found to induce the expression of latent HIV-1 (5).

The disease leishmaniasis was discovered in 1903, independently but simultaneously, by Sir William Boog Leishman, a British pathologist, and Charles Donovan, doctor in the Indian Medical Service (6,7). The most fatal species of *Leishmania* was termed *Leishmania donovani*. It is the causative agent of visceral leishmaniasis (VL) or Kala Azar, a colloquial name in India, which translates to "black plague", or Dum Dum Fever (7). Specifically, it is caused by the *L. donovani* and *L. infantum* species, and has a mortality rate of almost 100% if left untreated. More than 90% of VL cases occur in Bangladesh, Brazil, India and Sudan (Fig. 1-1A) (1). VL is caused by widespread parasite infection in the lymphatics. It is characterized by irregular bouts of fever, substantial weight loss, swelling of the spleen and liver, and anaemia (Fig. 1-1B).

The other major form of leishmaniasis is the cutaneous form (CL) also known as Baghdad ulcer, Delhi boil or Bouton d'Orient (boil of the orient). More than 90% of CL cases occur in Iran, Afghanistan, Syria, Saudi Arabia, Brazil and Peru (Fig. 1-1A) (1). Cutaneous forms of leishmaniasis are most prevalent and remain localized to the skin (8). The cutaneous sores develop as a vascularized papule on the skin at the site of the insect bite becomes ulcerated, erupts, and spreads to form a lesion (Fig. 1-1C) (8). The lesions can cause permanent

scarring when they heal especially with the onset of a secondary bacterial infection (8). The cutaneous form can be further categorized into dermal cutaneous (DCL) and mucocutaneous (MCL). DCL the most common of the cutaneous forms, is caused by the *L. mexicana* and *L. braziliensis* complexes in the New World and by *L. tropica* and *L. major* species in the Old World (9). It can leave unsightly scars from one to hundreds of skin lesions which self-heal within a few months. The DCL form can exacerbate into a "diffuse" form. It produces disseminated and chronic skin lesions resembling those of leprotamous leprosy. The diffuse form is difficult to treat and is mainly a progressive stage of infections by *L. mexicana amazonensis* and *L. mexicana pinnafoi* that spread to macrophages throughout the skin (10). MCL, caused by the *L. braziliensis* species, begins with skin ulcers that spread, causing dreadful and massive tissue destruction especially of the nose and mouth.

1.1.2. The Causative Agent: Life Cycle and Parasite Survival

1.1.2.a Taxonomy and Morphology

Leishmania belong to the order kinetoplastida, which derives its name from a unique organelle similar to the mitochondria, the kinetoplast (11). The

Chapter 1: INTRODUCTION

kinetoplasts have an extraordinary amount of circular DNA existing in two subsets, which replicates independently but synchronously with the cell nucleus (12). Maxicircles are the canonical, circular mitochondrial genome with the core genes for transcription that code for ribosomal RNA and structural genes, and minicircles encode for the specific guide RNA corresponding to the core genes that are catenated into a substantial mass of DNA referred to as the kinetosome (11). The guide RNA are used as templates to edit the main messenger RNA of the core genes by either inserting or deleting numerous uridine residues to create the final version of the coding sequence (11). Thus, the final sequence of the messenger RNA required for translation is a combination of two these two disparate DNA templates and unique process of RNA editing requiring uridines, pyrimidine nucleosides.

Leishmania belong to the family *Trypanosomatidae*, which are flagellated and either have a monogenetic or digenetic life cycle (13,14). *Leishmania* belong to the digenetic taxa, which alternate between the promastigote and amastigote forms. Promastigotes have a spindle shaped body with a single flagellum and persist in the insect vector, while amastigotes are spherical in shape with only a flagellar remnant, in the mammalian host where they mainly infect reticuloendothelial cells and macrophages (Fig. 1-2 A & B). The flagellum extends out of an invagination of the plasma membrane at the anterior end, termed the flagellar pocket. Membrane proteins traffic through the *trans* Golgi network composed of

tubovesicular structures and are inserted by vesicular fusion into the membrane of the flagellar pocket (15). It lacks a closely spaced sub-pellicular microtubule network, which is located beneath but attached to the plasma membrane of the cell body to maintain the shape of these parasites (16). The flagellar pocket is the main site of endo and exocytosis, and its membrane may also serve as a station for sorting proteins destined for the flagellar membrane from those for the pellicular plasma membrane (17). From there, membrane proteins can move by lateral diffusion to the surface of both the cell body and flagellum (18)

The promastigote form has been adapted for laboratory propagation and is therefore used as the primary form for scientific inquiry. The digentic switch between promastigotes and amastigotes had been achieved in axenic cultures for *L. donovani* previously, but the amastigotes were not infective (19). Recently, the digentic switch was achieved *in vitro* for *L. donovani* that retain infectivity (13). Along with gross morphological differences, even organelle morphology shifts have been observed with the life stage of the parasite *in vitro*. For example, the morphology of the multivesicular tubular compartment (MVT) or the "crapasome", varies with the growth stage of *Leishmania* (20,21). The MVT is a terminal lysosome thought to be the default destination for many integral membrane proteins in *Leishmania* in the absence of a targeting sequence, inability to interact with sorting machinery, and overexpression (20,21). In rapidly dividing *Leishmania* promastigotes, a population of 200 nm multivesicular bodies, which

Chapter 1: INTRODUCTION

extend from the *trans* Golgi network, fuse into a rod-like MVT that extends along the anterior-posterior axis of the cell (15,20,21). As promastigotes reach stationary phase, the rod-like MVT collapses into multiple electron dense vacuoles (21,22); finally, these vacuoles enlarge in the amastigote stage and are termed megasomes (23,24).

Human infection is caused by about 21 of 30 *Leishmania* species that infect mammals (3). The different species are morphologically indistinguishable, but they can be differentiated by isoenzyme analysis, molecular methods, or monoclonal antibodies (3). Five major *Leishmania* species, *L. tropica*, *L. major*, *L. donovani*, *L. braziliensis*, and *L. mexicana* cause leishmaniasis (25). Interestingly, *Leishmania* species differ in their ability to withstand temperature stress, which is one of the determinants for the tropism of the species (26). *L. major* and *L. mexicana* amastigotes multiply better at 35°C than at 37°C and are therefore restricted to skin (cutaneous) lesions where the temperature is lower. On the other hand, *L. donovani* amastigotes multiply equally well at 37°C and 35°C and therefore establish lesions in visceral organs where the temperature is 37°C.

1.1.2.b. Sandfly Vector: Survival and Attachment

The life-cycle of *Leishmania* (Fig. 1-2A) starts when a female sandfly (subfamily *Phlebotominae*), a tiny sand-colored blood-feeding fly that breeds in

forest areas, caves, or the burrows of small rodents, ingests a blood meal via the proboscis from an infected host (1). Old World forms of *Leishmania* are transmitted by sandflies of the genus *Phlebotomus*, while New World forms are transmitted mainly by flies of the genus *Lutzomyia* (1). Sandflies are infected by ingesting blood from infected reservoir hosts (small mammals) or from infected people (1). Amastigote loaded macrophages are introduced into the sandfly midgut and enclosed in a sac-like vacuole, where the amastigotes continue to go through a few cell divisions (27). Transformation into non-infectious motile promastigotes occurs when the change in the amastigote environment is sensed and a series of metabolic changes are initiated (27).

There are several discrete developmental stages of the promastigote form in the sandfly. First, amastigotes (2-3 μm) transform into short ellipsoid procyclic promastigotes that are about 6-8 μm long. After the procyclics reach a certain cell density and the nutrients in the blood meal have been depleted, they gradually transform into the more elongated nectomonad forms that are about 15-20 μm long. After three days, the sac-like vacuole breaks down and the nectomonads migrate to the anterior midgut where they attach to the epithelium by inserting their flagella between the microvilli (27). At the molecular level, the attachment of *Leishmania* to the midgut involves the interaction of the parasite lipophosphoglycan (LPG) coat with lectin and lectin-like molecules in the sandfly gut (Fig. 1-3A) (28-33). LPG is one of the most abundant forms of glycosylphos-

Chapter 1: INTRODUCTION

phatidyl inositol (GPI) anchored molecules on the surface of the promastigote, which forms a dense glycocalyx coat over the entire surface of the parasite including the flagellum (34). It is a tripartite molecule that consists of a Gal-Man-PO₄ repeat unit backbone attached to a lipid anchor via a glycan core (35). Although, the phosphoglycan moieties from all *Leishmania* species share a common backbone of repeating disaccharide units of PO₄-6Galβ(1>4)Manα1, they exhibit polymorphisms at position 3 of the Gal residues that allow particular species of *Leishmania* to colonize a specific sandfly species (34,36-38,39 Sacks, 2000 #37). For example, the *L. major* lipophosphoglycan (LPG), which contains several glycan side chains, binds strongly to the midgut of *Phlebotomus papatasi*, the natural host. *L. donovani* LPG, on the other hand, lacks any substituted glycan side chains and binds exclusively to the midgut of *P. argentipes* (34). Along with LPG, the survival of *Leishmania* in the insect vector is also facilitated by a zinc metalloprotease gp63, an abundant promastigote surface GPI-anchored protein that consists of a 63 kDa zinc protease attached to the glycan core (Fig. 1-3B) (35). Gp63 protects the parasites from hydrolytic enzymes of the sandfly midgut as the promastigotes protrude from the intestinal microvilli (30,34,40). About five days after ingestion of the bloodmeal, the promastigotes reach the final stage of highly motile and infectious metacyclic promastigotes that colonize the anterior midgut and foregut of the sandfly lumen (27). LPG undergoes structural changes involving size and heightened expres-

sion of terminally exposed sugars that cause detachment from the midgut and allow the promastigotes to migrate forward into the mouthparts (27,29).

1.1.2.c. Human Host: Phagocytosis and Defiance of the Immune System

When a parasitized female sandfly ingests a blood meal from a naive host, promastigotes are delivered and the amastigote part of the life cycle is initiated. *Leishmania* lack any specialized mechanism to actively penetrate cells and therefore depend on the phagocytic potential of the host cell (41). Entry of parasites into mononuclear phagocytes is a receptor-mediated endocytosis process involving complement receptor types I and III (CR1 and CR3) on the surface of the macrophages and the complement for the CRs on the parasite (C3b) (42,43). Parasite component C3b is the ligand for the macrophage receptor CR1, which initiates the production of nitric oxide (NO), a potent microbicidal agent involved in the killing of a range of pathogens. Gp63 binds C3b and enhances the rate of cleavage of C3b to the inactive form iC3b (44). The generated iC3b now serves as a ligand for the macrophage receptor CR3, which enhances binding of the parasite to the macrophage and more specifically, internalization and inhibition of interleukin-12 (IL-12) production thus, hindering

Chapter 1: INTRODUCTION

the microbicidal oxidative burst of the host immune response towards *Leishmania* (44).

Humans exhibit two types of immunity: humoral, which is antibody mediated, and cell-mediated, which involves the activation of T-lymphocytes (T-cells). Immunity against *Leishmania* is cell-mediated, because parasites escape the humoral response by residing within macrophage phagolysosome where antibodies have no effect (2). Each T-cell subset, T4 and T8, expresses a unique CD membrane protein, CD4 and CD8 respectively. The CD molecules bind the antigen presenting molecules on infected cells, major histocompatibility molecule (MHC). The T cells also express T-cell receptors (TCR), which bind to the antigen peptide loaded on the MHC molecule. Thus, the infected cells present the antigen at the membrane bound to a MHC molecule. The TCRs on naive T-cells recognize the antigen and the interaction is stabilized by the added association of the CD molecule on the naive T-cell with the MHC molecule on the infected cell. This interaction activates T8 cells that cause cytotoxic cell lysis, while it induces the maturation of T4 cells into another subset, Th1 and Th2 that further regulate the immune response through cytokine production such as IL-12. Finally, gp63 contributes to the leishmanial defense by cleaving the CD4 molecule on T4 cells, which would prevent the maturation of T4 into Th1 cells and subsequently the production of IL-12 that would initiate the microbicidal oxidative burst (45).

Phagocytosis of microorganisms by the macrophage usually triggers the microbicidal oxidative burst characterized by an increased uptake of oxygen. The two main enzymes that catalyze the oxidative burst are NADPH oxidase, which leads to the generation of microbicidal hydrogen peroxide and superoxide radicals, and inducible nitric oxide synthetase (iNOS), which leads to the production of nitric oxide from L-arginine and molecular oxygen (2,46). The iNOS is activated by interferon-gamma (IFN- γ) secreted by Th1, mature T4-lymphocytes that are induced upon IL-12 production from macrophages engaging in phagocytosis. LPG can regulate the activity of iNOS and therefore profoundly affect the survival of *Leishmania* within macrophages (47). On the other hand, NADPH oxidases are activated upon phosphorylation by protein kinase C (PKC) (48). However, LPG and gp63 can block the oxidative burst through abnormal activation of PKC by calcium chelation (29,49-51) and reduction of its translocation to the membrane (52). LPG is also capable of scavenging oxygen free radicals due to its repetitive, oxidizable, phosphorylated, disaccharide units (41). *Leishmania* amastigotes possess large amounts of superoxide dismutase and catalase to convert the superoxide anion to hydrogen peroxide (41,48).

Following endocytosis, phagosomes containing *Leishmania* fuse with lysosomes and or late endosomes to form the parasitophorous vacuole (PV) (53). Like lysosomes, PVs have an acidic lumen with a pH of 5 and contain

Chapter 1: INTRODUCTION

several active acidic hydrolases, which degrade the pathogen proteins into antigens. Promastigotes are more susceptible to the lysosomal hydrolases. The promastigote LPG has the ability to transiently inhibit phagosome-endosome fusion and allow promastigotes to initiate transformation into amastigotes. This continues after fusion for 2-5 days depending on the *Leishmania* species (53,54). LPG repeating units may inhibit phagosome-endosome fusion by reducing the fusogenic properties of the membranes due to steric repulsion or by imparting rigidity to the parasite plasma membrane (29). The promastigote to amastigote transformation is accompanied by the reduction or loss of LPG expression and concomitant phagosome-endosome fusion (54). Finally, if the phagolysosome does form before complete transformation, gp63 assumes a protective function by inhibiting degradative phagolysosomal enzymes (4,55).

The temperature shift to 37°C and change in pH to 5 inside the PV triggers various physiological changes that complete the transformation to amastigotes. Interestingly, the various isoforms of gp63 and other membrane proteins that function optimally at pH 7.4 in the promastigote stage are adjusted to function optimally at pH 5.0 in the amastigote stage. However, the proton translocating ATPase located at the amastigote plasma membrane has been implicated in creating a transmembrane proton electrochemical gradient and in regulating internal parasite pH at physiological levels (26,56). To persist in the macrophages, amastigotes change their surface coats by downregulating LPG and

gp63 expression and increasing the level of glycoinositol phospholipids (GIPLs), GIPLs are a family of free GPIs linked with a lipid anchor via a glycan core (57) (Fig. 1-3 A & C). GIPLs are involved in various mechanisms to maintain *Leishmania* within the macrophages: they mediate amastigote binding to macrophages (58), promote survival by inhibiting microbicidal NO macrophage production (41), protect against the acidic medium and hydrolases within the PV (53), inhibit MHC-I and II expression and peptide loading for the few MHC that are produced (59), and PKC inhibition (29,60). Finally, amastigotes have the ability to internalize and degrade MHC-II molecules that reach the PV in organelles called megasomes, which are rich in cysteine proteases (53). Thus, the parasites reduce the number of parasite antigen-MHC II complexes on the surface of the macrophage and escape recognition by the host immune system (53). It is commonly accepted that after several cycles of replication, the macrophage bursts (lytic cycle) to release the amastigotes for reinfection. It may also be possible that the release of amastigotes occurs by the fusion of the PV with the macrophage plasma membrane (53). Little is known about the amastigote re-entry into the macrophages. In summary, throughout their life cycle, *Leishmania* attack every level of the human immune response.

Chapter 1: INTRODUCTION

1.2. Therapies

1.2.1. Current Therapies

Pentavalent antimonials (Sb(V)) were the first agents of therapy introduced in the 1940s, and remain to be the mainstay of therapy for all forms of *Leishmaniasis* (61) (Fig. 1-4A). Two such drugs are stibogluconate sodium (Pentostam) and meglumine antimoniate (Glucantime), which are efficacious and as well as toxic (62,63). They are intravenously administered with the dosage of 20 mg of Sb(V) per kg body weight per day (63). The mechanism of action is uncertain, but it appears that pentavalent antimony concentrates in cells of reticuloendothelial origin, a site where *Leishmania* reside in humans (63). It is generally agreed that the reduced trivalent form Sb(III) of Sb(V) is toxic to *Leishmania* (61). Side effects such as pancreatitis can be severe, and fatality may even occur due to cardiac arrhythmia for persons with underlying heart disease (63). A slow resistance to antimonials began to develop in the 1970s, and today resistance to Sb(V) is endemic at a rate of more than 50% in the state of Bihar, India. Furthermore, 10-25% of the treatments fail or a relapse occurs, in which case a second line of drugs is used, pentamidine and amphotericin B (AmpB) that will be discussed below (64). Also, antimonials have reduced

activity in the absence of a T lymphocyte mediated immune response, as would be the case in an immunocompromised patient infected with HIV (5,65).

Pentamidine is a second line drug against many leishmanial infections, but its efficacy has also rapidly declined in India (61) (Fig. 1-4C). Another reason for its limited use is its toxicity (62). The cellular target of pentamidine is unknown, although it causes competitive inhibition of polyamine transport suggesting that it possibly enters into *Leishmania* through the parasite polyamine transport system (61). The first of the leishmanial polyamine transporters has just been cloned and characterized (Hasne *et al*, unpublished). Perhaps, an understanding of the ligand binding site and translocation mechanism will aid in the development of pentamidine analogs that are less toxic. Furthermore, a knockout of the polyamine transporter will confirm the mode of pentamidine entry.

Another second line drug for leishmaniasis is AmpB deoxycholate and liposomal AmpB (62) (Fig. 1-4B). Amphotericin, an antifungal, binds to sterols and probably damages the surface membrane of *Leishmania* (63). The disadvantage with AmpB deoxycholate is its intravenous administration over extended periods of time and its side effects such as fever, malaise, and renal failure (63). The most recent advance has been the use of liposomal AmpB (AmBisome) for the treatment of VL (63). Liposomes are preferentially taken up by mononuclear phagocytes and reticuloendothelial cells, the two target cells of *Leishmania* (63). The liposomal form is substantially less toxic to the human host and has an

Chapter 1: INTRODUCTION

extended plasma half-life (62,63). It is the first drug to receive the Food and Drug Administration (FDA) approval for treatment of VL and could become the first line drug since it has been effective in cases where antimonials have failed (62,63). The major hurdle limiting use of the AmBisome is its high cost (63), which could be reduced by alternative cheaper liposomal formulations (66,67). Although resistance to AmpB is not yet widespread, resistance could occur as it is easy to derive resistant strains in the laboratory (61).

1.2.2. Therapies under Development

Although a vaccine would be the best solution for combating leishmaniasis, the results have not been promising. Current leishmaniasis vaccine candidates are killed or attenuated whole promastigotes, synthetic and recombinant peptides of molecules such as lipophosphoglycan, and recombinant, live, attenuated vectors (2,3,36,68). However, vaccine trials in South America and the Middle East have, unfortunately, met with mixed success (25). However, there are some promising chemotherapeutic drugs under development.

Since most of the treatments available are intravenous, it is necessary to develop topical treatments for CL where the infection is mainly at the skin. Paromomycin (PM), an aminoglycoside antibiotic, is a promising topical treatment for CL currently in phase III trials (62) (Fig. 1-4D). Although this drug was

identified in 1960s, its development has been slow due to poor bioavailability (62). Aladara, presently used to treat genital warts, is yet another promising drug currently in phase II trials (62) (Fig. 1-4F). It is a topical cream with the active ingredient imidazoquinoline imiquimod, an immune system modifier which mimics the action of interferon γ (INF- γ), a cytokine that induces nitric oxide production in macrophages to cause parasite lysis.

One of the current drugs under development, which has exhibited promise, is miltefosine (Fig. 1-4E). It was recently shown to be effective in Indian field trials (63). Miltefosine is a phosphocholine analog that interferes with cell-signaling pathways and membrane synthesis (63). It is related to lecithin (phosphatidylcholine) and was originally developed as a cancer drug, but it did not have efficacy towards tumors when administered orally (63). In phase II trials (tested on laboratory subjects), miltefosine appears to be highly effective against VL, however gastrointestinal side-effects were frequent and altered levels of reversible transaminase and creatinine were also observed (63). The efficacy of miltefosine was remarkable in phase III trials (controlled test group of a couple hundred people), which had a 94% success rate against VL (69). Miltefosine is now registered for phase IV trials (field study involving a village) in India and is reported to have a high success rate (69). Like AmpB, resistance to miltefosine can occur since resistant laboratory strains are easy to derive (61).

Chapter 1: INTRODUCTION

1.2.3. New Avenues for Therapy Development

1.2.3.a. Differences between the Host and Parasite

Due to the failed attempts of vaccine development, toxicity of current therapies, and the unavoidable phenomenon of drug resistance, the need for new therapies is acute. A drug would be fundamentally useful if it is toxic to the parasite without affecting the host. Such a drug would target a discrepancy between the parasite and the host. The kinetoplast and the glycosome are two unique organelles that are targets for drug development (Fig. 1-2B). Although, no drugs that specifically inhibit the kinetoplast have been identified (11), the mode of action of miltefosine in *Leishmania* is reported to be the inhibition of the glycosomal enzyme alkyl-specific-acyl-CoA acyltransferase involved in ether-lipid remodeling (61). The glycosome is evolutionarily related to the peroxisomes and glyoxysomes of higher eukaryotes. Typically a cell contains 65-250 glycosomes, comprising 4 percent of the total cell volume (70). Like peroxisomes, glycosomes contain enzymes of fatty acid oxidation and pyrimidine synthesis. Unlike peroxisomes, glycosomes also contain the first seven enzymes of the glycolytic pathway and two glycerol metabolism enzymes (71). Interestingly, there is a dramatic reduction in the rate of respiration and glucose catabolism

from the promastigotes to the amastigotes (43) in which fatty acid metabolism is actually the predominant source of energy for amastigotes (43). Thus, perhaps glycosomes behave more like their peroxisome counterparts in the amastigote stage. Interestingly, majority of the glycosomal enzymes are clearly more related to their prokaryotic, algae, and plant counterparts bolstering its validity as a drug target (11). Besides energy metabolism pathways, the glycosome is also home to enzymes of other important pathways such the purine salvage pathway. In particular, the key enzymes hypoxanthine guanine phosphoribosyl transferase (HGPRT) and xanthine phosphoribosyl transferase (XPRT) are localized to the glycosome via a specific carboxy terminus SKL tripeptide (Fig. 1-5) (72,73).

1.2.3.b. Purine Salvage

A metabolic difference that exists between all known protozoan parasites to date and the human host is the inability of the parasites to synthesize purines *de novo*. Therefore, they must rely on salvage pathways for these essential nutrients. Purine and pyrimidine nucleotides are fundamental in several biochemical molecules such as nucleic acid building blocks, cellular energy sources, signaling molecules, and as components of coenzymes NAD⁺, FAD, and coenzyme A. Delivering a toxic compound to the parasite by exploiting the purine salvage pathway would be feasible without harming the host. The majority of the

Chapter 1: INTRODUCTION

mammalian cells possess two pathways for the synthesis of purine nucleotides. *De novo* pathway leads to the synthesis of inosine monophosphate (IMP) from non-purine precursors such as amino acids and carbon dioxide. A salvage pathway reutilizes preformed purines (74). The *de novo* pathway consists of eleven enzymatic reactions that assemble the purine ring on a phosphoribosyl (PRPP, ribose-5'-phosphate) moiety, leading to the synthesis of IMP, the precursor for both adenosine (AMP) and guanosine (GMP) nucleotides (75). Most mammalian cells also possess a purine salvage pathway and bone marrow cells actually only possess the purine salvage pathway (76). Salvage pathways in mammals are similar to those in *Leishmania*, but less redundant.

Once the purine enters *Leishmania* via nucleoside transporters, discussed in detail in the next section, it is captured and interconverted to a phosphorylated nucleotide by a complex, yet redundant purine salvage pathway (Fig. 1-5). Central to the *Leishmania* salvage pathway, are the reactions catalyzed by the PRPP transferase (PRT) enzymes, $\text{PRPP} + \text{purine base} \rightarrow \text{purinePRPP}$. Before the PRT reaction can proceed, the reactants must first be generated. The first step of purine salvage which is the uptake of these nutrients into the parasite from the host milieu. Nucleoside transporters are only capable of translocating purine nucleosides (dephosphorylated purine-ribose) and nucleobases. *L. donovani* have membrane bound 5' and 3' nucleotidase activities and a surface acid phosphatase activity, which play an important role in purine salvage by

generating purine nucleosides by dephosphorylating nucleotides (phosphorylated purine-ribose) (77). The captured nucleoside is first hydrolyzed to its corresponding purine base by nucleoside hydrolases (NH), nucleoside \rightarrow nucleobase + ribose. Each NH activity is specific for a different set of substrates: inosine, cytosine, and xanthosine (IUNH); deoxynucleosides; and inosine and guanosine (78). There is also an adenosine phosphorylase activity that cleaves adenosine to adenine (78). The second reactant for the PRT reaction is PRPP, which is synthesized from PRPP synthetase. Recently, three PRPP synthetases were mined from the *Leishmania* genome database and are currently under characterization (Jan Zarella-Boitz unpublished). The nucleobases are then appended with a PRPP moiety by the PRT enzymes.

L. donovani express three different activities: Hypoxanthine Guanine (HG) PRT, Adenine (A) PRT, and Xanthine (X) PRT (Fig. 1-5) (78). Mammalian cells lack XPRT (78). *Leishmania donovani* (Ld) HGPRT and APRT exhibit absolute specificity for the purines for which they are named (78). However, XPRT recognizes hypoxanthine and guanine with xanthine as the preferred substrate (78). HGRPT and XPRT also contain a glycosomal targeting carboxy terminal tripeptide (SKL) and, indeed, they have been shown to target to the glycosome (78). Conversely, APRT is a cytosolic enzyme (78). Interestingly, APRT does not play a critical role in adenosine salvage in promastigotes; rather, it seems to have a prominent role in amastigotes (78). Thus in amastigotes, adenosine may be

Chapter 1: INTRODUCTION

either deaminated to inosine and then cleaved by NH or directly phosphorylated by adenosine kinase (AK) (78). This observation is corroborated by the fact that in promastigotes, extremely active enzymes that interconvert Adenosine → Inosine → Hypoxanthine through adenine/adenosine deaminase (AD), and guanine → xanthine by guanine deaminase (GD). Hypoxanthine and xanthine are used by the HGPRT and XPRT (78). Gene knockout studies of the PRTases, where each of the PRTs have been singly knocked out by gene replacement with a drug marker, have all yielded viable promastigotes. This shows that none of the PRTases are essential by themselves (78). The effect of these PRTase knockouts in amastigotes is presently being studied with the *L. donovani* infective cell line recently isolated (Jan Zarella-Boitz unpublished).

Leishmania, like in most organisms, can interconvert purine nucleosides. IMP (hypoxanthine-PRPP), product of the HGPRT reaction, can be converted to both AMP and GMP by alternative pathways. For AMP synthesis, adenylosuccinate synthetase (ASS) catalyzes the following reaction: $\text{IMP} + \text{Asp} \rightarrow \text{succino-AMP}$, which is then cleaved by succino-AMP lyase to AMP and fumarate (76,79). GMP reductase catalyzes the reduction of GMP to IMP (74). LdASS, GMP reductase, succino-AMP lyase, and HGPRT are unique in that they can accept allopurinol ribonucleotide monophosphate and formycin B monophosphate as substrates, both of which are toxic nucleoside analogs (Fig. 1-6 & 7A) (78). Furthermore, *L. donovani* also has nucleoside phosphotransferase (NPT), impli-

cated in the metabolism to the nucleotide level of anti leishmanial pyrazolopyrimidine (purine) nucleoside analogs, allopurinol riboside, formycin B, and 4-thiopurinol riboside, but whether this enzyme recognizes naturally occurring purines is unknown (78).

Allopurinol, a pyrazolo[3,4-d]-pyrimidine base (purine analog), has been clinically tested and may be efficacious against certain forms of leishmanial infections (61). Purine analogs are aminated to adenine nucleotide analogs and have been shown to kill *Leishmania* species *in vitro* and in animal models (63). They stop protein synthesis and result in breakdown of mRNA (Fig. 1-6) (63). The efficacy of various purine analogs has not been sufficient in humans to be recommended as a routine drug (63). However, allopurinol has suppressive activity against canine leishmaniasis and has been considered as part of its maintenance therapy (80). Purine analogs such as pyrazolo (3,4-d) pyrimidine bases are inefficient substrates for hypoxanthine guanine phosphoribosyl transferase (HGPRT). HGPRT is a key purine salvage enzyme that catalyzes the formation of IMP and guanosine monophosphate by appending a phosphoribosyl moiety to hypoxanthine and guanine bases respectively. This converts them to a toxic phosphorylated metabolite (78). These findings do lend encouragement to researchers of purine salvage for the design of more efficacious drugs.

Chapter 1: INTRODUCTION

Unfortunately, purine analog resistance has already been encountered in *Leishmania*. One mechanism is the appearance of cryptic mutations within essential transporters and genes under drug pressure. For example, in the adenosine-pyrimidine nucleoside transporter (LdNT1), point mutations were shown to confer resistance to tubercidin, a toxic adenosine analog (Fig. 1-7B) (81). *Leishmania* can also respond to purine analogs by amplifying a specific portion of its genome (61). The *TOR* gene, similar to transcription factor genes, was shown to confer resistance to several purine analogs including allopurinol (61). The *TOR* gene product appears to modulate the activity of purine nucleoside transporters by an unknown mechanism (61). Thus, new drugs are constantly needed to combat the phenomenon of drug resistance. The mode of entry for a toxic nucleoside analog is the nucleoside transporter. Understanding the function of the translocation mechanism is crucial for the development of drugs to deliver a toxic meal to the uninvited guests. The focus of this thesis is purine nucleoside transport, which is the first step in purine salvage.

1.3. Nucleoside Transporters

1.3.1. Transport Processes: Overview

Section: 1.3. Nucleoside Transporters

Transport proteins mediate the uptake of essential hydrophilic molecules through the impermeable lipid bilayer. There are two main types of transport proteins, channels and transporters. These create aqueous pores surrounded by multiple transmembrane spanning domains within the hydrophobic lipid bilayer to regulate the passage of essential molecules. The major difference between channels and transporters is that a channel pore mediates facilitated diffusion by a “gated” mechanism, which means the channel opens in response to a chemical or mechanical stimuli. However, a transporter mediates facilitated or active diffusion by a conformational change induced upon ligand binding. This is analogous to classical enzyme kinetics where the “reaction” step of enzymes is equivalent to the “translocation” step of transporters. A classical example of a channel type transport protein is the potassium channel, which is critical in potassium cation flux in neurons to facilitate the transmission of signal (82). It is thought to be selective by the size of its pore and stimulated (opened) by a voltage sensitive “gate”. The gate is a loop that occludes the pore when the channel is closed (82). A classical example of a transporter type transport protein is the lactose permease of *E. coli*, which is proton and lactose symporter (83). Lactose permease belongs to the major facilitator superfamily (MFS) whose members have twelve transmembrane domains and function as monomers (83). Lactose permease uses a proton gradient to drive the translocation of a lactose molecule (83). The binding of the ligand to the transporter causes a global

Chapter 1: INTRODUCTION

conformational change. The ligand bound and unbound forms of lactose permease have recently been crystallized (83).

Nucleoside transporters play an important role in the physiology of living organisms by salvaging nucleosides. Many antiviral and anticancer nucleoside drugs are ligands of nucleoside transporters, such as cytarabine and zalcitabine respectively (84). Also, since protozoan parasites must solely depend on the salvage of purines from their host to survive, nucleoside analogs are attractive as antiparasitic drugs that can be delivered into the parasite via the nucleoside transporter. Understanding the basic molecular mechanism of nucleoside transport should enable the design of effective drugs since the ability of the transporter to transport these drugs is critical for the effectiveness of the therapy. However, rational drug design is hindered by the absence of high-resolution structural data on the transporters. For the past few decades, research groups have been slowly piecing together the puzzle of nucleoside transport by various mutational approaches, discussed in detail below.

Mammalian cells have two distinct types of nucleoside transporters, concentrative (CNT) and equilibrative (ENT). All the cloned and characterized CNTs are secondary active transporters that utilize sodium or proton gradients to drive the uphill transport of their nucleoside substrates (85). The gradients are established by primary active transporters that utilize energy to cause a conformational change resulting in translocation of ions against their concentration gradient, an

example is the ATPase family that transport ions coupled to ATP hydrolysis. CNTs are found in prokaryotes and eukaryotes. Another example is the human nucleoside/sodium symporter (translocation of the both ligands in the same direction) hCNT1 (86). On the other hand, ENTs are facilitative transporters that transport substrates down their concentration gradients. Protozoan parasite nucleoside transporters belong to the ENTs, which are mainly found in eukaryotes with one putative bacterial member recently mined from the databases (87). The ENTs are the focus of this thesis.

1.3.2. Equilibrative Nucleoside Transporters (ENT):

1.3.2.a. General Characteristics: Human and *Leishmania* ENTs

ENTs have a putative membrane topology consisting of 11 transmembrane domains (TM) with an extracellular large loop between TMs1 and 2, an intracellular large loop between TMs 6 and 7, a cytoplasmic amino terminus, and a carboxy extracellular terminus (Fig. 1-8). The extracellular loop of TMs 1-2 is usually glycosylated in the mammalian proteins. The predicted topology has been shown to be correct for hENT1 (human equilibrative nucleoside transporter 1), the original member of this family, by glycosylation scanning mutagenesis and

Chapter 1: INTRODUCTION

use of antibodies as topological probes (88,89). Although sequence identity between various family members is less than 40%, pairwise alignments between various members of the ENTs revealed conserved residues, which now serve as signature motifs for this family (Fig. 1-8) (78,90). These residues are mainly within membrane spanning domains with no conserved residues in TMs 2, 4, and 6. Furthermore, the majority of the signature motifs are in TMs 7 - 10.

The human ENTs have also been termed the Solute Carrier 29 (SLC29) family of proteins (84). Human ENTs have been classified into two subtypes depending on their sensitivity (*es* subtype) or insensitivity (*ei* subtype) to the inhibition by 6-thiopurine ribonucleoside nitrobenzylthioinosine (NBMPR) at nanomolar amounts (Fig. 1-9) (91). The *es* subtype is also inhibited by dipyridamole, dilazep, and draflazine. Dilazep and draflazine are used clinically as vasodilators (Fig. 1-9) (84). Studies with intact cultures of human K562 leukemia cells have shown that at physiological temperatures, the *es* processes exhibit a higher transporter efficiency for adenosine and uridine than the *ei* processes (92). Human ENT1 belongs to the *es* transport process and hENT2 belongs to the *ei* transport process (93-97). A third member of the human ENTs was recently reported from data base mining, hENT3 (98). However, it has not yet been functionally characterized since its expression cannot be detected even in oocytes. Human ENT3 could be an organellar transporter since it has putative dileucine lysosomal targeting motifs and a charged amino terminus (99,100).

Section: 1.3. Nucleoside Transporters

All the protozoan parasite nucleoside and nucleobase transporters cloned and characterized to date belong to the ENTs based on their secondary topology predictions and the presence of signature motifs. *Leishmania donovani* have two types of nucleoside transporters that display non-overlapping substrate specificities and recognize their purine ligands with high affinity. LdNT1 transports adenosine and pyrimidine nucleosides with an affinity of 0.2 μM and 6 μM respectively, and LdNT2 transports inosine and guanosine with an affinity of 0.3 μM and 0.6 μM respectively. Transfection of a *L. donovani* cosmid library into nucleoside transport-deficient *L. donovani* provided an avenue for cloning the *LdNT1* and *LdNT2* genes by functional rescue of the nucleoside transport-deficient phenotype (101,102). These transporters display a 30% sequence identity to each other and to the human ENTs. *Leishmania* are capable of transporting any preformed purine or purine nucleoside with the exception of xanthosine (90). Recently, two other ENT homologs have been identified from *Leishmania major* NT3 and NT4, which are nucleobase transporters (103,104). Whether LdNT1 and LdNT2 are expressed in the amastigote is not yet determined (90). However, a partial cDNA sequence from *L. major* amastigotes with high homology to LdNT2 has been deposited in the GenBank database (90). Interestingly, recent studies on *L. donovani* amastigotes revealed two distinct adenosine transport activities, one was similar to LdNT1 and the second transported adenosine, inosine, and guanosine (90). Transport is upregulated under

Chapter 1: INTRODUCTION

conditions of purine depletion. It is modulated by the TOR protein (Toxic nucleoside resistance protein), named after its identification in *L. donovani* cells selected for resistance to the toxic adenosine analog, tubercidin (Fig. 1-7B) (90). TOR comprises some 478 amino acids and is similar to mammalian transcription activator OCT-6 (90). When expressed in *Leishmania* TOR represses purine nucleoside and more significantly nucleobase transport (90). The mechanism of action is unknown.

The protozoan parasite ENTs are similar to the mammalian ENTs since they have the signature residues and share a similar topology, but there are some differences. They have higher permeant affinities (K_m values) than the mammalian counterparts (low or sub μM as opposed to mM) (90,105,106). The parasite ENTs have specific ligand selectivities whereas the mammalian counterparts are less selective since they transport a range of purine and pyrimidine nucleosides and analogs (90,105,106). Specifically, LdNT1 transports adenosine and pyrimidines and LdNT2 transports inosine and guanosine. Finally, LdNT1 and LdNT2 appear to be proton-dependent concentrative type transporters in a two-electrode voltage clamp study done in *Xenopus* oocytes (107) whereas the mammalian ENTs are strictly facilitative (91). However, the leishmanial nucleoside transporters do not share a predicted topology or sequence identity with the CNTs, and thus are still grouped under the ENT family.

1.3.2.b. Structure-Function of ENTs

Structure-function studies of the ENT proteins have revealed some interesting insights into the ligand binding domain and the translocation mechanism of the ENTs (Fig. 1-10). Chimera studies were instrumental in placing TMs 3 – 6 in the putative ligand binding domain. Since both rat ENTs (rENT1 and rENT2) are less sensitive to dipyridamole than their human and mouse counterparts (108), chimeras between hENT1 and rENT1 indicated that TMs 3 - 6 are important for interaction with dilazep and dipyradamole (109). These data were bolstered by chimeras between rENT1 (*es*) and rENT2 (*ei*), which indicated that TMs 3 - 6 are important for interactions with NBMPR (110). A smaller region encompassing TMs 5 - 6 was further characterized with the rENT chimeras to be important for nucleobase translocation (111). Further mutagenesis of amino acids and solvent accessibility studies implicate TMs 1, 2, 4, and 5 in ligand binding and TM7 in the translocation mechanism.

Reverse genetics suggest that residues in TM4 likely play a critical roles in ligand binding. Gly¹⁵⁴ of TM4 in hENT1 has been shown to lose NBMPR binding when mutated to a Ser (112). Interestingly, Ser is the homologous residue at position 154 in hENT2 (*ei* subtype). A subsequent study on Cys¹⁴⁰ of rENT2 in TM4, the homologous position to Gly¹⁵⁴, places Cys¹⁴⁰ in the hydrophilic pore of the transporter through modification of the Cys residue with an impremeant thiol-

Chapter 1: INTRODUCTION

reactive reagent, *p*-chloromercuriphenyl sulfonate, which was able to inhibit uridine transport in rENT2 (113). Furthermore, a C140S mutation, which is functionally similar to wild-type rENT2, is not inhibited by *p*-chloromercuriphenyl sulphonate (113). Taken together, these data corroborate the chimera results and identify a critical position in TM4 that may be involved in ligand selectivity and line the ligand binding domain.

Through extensive mutagenesis analysis, TM5 of LdNT1 and hENT1 have been implicated to be crucial for ligand binding. In a *Leishmania* cell line isolated for resistance to the toxic adenosine analog tubercidin (TUBA5 cell line) (81), Gly¹⁸³ in TM5 of LdNT1 was mutated to G183D. This caused drastic reductions in the maximal velocity for adenosine transport, but it targeted properly to the plasma membrane. Strikingly, a G183A mutation of LdNT1 disrupted pyrimidine transport without affecting adenosine transport capability, suggesting that the region of Gly¹⁸³ may be implicated in ligand selectivity. These data were corroborated with a site-directed mutagenesis study on highly conserved Gly residues 179 and 184 in TM5 of hENT1 (114). When Gly¹⁷⁹ was mutated to an Ala, uridine transport and inhibition by NMBPR were diminished, but for G179L, C, and V mutations only uridine transport was not detected. Baldwin *et al* suggest that although these data postulate Gly¹⁷⁹ in ligand binding, the drastic effect of mutating this absolutely conserved residue would also be consistent with helix-helix packing (84). This hypothesis was bolstered by the observation that the

homologous position of Gly¹⁷⁹ in hENT1 is not solvent accessible in a study described below on LdNT1. Furthermore, mutations at Gly¹⁸⁴, the homologous residue to Gly¹⁸³ of LdNT2, seem to mainly affect membrane targeting and/or correct folding of hENT1. The emerging data on TM5 of the ENTs prompted Landfear *et al* to determine the role of TM5 in forming a portion of the aqueous channel. A substituted-cysteine accessibility method was employed, which involves generating a Cys-less mutant and then scanning a TM with Cys substitutions to assess their reactivity with permeant and impermeant thiol reactive compounds (115). LdNT1 has 5 Cys, which are not conserved and were dispensable (115). Subsequent Cys replacements through predicted TM5 sequence of LdNT1 revealed six positions (M176C, T186C, S187C, Q190C, V193C, and K194C) that were inhibited by incubation with sulfhydryl-specific methanethio-sulfonate reagents, suggesting their solvent accessibility to the permeation pathway (116). Interestingly, these residues map to the hydrophilic face of TM5 on a helical wheel diagram (116). Taken together, these data bolster the chimeric studies and demonstrate that TM5 is critical in ligand selectivity and that TM5 lines the hydrophilic pore along with TM4. Finally, in the TUBA5 cell line, a C337Y mutant was also identified in TM7 of LdNT1, which caused drastic reductions of the maximal velocity for adenosine transport although it targeted properly to the plasma membrane (81). These data suggested that TM7, which is in the second half of the ENTs is critical for the translocation mechanism.

Chapter 1: INTRODUCTION

Studies with the rENT chimeras have also established that TMs 1-6 were required for the transport of the 3'-deoxynucleoside drugs (117). These data suggested that TMs 1 and 2 may also be involved in ligand binding and translocation. An M33I mutation in TM1 of hENT1 was identified in a forward genetic screen of random mutants selected for dipyridamole inhibition (118). M33I exhibited decreased dipyridamole inhibition of uridine transport (118). Interestingly, hENT2 (*ei* subtype) has an isoleucine at this position. A reciprocal I33M mutation in hENT2 changed it to *es* specificity (118). Furthermore, an L92Q mutation in TM2 of hENT1 was identified in a forward genetic yeast screen, which altered the ubiquitous selectivity of hENT1 to be exclusive for inosine and guanosine (119). L92Q also increased the sensitivity of hENT1 to NBMPR and dilazep (119). Taken together, these data bolster the rENT chimera results that TMs 1 and 2 are implicated in the ligand binding and translocation of the ENTs.

A comprehensive evolutionary study performed through sequence analysis by Acimovic and Coe (87) on 45 known and putative members of the ENTs revealed four conserved regions: TM1; TM4-loop-TM5; TM8; TM9-loop-TM10. Interestingly, Gly¹⁵⁴ in TM4 of hENT1, Gly^{179 and 184} in TM5 of hENT1, Gly¹⁸³ in TM5 of LdNT1, and Met³³ in TM1 of hENT1 mentioned above all lie within these conserved regions (Fig. 1-10). Taken together with the mutagenesis data discussed above, perhaps, TMs 1, 4, 5, 8, 9, and 10 form the core of the ENTs, and TMs 1, 4, and 5 are proximal to the ligand binding pore.

Another avenue for probing the structure of a binding cavity is to understand the molecular requirements of the ligand for recognition by scanning a library of analogues. Recently, a three-dimensional quantitative structure-activity relationship (3D-QSAR) was used to map the molecular requirements for specificity in the ENTs (120) (Fig. 1-7C). In this study the analogues of the ligand were modeled to determine whether they are feasible inhibitors. Candidate analogues were then experimentally tested for their inhibition of hENT1 transport function, which displayed a preference mainly for electrostatic and steric interactions with the ligand. However, a hydrogen bond formation with the 3'-hydroxyl is essential for binding (Fig. 1-7C). Indeed, various analog studies have been done in the past with the main conclusion that the 3' hydroxyl of the ribose is critical for ligand binding (84). Furthermore, the amino acids that interact with the 3'-hydroxyl of the ribose are likely within TMs 7-11 since rENT chimaeras have shown that TMs 1-6 were sufficient for the transport of the 3'-deoxynucleoside drugs (117).

Finally, PSI-BLAST mining has revealed that the human protein CLN3 has a distant but significant (expect value $3e^{-73}$ after four iterations) sequence similarity to hENT1 (84). BLAST is a basic local alignment search tool that identifies homologous sequences by generating pairwise alignments (121). PSI-BLAST is a position specific iterative BLAST, which generates multiple alignments to build profiles which are used in subsequent iterative searches to increase specificity in

Chapter 1: INTRODUCTION

searches (121). Human CLN3, battenin, is a 438 residue lysosomal arginine transporter proposed to play a role in lysosomal pH homeostasis and mutations in the corresponding gene are associated with the neurodegenerative disease, neuronal ceroid lipofuscinosis (122-124). Battenin is predicted to exhibit a similar transmembrane topology to the ENTs (84). Although the identification of this homolog is interesting, unfortunately it is not very helpful since this transporter has only recently been cloned and is currently under preliminary characterization.

1.3.2.c. Contribution of this thesis

The power of mutagenesis studies is revealed by the elegant work on lactose permease and rhodopsin, which led to a molecular mechanism for translocation that was later corroborated by a crystal structure (83,125). One of the major general conclusions that have been deduced from the plethora of data on the lactose permease is that only a few mutations alter or destroy the function of the transporter. These do so because specific contacts between the solute, ion, or substrate and the transporter are disrupted, or conformational changes required for the transport process are prevented (126). In the absence of a crystal structure and the paucity of structural and mechanistic information on the ENTs, which were only cloned and molecularly characterized less than a decade ago, mutagenesis analyses are necessitated to understand important transporters that

Section: 1.3. Nucleoside Transporters

are the mode of delivery for various anticancer, antiviral, and antiparasitic drugs. Members of the ENTs have a similar topology of eleven transmembrane domains, a large intracellular TM 6 – TM 7 loop, and a cytoplasmic amino terminus (88). Furthermore, multiple sequence alignments of the ENT family members revealed conserved residues that now serve as “signatures” for the family (87,90). Conservation of a residue within a family that has very low sequence identity (on average less than 30%) and high ligand disparity suggests that the residue has been evolutionarily favored for either structural integrity and/or the translocation mechanism (87,90). Two of these charged conserved residues are striking, Asp³⁸⁹ and Arg³⁹³ that are predicted at the cytoplasmic end of TM8 (Fig. 1-8). In a relative phenotypic propensity study done on mutations in 240 proteins that result in a disease, it was found that even though ionizable residues are often the least common species in transmembrane domains, these residues ostensibly play vital roles in transmembrane helices (127).

Site-directed mutagenesis at these residues revealed that Arg³⁹³ is critical for transporter expression and targeting (Chapter 2). However, the Asp³⁸⁹ is also critical for transporter function since even conservative mutations dramatically compromise transport capability without affecting protein expression and ligand affinity (Chapter 2). Subsequently, a second-site suppressor screen with a nonfunctional D389N mutant in yeast revealed that mutations at Asp³⁸⁹ impart a constraint on *Idnt2* that may be relaxed by an array of mutations mainly within

Chapter 1: INTRODUCTION

TMs 1 - 8 (Chapter 3). Further investigation suggested that Asn¹⁷⁵ at the cusp of TM 5 and the intracellular TM 4 - 5 loop is a critical second-site suppressor of D389N (Chapter 3). To investigate whether the second-site mutations would cluster on a three-dimensional model, a tertiary structure prediction by threading analyses, a method to identify protein templates that are similar at the secondary structure level, was undertaken. These studies have demonstrated that the ENT helix packing is similar to the MFS family, suggesting a conservation of structural similarity through evolution (Chapter 3). Furthermore, all the second-site mutations do, indeed, cluster on the model, and Asn¹⁷⁵ is proximal to Asp³⁸⁹ in the tertiary topology model (Chapter 3).

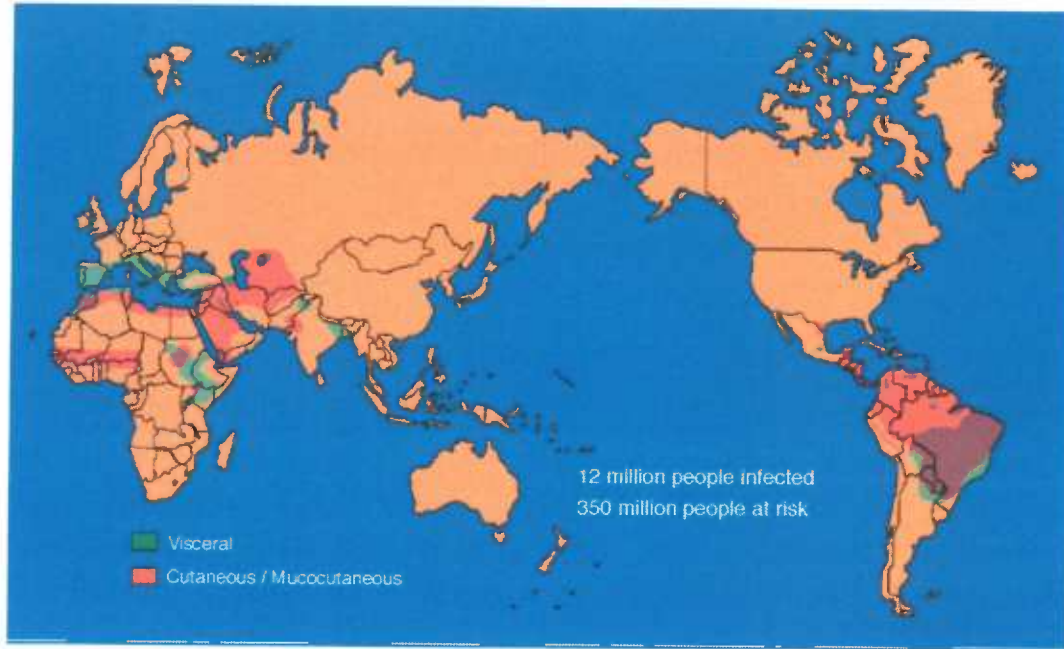
1.4. Figures

FIG. 1.1. Leishmaniasis distribution and pathology (128).

Panel A, Leishmaniasis is predominant in tropical countries. Panel B, Pathology of visceral leishmaniasis is enlargement of the spleen and liver. Panel C, Pathology of cutaneous leishmaniasis is lesion formation.

Chapter 1: INTRODUCTION

A



B



C

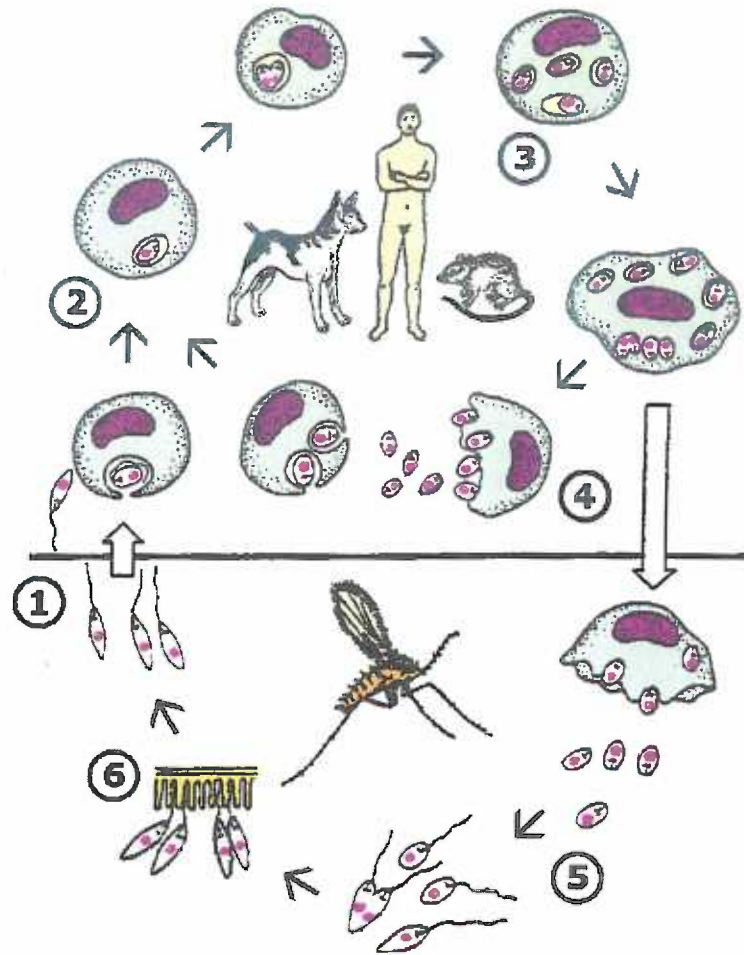


FIG. 1.2. Leishmania life-cycle and Promastigote Cell Biology (128).

Panel A, Life-Cycle. 1. sandfly bite introduces promastigotes into human host. 2. promastigotes transform into amastigotes and settle into the phagolysosome or PV. 3. amastigotes multiply. 4. lysogeny occurs when the amastigotes are released. 5. sandfly takes a blood meal and becomes infected where amastigotes transform to promastigotes. 6. promastigotes reside within the gut by attaching to the microvilli via their flagella. Panel B, Promastigote cell biology. The unique organelles of *Leishmania* are the glycosome, kinetoplast, flagellum, and the flagellar pocket.

Chapter 1: INTRODUCTION

A



B

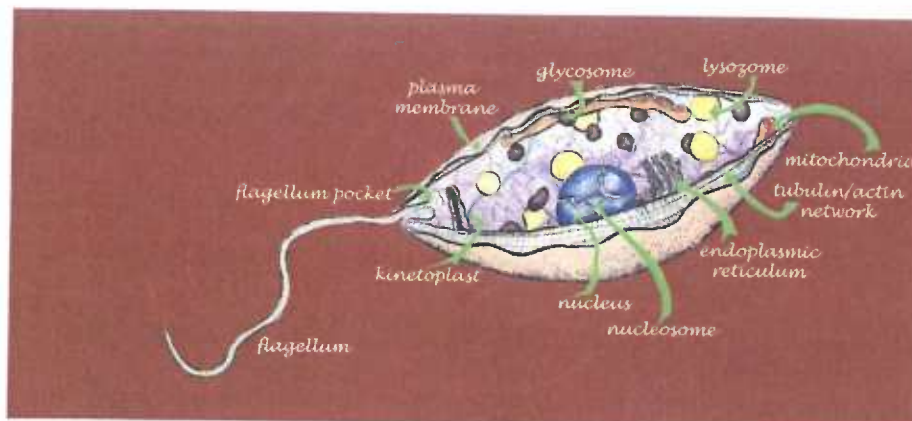
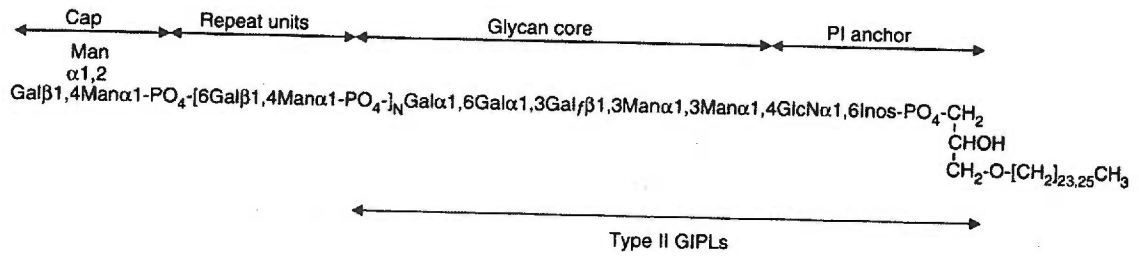


FIG. 1.3. Structures of Leishmania surface glycoconjugates (48).

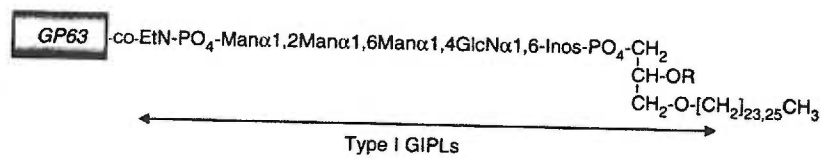
Panel A, LPG (lipophosphoglycan), the predominant glycoconjugate of promastigotes, consists of a Gal-Man-PO₄ repeat unit backbone attached to a lipid anchor via a glycan core. The structure of *L. donovani* promastigote LPG is shown. Type II GIPLs share the LPG anchor and glycan core structure. Panel B, Structure of GP63/glycoprotein anchors, also shared by Type I GIPLs. Panel C, Structure of hybrid GIPLs. 'R' represents an ester-linked fatty acid.

Chapter 1: INTRODUCTION

A. LPG and Type II GIPLs



B. Protein anchors and Type I GIPLs



C. Hybrid GIPLs

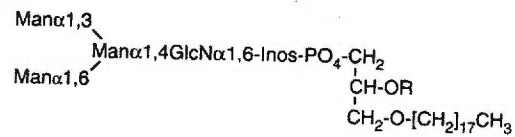


FIG. 1.4. Chemical structures of chemotherapy agents for leishmaniasis (62).

Panels A, B, and C are the present therapies employed. Panels D, E, and F are the therapies under development.

Chapter 1: INTRODUCTION

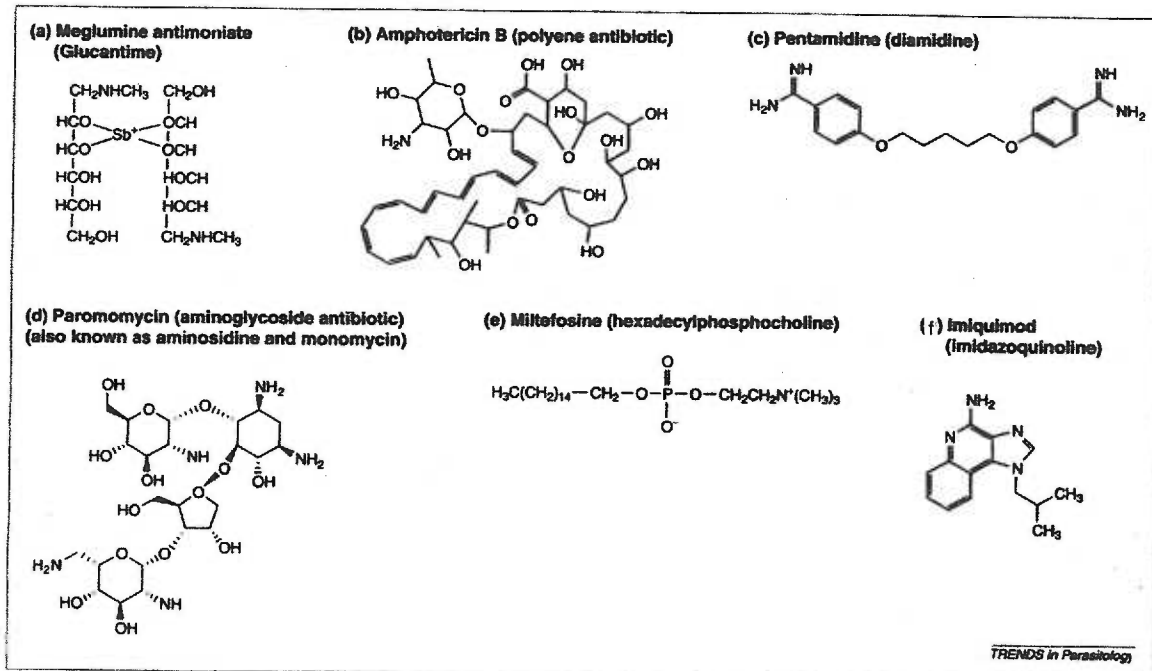


FIG. 1.5. Leishmania purine salvage pathway (129).

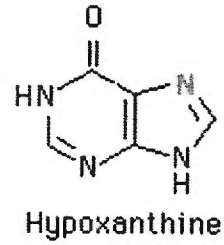
PRPP denotes the phosphoribosyl moiety that is appended onto the nucleobase by the the phosphoribosyltransferases (PRT) to generate nucleotides.

HGPRT, denotes hypoxanthine-guanine phosphoribosyltransferase; XPRT denotes xanthine phosphoribosyltransferase; and APRT denotes adenosine phosphoribosyltransferase. The products of the PRT reactions are XMP, IMP, GMP, AMP, which are xanthine, inosine, guanosine, and adenosine mono phosphates respectively.

Chapter 1: INTRODUCTION



A



B

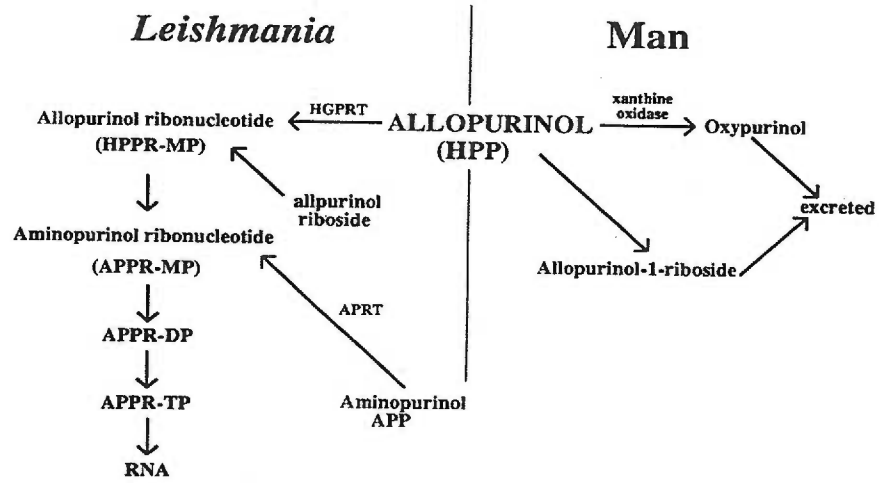
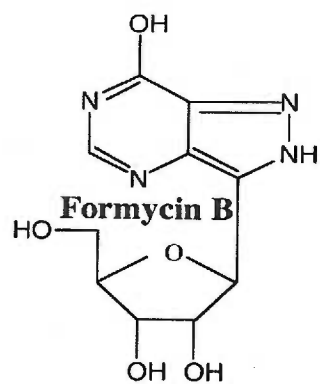


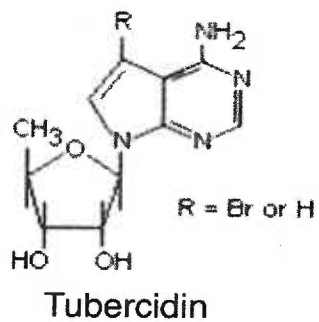
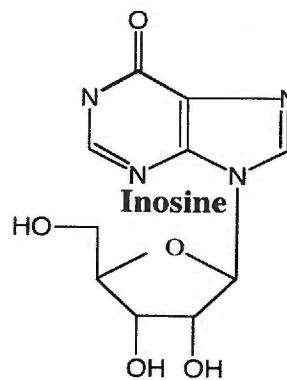
FIG. 1.7. Chemical structures of purines (128).

Panel A, Inosine and its toxic analog formycin B. Panel B, Adenosine and its toxic analog tubercidin. Panel C, a generic purine structure with all the positions numbered.

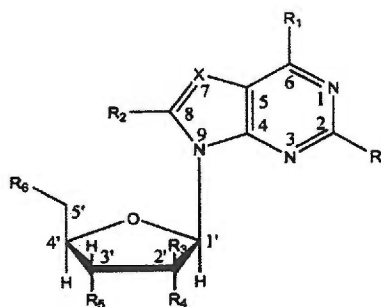
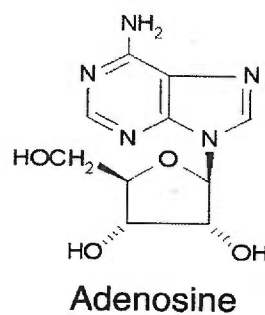
Chapter 1: INTRODUCTION



A



B



C

FIG. 1.8. Predicted topology and conserved residues (labeled) of the equilibrative nucleoside transporter (ENT) family (78).

Chapter 1: INTRODUCTION

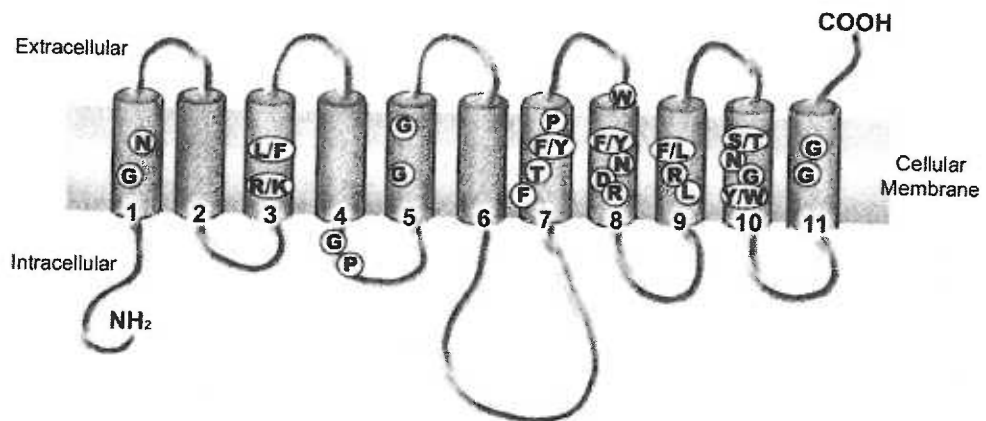


FIG 1.9. Substrate and inhibitor specificity of hENT1 and hENT2 (84).

Chapter 1: INTRODUCTION

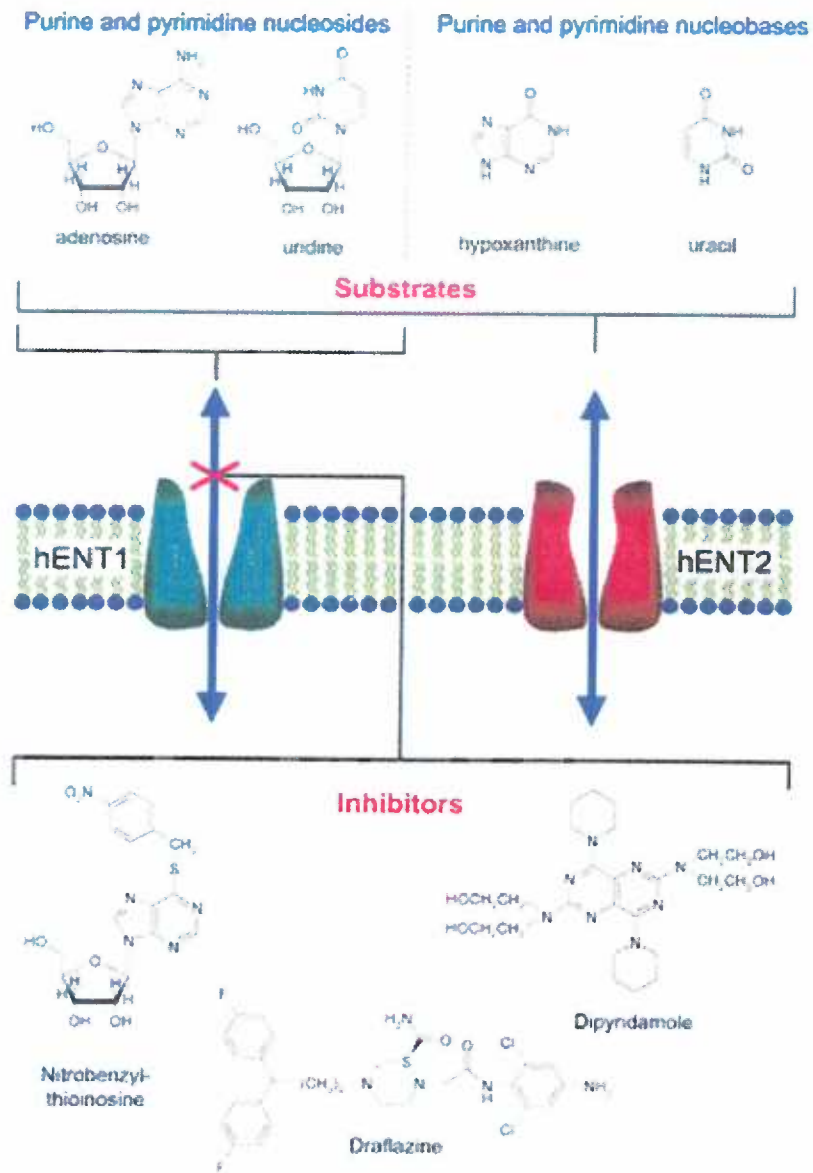


FIG. 1.10. Schematic of the main findings of the structure function of the ENTs (129).

Royal blue outline, highlights the evolutionarily conserved regions. *Pink*, TMs required for nucleobase transport. *Cyan and Pink*, TMs required for NMBPR binding. *Cyan, Pink, and Yellow*, TMs required for 3'-deoxyribose nucleoside analog transport. Met³³ in TM1, Leu⁹² in TM2, Gly¹⁵⁴ in TM4 of hENT1 and Gly¹⁸³ in TM5 of LdNT1 have been implicated in ligand selectivity and binding. Cys³³⁷ in TM7 of LdNT1 has been implicated in the translocation mechanism.

Chapter 1: INTRODUCTION



1.5. References

1. <http://www.who.int/tdr/diseases/leish/default.htm>.
2. <http://www.microbiology.wustl.edu/training/med/micpath99/11beverley>.
3. http://www.cdc.gov/ncidod/dpd/parasites/leishmania/factsheet_leishmania.htm.
4. Cunningham, A. (2002) *Experimental and Molecular Pathology* **72**, 132-141
5. Alvar, J., Canavate, C., Gutierrez-Solar, B., Jimenez, M., Laguna, F., Lopez-Velez, R., Molina, R., and Moreno, J. (1997) *Clin Microbiol Rev* **10**, 298-319
6. <http://www.1shtm.ac.uk/library/archives/leishman.html>.
7. http://www.4reference.net/encyclopedias/wikipedia/William_Boog_Leishman.html.

Chapter 1: INTRODUCTION

8. Bogtish, B. J. a. C., T.C. (1998) *Human Parasitology*, Second Ed., Academic Press, San Diego, CA
9. Berman, J. D. (1997) *Clin Infect Dis* **24**, 684-703
10. Jeronimo, S. M., and Pearson, R. D. (1992) *Subcell Biochem* **18**, 1-37
11. McFadden, G. I. (2003) in *Molecular Medical Parasitology* (Marr, J. J., Nilsen, T.W. and Komuniecki, R.W., ed), Academic Press, San Diego, CA
12. Alfonzo, J. D., Thiemann, O., and Simpson, L. (1997) *Nucleic Acids Res* **25**, 3751-3759
13. Fernandes, A. P., Nelson, K., and Beverley, S. M. (1993) *Proc Natl Acad Sci U S A* **90**, 11608-11612
14. Donelson, J. E., Gardner, M. J., and El-Sayed, N. M. (1999) *Proc Natl Acad Sci U S A* **96**, 2579-2581
15. Weise, F., Stierhof, Y. D., Kuhn, C., Wiese, M., and Overath, P. (2000) *J Cell Sci* **113 Pt 24**, 4587-4603

Section: 1.5. References

16. Gull, K. (1999) *Annu Rev Microbiol* **53**, 629-655
17. Snapp, E. L., and Landfear, S. M. (1997) *J Cell Biol* **139**, 1775-1783
18. Overath, P., Stierhof, Y-D. & Wiese, M. (1997) *Trends Cell Biol* **7**, 27-33
19. Doyle, P. S., Engel, J. C., Pimenta, P. F., da Silva, P. P., and Dwyer, D. M. (1991) *Exp Parasitol* **73**, 326-334
20. Ghedin, E., Debrabant, A., Engel, J. C., and Dwyer, D. M. (2001) *Traffic* **2**, 175-188
21. Mullin, K. A., Foth, B. J., Ilgoutz, S. C., Callaghan, J. M., Zawadzki, J. L., McFadden, G. I., and McConville, M. J. (2001) *Mol Biol Cell* **12**, 2364-2377
22. Pimenta, P. F., Saraiva, E. M., and Sacks, D. L. (1991) *Exp Parasitol* **72**, 191-204
23. Coombs, G. H., Tetley, L., Moss, V. A., and Vickerman, K. (1986) *Parasitology* **92 (Pt 1)**, 13-23

Chapter 1: INTRODUCTION

24. Ueda-Nakamura, T., Attias, M., and de Souza, W. (2001) *Parasitol Res* **87**, 89-97
25. <http://martin.parasitology.mcgill.ca/jimspage/biol/leish.htm>.
26. Zilberstein, D., and Shapira, M. (1994) *Annu Rev Microbiol* **48**, 449-470
27. Bates, P. A. (1994) *Exp Parasitol* **79**, 215-218
28. McConville, M. J., Turco, S. J., Ferguson, M. A., and Sacks, D. L. (1992) *Embo J* **11**, 3593-3600
29. Descoteaux, A., and Turco, S. J. (1999) *Biochim Biophys Acta* **1455**, 341-352
30. Alexander, J., Satoskar, A. R., and Russell, D. G. (1999) *J Cell Sci* **112 Pt 18**, 2993-3002
31. Pimenta, P. F., Turco, S. J., McConville, M. J., Lawyer, P. G., Perkins, P. V., and Sacks, D. L. (1992) *Science* **256**, 1812-1815

Section: 1.5. References

32. Butcher, B. A., Turco, S. J., Hilty, B. A., Pimenta, P. F., Panunzio, M., and Sacks, D. L. (1996) *J Biol Chem* **271**, 20573-20579
33. Wallbanks, K. R., Ingram, G. A., and Molyneux, D. H. (1986) *Trop Med Parasitol* **37**, 409-413
34. Pimenta, P. F., Saraiva, E. M., Rowton, E., Modi, G. B., Garraway, L. A., Beverley, S. M., Turco, S. J., and Sacks, D. L. (1994) *Proc Natl Acad Sci U S A* **91**, 9155-9156
35. Turco, S. J. (2003) in *Molecular Medical Parasitology* (Marr, J. J., Nilsen, T.W. and Komuniecki, R.W., ed), Academic Press, San Diego, CA
36. Herwaldt, B. L. (1999) *Lancet* **354**, 1191-1199
37. Desjeux, P. (1996) *Clin Dermatol* **14**, 417-423
38. Shaw, J. J. (1994) *Mem Inst Oswaldo Cruz* **89**, 471-478
39. Ashford, R. W. (1997) *Ann Trop Med Parasitol* **91**, 693-701

Chapter 1: INTRODUCTION

40. Davies, C. R., Cooper, A. M., Peacock, C., Lane, R. P., and Blackwell, J. M. (1990) *Parasitology* **101 Pt 3**, 337-343
41. Zambrano-Villa, S., Rosales-Borjas, D., Carrero, J. C., and Ortiz-Ortiz, L. (2002) *Trends Parasitol* **18**, 272-278
42. Alexander, J., and Russell, D. G. (1992) *Adv Parasitol* **31**, 175-254
43. Mael, J. (1990) *J Leukoc Biol* **47**, 187-193
44. Brittingham, A., Morrison, C. J., McMaster, W. R., McGwire, B. S., Chang, K. P., and Mosser, D. M. (1995) *J Immunol* **155**, 3102-3111
45. Locksley, R. M., Reiner, S. L., Hatam, F., Littman, D. R., and Killeen, N. (1993) *Science* **261**, 1448-1451
46. Kane, M. M., and Mosser, D. M. (2000) *Curr Opin Hematol* **7**, 26-31
47. Proudfoot, L., Nikolaev, A. V., Feng, G. J., Wei, W. Q., Ferguson, M. A., Brimacombe, J. S., and Liew, F. Y. (1996) *Proc Natl Acad Sci U S A* **93**, 10984-10989

Section: 1.5. References

48. Turco, S. J. (1992) *The lipophosphoglycan of Leishmania*. Subcellular Biochemistry, Intracellular Parasites (Avila, J. L. H., J.R., Ed.), 18, Plenum, NY
49. Olivier, M., Baimbridge, K. G., and Reiner, N. E. (1992) *J Immunol* **148**, 1188-1196
50. Gorak, P. M., Engwerda, C. R., and Kaye, P. M. (1998) *Eur J Immunol* **28**, 687-695
51. Descoteaux, A., Turco, S. J., Sacks, D. L., and Matlashewski, G. (1991) *J Immunol* **146**, 2747-2753
52. Giorgione, J. R., Turco, S. J., and Epand, R. M. (1996) *Proc Natl Acad Sci U S A* **93**, 11634-11639
53. Antoine, J. C., Prina, E., Lang, T., and Courret, N. (1998) *Trends Microbiol* **6**, 392-401
54. Desjardins, M., and Descoteaux, A. (1997) *J Exp Med* **185**, 2061-2068

Chapter 1: INTRODUCTION

55. Phillips, C. L., Ullman, B., Brennan, R. G., and Hill, C. P. (1999) *Embo J* **18**, 3533-3545
56. Vieira, L., Slotki, I., and Cabantchik, Z. I. (1995) *J Biol Chem* **270**, 5299-5304
57. Ilgoutz, S. C., Mullin, K. A., Southwell, B. R., and McConville, M. J. (1999) *Embo J* **18**, 3643-3654
58. Peters, C., Aebischer, T., Stierhof, Y. D., Fuchs, M., and Overath, P. (1995) *J Cell Sci* **108 (Pt 12)**, 3715-3724
59. Reiner, N. E., Ng, W., and McMaster, W. R. (1987) *J Immunol* **138**, 1926-1932
60. McNeely, T. B., Rosen, G., Londner, M. V., and Turco, S. J. (1989) *Biochem J* **259**, 601-604
61. Ouellette, M. a. W., S.A. (2003) in *Molecular Medical Parasitology* (Marr, J. J., Nilsen, T.W. and Komuniecki, R.W., ed), Academic Press, San Diego, CA

Section: 1.5. References

62. Croft, S. L., and Coombs, G. H. (2003) *Trends Parasitol* **19**, 502-508
63. Pearson, R. D., Hewlett, E.L., Petri, Jr., W.A. (2003) in *Molecular Medical Parasitology* (Marr, J. J., Nilsen, T.W. and Komuniecki, R.W., ed), Academic Press, San Diego, CA
64. Guerin, P. J., Olliaro, P., Sundar, S., Boelaert, M., Croft, S. L., Desjeux, P., Wasunna, M. K., and Bryceson, A. D. (2002) *Lancet Infect Dis* **2**, 494-501
65. Murray, H. W., Oca, M. J., Granger, A. M., and Schreiber, R. D. (1989) *J Clin Invest* **83**, 1253-1257
66. Bodhe, P. V., Kotwani, R. N., Kirodian, B. G., Pathare, A. V., Pandey, A. K., Thakur, C. P., and Kshirsagar, N. A. (1999) *Trans R Soc Trop Med Hyg* **93**, 314-318
67. Petit, C., Yardley, V., Gaboriau, F., Bolard, J., and Croft, S. L. (1999) *Antimicrob Agents Chemother* **43**, 390-392
68. Modabber, F. (1995) *Ann Trop Med Parasitol* **89 Suppl 1**, 83-88

Chapter 1: INTRODUCTION

69. Sundar, S., Jha, T. K., Thakur, C. P., Engel, J., Sindermann, H., Fischer, C., Junge, K., Bryceson, A., and Berman, J. (2002) *N Engl J Med* **347**, 1739-1746
70. http://www.cellml.org/examples/repository/bakker_model_2000_doc.html.
71. Clayton, C., Hausler, T., and Blattner, J. (1995) *Microbiol Rev* **59**, 325-344
72. Shih, S., Hwang, H. Y., Carter, D., Stenberg, P., and Ullman, B. (1998) *J Biol Chem* **273**, 1534-1541
73. Zarella-Boitz, J. M., Rager, N., Jardim, A., and Ullman, B. (2004) *Mol Biochem Parasitol* **134**, 43-51
74. Berens, R. L., Krug, E.C. & Marr, J.J. (1995) in *Biochemistry and Molecular Biology of Parasites* (Marr, J. J. M., M., ed), Academic Press, New York
75. Becker, M. A. R., B.J. (1995) in *Metabolic and Molecular Bases of Inherited Disease* (Scriver, C. R., Beaudet, A.L., Sly, W.S. & Valle, S., ed), McGraw-Hill, New York

Section: 1.5. References

76. Marr, J. J. B., R.L. (1985) in *Leishmania in Human Parasitic Diseases* (Chang, K. P. B., R.S., ed) Vol. 1, Elsevier, Amsterdam
77. Gottlieb, M. (1985) *Science* **227**, 72-74
78. Carter, N. S., Rager, N. & Ullman, B. (2003) in *Molecular Medical Parasitology* (Marr, J. J., Nilsen, T.W. and Komuniecki, R.W., ed), Academic Press, San Diego, CA
79. Spector, T., Jones, T. E., and Elion, G. B. (1979) *J Biol Chem* **254**, 8422-8426
80. Koutinas, A. F., Saridomichelakis, M. N., Mylonakis, M. E., Leontides, L., Polizopoulou, Z., Billinis, C., Argyriadis, D., Diakou, N., and Papadopoulos, O. (2001) *Vet Parasitol* **98**, 247-261
81. Vasudevan, G., Ullman, B., and Landfear, S. M. (2001) *Proc Natl Acad Sci U S A* **98**, 6092-6097
82. Doyle, D. A. (2004) *Eur Biophys J*

Chapter 1: INTRODUCTION

83. Abramson, J., Smirnova, I., Kasho, V., Verner, G., Kaback, H. R., and Iwata, S. (2003) *Science* **301**, 610-615
84. Baldwin, S. A., Beal, P. R., Yao, S. Y., King, A. E., Cass, C. E., and Young, J. D. (2004) *Pflugers Arch* **447**, 735-743
85. Cass, C. E., Young, J. D., and Baldwin, S. A. (1998) *Biochem Cell Biol* **76**, 761-770
86. Lostao, M. P., Mata, J. F., Larrayoz, I. M., Inzillo, S. M., Casado, F. J., and Pastor-Anglada, M. (2000) *FEBS Lett* **481**, 137-140
87. Acimovic, Y., and Coe, I. R. (2002) *Mol Biol Evol* **19**, 2199-2210
88. Sundaram, M., Yao, S. Y., Ingram, J. C., Berry, Z. A., Abidi, F., Cass, C. E., Baldwin, S. A., and Young, J. D. (2001) *J Biol Chem* **276**, 45270-45275
89. Griffiths, M., Beaumont, N., Yao, S. Y., Sundaram, M., Boumah, C. E., Davies, A., Kwong, F. Y., Coe, I., Cass, C. E., Young, J. D., and Baldwin, S. A. (1997) *Nat Med* **3**, 89-93

Section: 1.5. References

90. Carter, N. S., Landfear, S. M., and Ullman, B. (2001) *Trends Parasitol* **17**, 142-145
91. Baldwin, S. A., Mackey, J. R., Cass, C. E., and Young, J. D. (1999) *Mol Med Today* **5**, 216-224
92. Boleti, H., Coe, I. R., Baldwin, S. A., Young, J. D., and Cass, C. E. (1997) *Neuropharmacology* **36**, 1167-1179
93. Cass, C. E., Young, J.D., Baldwin, S.A., Cabrita, M.A., Graham, K.A., Griffiths, M., Jennings, L.L., Mackey, J.R., Ng, A.M., Ritzel, M.W., Vickers, M.F., and Yao, S.Y. (1999) in *Membrane Transporters as Drug Targets* (Amidon, G. L. S., W., ed) Vol. 12, Kluwer Academic/Plenum Publishers, New York
94. Belt, J. A., Marina, N. M., Phelps, D. A., and Crawford, C. R. (1993) *Adv Enzyme Regul* **33**, 235-252
95. Cass, C. E. (1995) in *Drug Transport in antimicrobial and anticancer therapy* (Georgopapadakou, N. H., ed), Marcel Dekker, New York

Chapter 1: INTRODUCTION

96. Griffith, D. A., and Jarvis, S. M. (1996) *Biochim Biophys Acta* **1286**, 153-181
97. Oliver, J. M., and Paterson, A. R. (1971) *Can J Biochem* **49**, 262-270
98. Hyde, R. J., Cass, C. E., Young, J. D., and Baldwin, S. A. (2001) *Mol Membr Biol* **18**, 53-63
99. Cabrita, M. A., Baldwin, S. A., Young, J. D., and Cass, C. E. (2002) *Biochem Cell Biol* **80**, 623-638
100. Sandoval, I. V., Martinez-Arca, S., Valdueza, J., Palacios, S., and Holman, G. D. (2000) *J Biol Chem* **275**, 39874-39885
101. Vasudevan, G., Carter, N. S., Drew, M. E., Beverley, S. M., Sanchez, M. A., Seyfang, A., Ullman, B., and Landfear, S. M. (1998) *Proc Natl Acad Sci U S A* **95**, 9873-9878
102. Carter, N. S., Drew, M. E., Sanchez, M., Vasudevan, G., Landfear, S. M., and Ullman, B. (2000) *J Biol Chem* **275**, 20935-20941

Section: 1.5. References

103. Sanchez, M. A., Tryon, R., Pierce, S., Vasudevan, G., and Landfear, S. M. (2004) *Mol Membr Biol* **21**, 11-18
104. Al-Salabi, M. I., Wallace, L. J., and De Koning, H. P. (2003) *Mol Pharmacol* **63**, 814-820
105. Parker, M. D., Hyde, R. J., Yao, S. Y., McRobert, L., Cass, C. E., Young, J. D., McConkey, G. A., and Baldwin, S. A. (2000) *Biochem J* **349**, 67-75
106. Landfear, S. M. (2001) *Biochem Pharmacol* **62**, 149-155
107. Stein, A., Vasudevan, G., Carter, N. S., Ullman, B., Landfear, S. M., and Kavanaugh, M. P. (2003) *J Biol Chem* **278**, 35127-35134
108. Yao, S. Y., Ng, A. M., Muzyka, W. R., Griffiths, M., Cass, C. E., Baldwin, S. A., and Young, J. D. (1997) *J Biol Chem* **272**, 28423-28430
109. Sundaram, M., Yao, S. Y., Ng, A. M., Griffiths, M., Cass, C. E., Baldwin, S. A., and Young, J. D. (1998) *J Biol Chem* **273**, 21519-21525

Chapter 1: INTRODUCTION

110. Sundaram, M., Yao, S. Y., Ng, A. M., Cass, C. E., Baldwin, S. A., and Young, J. D. (2001) *Biochemistry* **40**, 8146-8151
111. Yao, S. Y., Ng, A. M., Vickers, M. F., Sundaram, M., Cass, C. E., Baldwin, S. A., and Young, J. D. (2002) *J Biol Chem* **277**, 24938-24948
112. SenGupta, D. J., and Unadkat, J. D. (2004) *Biochem Pharmacol* **67**, 453-458
113. Yao, S. Y., Sundaram, M., Chomey, E. G., Cass, C. E., Baldwin, S. A., and Young, J. D. (2001) *Biochem J* **353**, 387-393
114. SenGupta, D. J., Lum, P. Y., Lai, Y., Shubochkina, E., Bakken, A. H., Schneider, G., and Unadkat, J. D. (2002) *Biochemistry* **41**, 1512-1519
115. Vasudevan, G. (2001) in *Biochemistry and Molecular Biology*, Oregon Health and Science University, Portland
116. Valdes, R., Vasudevan, G., Conklin, D., Landfear, S.M. (2004) *Biochemistry* manuscript in press.

Section: 1.5. References

117. Yao, S. Y., Ng, A. M., Sundaram, M., Cass, C. E., Baldwin, S. A., and Young, J. D. (2001) *Mol Membr Biol* **18**, 161-167
118. Visser, F., Vickers, M. F., Ng, A. M., Baldwin, S. A., Young, J. D., and Cass, C. E. (2002) *J Biol Chem* **277**, 395-401
119. Endres, C. J., SenGupta, D. J., and Unadkat, J. D. (2004) *Biochem J*
120. Chang, C., Swaan, P. W., Ngo, L. Y., Lum, P. Y., Patil, S. D., and Unadkat, J. D. (2004) *Mol Pharmacol* **65**, 558-570
121. Gibas, C. J., P. (2001) *Developing Bioinformatics Computer Skills*, First Ed. (LeJeune, L., Ed.), O'Reilly & Associates, Inc., Sebastopol, CA
122. Kim, Y., Ramirez-Montealegre, D., and Pearce, D. A. (2003) *Proc Natl Acad Sci U S A* **100**, 15458-15462
123. Mao, Q., Foster, B. J., Xia, H., and Davidson, B. L. (2003) *FEBS Lett* **541**, 40-46
124. Vesa, J., and Peltonen, L. (2002) *Curr Mol Med* **2**, 439-444

Chapter 1: INTRODUCTION

125. Palczewski, K., Kumasaka, T., Hori, T., Behnke, C. A., Motoshima, H., Fox, B. A., Le Trong, I., Teller, D. C., Okada, T., Stenkamp, R. E., Yamamoto, M., and Miyano, M. (2000) *Science* **289**, 739-745
126. Kaback, H. R., Sahin-Toth, M., and Weinglass, A. B. (2001) *Nat Rev Mol Cell Biol* **2**, 610-620
127. Partridge, A. W., Therien, A. G., and Deber, C. M. (2004) *Proteins* **54**, 648-656
128. <http://www.google.com/Images>
129. Rager, N. (2002), Portland, OR, Original Art work
130. Meshnick, S. R. M., J.J. (1982) in *Subcellular Biochemistry* (Avila, J. L. H., J.R., ed), pp. 401-441, Plenum, New York

Chapter 2

MANUSCRIPT 1

Functional Analysis of an Inosine-Guanosine Transporter from *Leishmania donovani*: The Role of Conserved Residues, Aspartate 389 and Arginine 393

Shirin Arastu-Kapur, Ethan Ford, Buddy Ullman, & Nicola S. Carter

From the Department of Biochemistry and Molecular Biology, Oregon Health & Science University, Portland, OR 97239

2.1 ABSTRACT

Equilibrative nucleoside transporters encompass two conserved, charged residues that occur within predicted transmembrane domain 8. To assess the role of these 'signature' residues in transporter function, the Asp³⁸⁹ and Arg³⁹³ residues within the LdNT2 nucleoside transporter from *Leishmania donovani* were mutated and the resultant phenotypes evaluated after transfection into *Δldnt2* parasites. Whereas an R393K mutant retained transporter activity similar to that of wild type LdNT2, the R393L, D389E, and D389N mutations resulted in dramatic losses of transport capability. Tagging the wild type and mutant *ldnt2* proteins with green fluorescent protein demonstrated that the D389N and D389E mutants targeted properly to the parasite cell surface and flagellum, whereas the expression of R393L at the cell surface was profoundly compromised.

To test whether Asp³⁸⁹ and Arg³⁹³ interact, a series of mutants was generated, D389R/R393, D389/R393D, and D389R/R393D, within the green fluorescent protein-tagged LdNT2 construct. Although all of these *ldnt2* mutants were transport deficient, D389R/R393D localized properly to the plasma membrane, while neither D389R/R393 nor D389/R393D could be detected. Moreover, a transport-incompetent D389N/R393N double *ldnt2* mutant also localized to the parasite membrane, whereas a D389L/R393L *ldnt2* mutant did not, suggesting that an interaction between residues 389 and 393 may be in-

volved in LdNT2 membrane targeting. These studies establish genetically that Asp³⁸⁹ is critical for optimal transporter function and that a positively charged or polar residue at Arg³⁹³ is essential for proper expression of LdNT2 at the plasma membrane.

2.2 INTRODUCTION

Leishmania donovani is the causative agent of visceral leishmaniasis, a disease that is invariably fatal if untreated. These protozoan parasites exhibit a digenetic lifecycle, existing as extracellular, flagellated promastigotes within the sandfly vector, and as intracellular amastigotes within the phagolysosome of macrophages and reticuloendothelial cells of the mammalian host. Since there is no immediate prospect of an antileishmanial vaccine, and current drug regimens are complicated by toxicity and curative failure, the need for new drugs to treat leishmaniasis is acute. Rational therapeutic approaches for antiparasitic drug development require the exploitation of fundamental biochemical differences between parasite and host. Perhaps the most striking metabolic discrepancy between parasites and their mammalian hosts is the disparate mechanisms by which they generate purine nucleotides. Whereas mammalian cells synthesize purine nucleotides from amino acids and 1-carbon compounds,

Chapter 2: MANUSCRIPT 1

all of the protozoan parasites studied to date are incapable of *de novo* synthesis of the purine ring (1). Thus, purine acquisition from the host is an indispensable nutritional function for which each genus of protozoan parasite has evolved a unique complement of purine salvage enzymes. The initial step in purine salvage involves the translocation of host purines across the parasite surface membranes, a process that is mediated by nucleoside and nucleobase transporters.

Nucleoside permeation into *L. donovani* is mediated by two high affinity transporters with non-overlapping ligand specificity, LdNT1 and LdNT2. LdNT1 transports adenosine and pyrimidine nucleosides, whereas LdNT2 is selective for inosine and guanosine (2,3). Mutants genetically deficient in either LdNT1 or LdNT2 activity have been created by negative selection, and the genes coding for these permeases were subsequently cloned from a cosmid library by functional rescue of nucleoside transport-deficient *Leishmania* (2,3). Based on their primary structures and predicted membrane topologies, LdNT1 and LdNT2 belong to the equilibrative nucleoside transporter (ENT) family first described in mammals (4).

Numerous putative members of the ENT family have subsequently been characterized (5) or unveiled within available genome databases (6). However, the elucidation of the functional determinants within the ENT family that govern ligand translocation and specificity are still largely unknown. Glycine

residues within transmembrane region 5 of hENT1 and LdNT1 have emerged as important determinants of uridine transport (7). However, by far the majority of analyses focused on the interactions between mammalian ENTs and their specific inhibitors, and thus, do not easily extrapolate to other members of the ENT family. These studies support a role for transmembrane (TM) domains 3-6 within hENT1 in the binding of the potent inhibitor 4-nitrobenzylthioinosine (8), while Met³³ within TM1 of hENT1 has emerged as a determinant of dipyridamole and dilazep sensitivity (9). The elucidation of functional determinants for ENT-mediated transport is hindered by the overall diversity that members of the ENT family exhibit for ligand selectivity and affinity (5). Although ENT members exhibit strikingly low amino acid sequence identities (5), multiple sequence alignments of ENT family members from both parasite and mammalian cells reveal a number of conserved or "signature" residues predominantly located in predicted TM spanning regions (5,6). The most striking of these residues are Asp and Arg, two charged residues that reside in predicted TM8 (see Fig. 2-1). The preservation of these residues and their topological prediction implies a role in the translocation mechanism. Using the LdNT2 inosine-guanosine transporter as a paradigm for all ENT family members, we describe studies on the role of these two conserved charged residues within LdNT2, Asp³⁸⁹ and Arg³⁹³. These investigations demonstrate that Asp³⁸⁹ is critical in the translocation mechanism and imply a structural role for both Asp³⁸⁹ and Arg³⁹³.

2.3 EXPERIMENTAL PROCEDURES

Cell Culture - *L. donovani* was cultured at 26 °C in DME-L medium (Invitrogen Life Technologies, Carlsbad, CA) as described (10). The construction and phenotypic characterization of the null mutant Δ *ldnt2* in which both wild type *LdNT2* copies have been eliminated by targeted gene replacement and loss-of-heterozygosity will be described elsewhere. The Δ *ldnt2* strain was cultured continuously in 50 µg/ml hygromycin (Roche Pharmaceuticals, Nutley, NJ) for which the selective marker, hygromycin phosphotransferase, used in the gene replacement strategy confers resistance. Cell lines generated by transfection of Δ *ldnt2* with plasmids pALTNEO (11) and pXG-GFP+2' (12) were selected and maintained in 25 µg/ml G418 (BioWhittaker, Inc., Walkersville, MD), as well as 50 µg/ml hygromycin.

Generation and Expression of Site-directed Mutants - Mutations in *LdNT2* were generated by the QuikChange® site-directed mutagenesis protocol, a polymerase chain reaction-based mutagenesis strategy (Stratagene, La Jolla, CA). Mutations were inserted within the *LdNT2* open reading frame that had been ligated into the pALTNEO leishmanial expression plasmid (11). Mutations were confirmed by sequencing and the mutant constructs transfected into the

Section: 2.3 EXPERIMENTAL PROCEDURES

Δdnt2 cell line using standard electroporation conditions (13). *Δdnt2* cells were also transfected with pALTNEO-*LdNT2* (wild type *LdNT2*). The wild type *LdNT2* open reading frame was subsequently cloned into the *Bam*HI site of pXG-GFP+2' (12), a leishmanial expression plasmid that tags proteins at the NH₂-terminus with the green fluorescent protein (GFP) and the mutants recreated using the QuikChange® method with the same mutagenic primers as above. All strains transfected with pXG-GFP+2' constructs were obtained by standard electroporation protocols as for the pALTNEO transfectants.

Formycin B Growth Curves - The *Δdnt2* parental knockout and its transfectants were tested for their sensitivity to formycin B (FoB) (Sigma Chemical Co., St. Louis, MO), an inosine isomer that is a potent inhibitor of *L. donovani* growth (14). Parasites were incubated with various concentrations of FoB and enumerated after ~6 days on a Coulter Counter Model ZM. The EC₅₀ value reported is the effective concentration of FoB that inhibits growth by 50%.

Transport Assays - Nucleoside transport measurements were performed by a previously described oil-stop method (15). Briefly, 10⁸ density of cells are incubated in radiolabeled ligand and then pelleted through a dibutylphthalate (Sigma) oil layer at the desired time point. Time courses were generated at 10 μM [³H]inosine (0.38 Ci/mmol) and 10 μM [³H]guanosine (0.06 Ci/mmol) and kinetic data obtained by measuring rates of inosine transport at concentrations between 0.3 nM and 10 μM. [³H]inosine (38.4 Ci/mmol) and [³H]guanosine (5.5

Chapter 2: MANUSCRIPT 1

Ci/mmol) were purchased from Moravek Biochemicals, Inc. (Brea, CA). Rates of uptake were calculated by linear regression analysis, and kinetic parameters were determined by the method of Hanes (16).

Integral Membrane Protein Preparations - Leishmania at a density of 1×10^7 parasites/ml were pelleted at 2000 X g, resuspended in 1.0 ml of double deionized water in which a Complete™ Mini, EDTA free protease inhibitor cocktail tablet (Roche Pharmaceuticals) had been dissolved, and lysed with one round of freezing at -70°C and thawing at room temperature (RT). The lysates were then sedimented in a microcentrifuge for 2 min at RT and the pellets resuspended on ice in 1.0 ml of 100 mM NaHCO₃, pH 11.0. After an additional 30 min of sedimentation in the microcentrifuge at 4°C , the pellet was resuspended in 2X Laemmli buffer (BioRad, Hercules, CA) supplemented with 8 M urea and stored at -20°C until further use.

Cell Surface Labeling - 1×10^8 cells were washed with phosphate buffered saline (PBS) and incubated on ice with 1 mg/ml EZ-Link Sulfo-NHS-LC-Biotin (Pierce Biotechnologies, Rockford, IL) in PBS for 2 h. The biotinylation reaction was quenched by washing the cells three times with 50 mM glycine made up in PBS. Cells were incubated on ice for 30 min in 100 μl of lysis buffer (50 mM Tris-HCl, pH 8.0, 100 mM NaCl, 1% NP40, and 10% glycerol). The cell lysate was pelleted in a microcentrifuge, after which the supernatant was removed to a new microcentrifuge tube and incubated for 1 h at RT with 20 μl of

Section: 2.3 EXPERIMENTAL PROCEDURES

packed streptavidin beads (Invitrogen Life Technologies) prewashed in lysis buffer. After the 1 h incubation the beads were washed two times with 1.0 ml of lysis buffer and resuspended in 20 μ l of 2X Laemmli buffer supplemented with 8 M urea. All samples were fractionated by SDS polyacrylamide gel electrophoresis on a 10 % slab gel using standard conditions (17) and biotinylated GFP-tagged LdNT2 protein detected by immunoblotting with a GFP monoclonal antibody (see below). To quantitate the amount of mutant and wild type GFP-tagged LdNT2 protein labeled at the cell surface, Western blot films were scanned using a Model GS-700 Imaging Densitometer (Bio-Rad, Hercules, CA) and the intensity of each band corresponding to GFP-tagged transporter assessed by the Molecular Analyst Software version 2.1.2 (Bio-Rad). Background signal was subtracted for each sample and the percentage of cell surface expression calculated for each mutant GFP-tagged transporter relative to wild type GFP-tagged LdNT2.

Immunoblotting - Protein samples were fractionated by SDS polyacrylamide gel electrophoresis on a 10 % slab gel using standard conditions (17). Immunoblotting was performed as described (18). A mouse GFP antibody (Living colors A.v. monoclonal JL-8, BD Biosciences, Palo Alto, CA) was used at a 1:1,000 dilution in PBS containing 0.01 % Tween 20 (Sigma Chemical Co.) and 5 % nonfat dry milk. Secondary antibody (goat anti-mouse conjugated to alkaline phosphatase, Jackson Immunoresearch, Westgrove, PA) was used at a 1:10,000

Chapter 2: MANUSCRIPT 1

dilution in PBS containing 0.01 % Tween 20 (Sigma Chemical Co.) and 5 % nonfat dry milk and signal detected by the CDP-Star chemiluminescence detection system (Roche Pharmaceuticals). A rabbit antibody to the *L. donovani* myo-inositol transporter (MIT) (19) was used at a 1:1,000 dilution in PBS containing 0.01 % Tween 20 (Sigma Chemical Co.) and 5 % nonfat dry milk as a control to normalize protein loading onto each lane of the slab gel. Goat anti-rabbit conjugated to horseradish peroxidase (Jackson Immunoresearch) was used at 1:10,000 to detect anti-*myo*-inositol transporter signal.

Fluorescence Microscopy – Lab-Tek® II Chambered Coverglass slides (Fisher Scientific, Pittsburgh, PA) were coated with a 1:10 dilution of poly-L-lysine (Sigma Chemical Co.) for 15 min. The chambers were rinsed with double deionized water to remove excess poly-L-lysine, allowed to dry for 1 h at 60 °C, and then cooled to RT. 1×10^7 *Leishmania* promastigotes were resuspended in 1.0 ml PBS, pipetted into the coverslip chamber, and allowed to attach for 15 min. Chambers were rinsed once with PBS and then overlaid with 500 μ l PBS. Images were acquired by Aurelie Snyder of the OHSU-MMI Research Core Facility at this institution (<http://www.ohsu.edu/core>) with the Applied Precision Deltavision® image restoration system. Deconvolution was performed using the iterative constrained algorithm of Sedat and Agard (20) and additional image processing performed on an SGI Octane workstation.

Section: 2.3 EXPERIMENTAL PROCEDURES

Immunofluorescence Microscopy (Live cells) – 1×10^7 Leishmania promastigotes were washed twice with 1.0 ml of PBS and resuspended in 30 μ l of immunofluorescence buffer (IFB) consisting of PBS, 1 % glucose, 10 % fetal calf serum. Cells were incubated on ice for 30 min with occasional mixing with either 50 μ l IFB containing mouse anti-GFP (Living colors A.v. monoclonal JL-8, BD Biosciences) diluted 1:100 or 50 μ l IFB containing rabbit anti-tubulin (ICN Pharmaceuticals, Inc. Costa Mesa, CA) diluted 1:10. Cells were washed twice with 1.0 ml of ice-cold IFB at 2000 X g and incubated on ice for 30 min with occasional mixing with either 30 μ l of goat anti-mouse or goat anti-rabbit conjugated to Rhodamine Red (ICN Pharmaceuticals, Inc.) and both diluted to 1:150 in IFB. Finally, cells were washed twice with 1.0 ml of ice-cold IFB at 2000 X g, resuspended in 250 μ l of ice-cold IFB, and then overlaid on Lab-Tek® II Chambered Coverglass slides (Fisher Scientific) coated with poly-L-lysine and processed for imaging as described in the previous section.

Immunofluorescence Microscopy (Permeabilized cells) – 1×10^7 Leishmania promastigotes were washed twice in 1.0 ml of PBS and resuspended in 500 μ l of fixative containing 4 % paraformaldehyde and 0.1 % glutaraldehyde made up in PBS. Cells in fixative were incubated for 30 min at RT after which time they were overlaid on Lab-Tek® II Chambered Coverglass slides (Fisher Scientific) coated with poly-L-lysine. Attached cells were washed twice with PBS containing 2% goat serum (PBS-gs) (Sigma Chemical Co.) and permeabilized

Chapter 2: MANUSCRIPT 1

with 500 μ l of PBS-gs containing 0.1% Triton-X-100 (Roche Pharmaceuticals) for 30 min at RT. At this time all subsequent steps were performed in the dark to prevent the bleaching of GFP within the permeabilized cells. Cells were incubated for 1 h at RT with either 250 μ l of mouse anti-GFP (Living colors A.v. monoclonal JL-8, BD Biosciences) diluted 1:100 in PBS-gs or 250 μ l of rabbit anti-tubulin (ICN Pharmaceuticals Inc.) diluted 1:10 in PBS-gs. Attached cells were washed twice with 1.0 ml of PBS-gs and then incubated at RT for 1 h with either 250 μ l of goat anti-mouse or goat anti-rabbit antibodies conjugated to Rhodamine Red (ICN Pharmaceuticals, Inc.) diluted 1:150 in PBS-gs. After this final incubation the cells were washed twice with 1.0 ml of PBS-gs and then overlaid with 500 μ l of PBS for imaging. The images were acquired as described previously above.

2.4 RESULTS

Creation and Growth Phenotype of Idnt2 Mutants - Multiple sequence alignments have revealed the presence of ~16 conserved amino acids residues among functionally characterized ENT family members from mammalian and parasitic organisms (5). Two of these, Asp³⁸⁹ and Arg³⁹³ in LdNT2, are charged, and according to the hidden Markov topological algorithm (21) are located within

Chapter 2: MANUSCRIPT 1

wild type transfectant. The only exception, Δ ldnt2[D389N], exhibited an EC₅₀ value of 5.7 μ M, a value close to that of the parental Δ ldnt2 line (Table I).

Transport Capabilities of the ldnt2 Mutants - The altered sensitivities of transfectant lines harboring Asp³⁸⁹ and Arg³⁹³ mutations toward FoB implied that LdNT2 transport capacity was impaired. To determine the effects of these mutations on transport directly, each of the transfectants was evaluated for [³H]inosine and [³H]guanosine uptake at a saturating ligand concentration for LdNT2 (10 μ M) (2). The ability of the transfectant cell lines to take up both 6-oxypurine nucleosides was directly proportional to the sensitivity of the strain to FoB (Fig. 2-2, Panels A and B). Whereas Δ ldnt2[R393K] cells incorporated both inosine and guanosine at a rate comparable to the wild type Δ ldnt2[LdNT2] transfectant, the capacities of the Δ ldnt2[D389E] and Δ ldnt2[R393L] lines to take up both ligands was less than 10% of the wild type transfectant (Fig. 2-2). The D389N mutation was even more incapacitating, since the Δ ldnt2[D389N] line, like the Δ ldnt2 knockout, exhibited no measurable [³H]inosine or [³H]guanosine uptake capability under these parameters. Because these radiolabel incorporation assays were carried out over a 4 min interval, uptake measurements were also performed over shorter intervals to assess impaired transport capabilities more accurately and to minimize metabolic contributions to the uptake measurements. The results of rapid transport assays (see Experimental Procedures), where the uptake of 10 μ M [³H]inosine or [³H]guanosine was measured over

intervals up to 10 s, correlated well with the results of the longer 4 min uptake assays (Fig. 2-2, Panels C and D).

To determine whether these transport-incapacitating mutations affected the affinity of the LdNT2 protein for ligand, transport assays were performed at varying [³H]inosine concentrations over time intervals where uptake was linear. K_m values of $0.4 \pm 0.19 \mu\text{M}$, $2.5 \pm 1.2 \mu\text{M}$, $1.8 \pm 1.1 \mu\text{M}$, and $2.0 \pm 1.6 \mu\text{M}$ were calculated by Hanes analysis for $\Delta ldnt2[LdNT2]$, $\Delta ldnt2[R393K]$, $\Delta ldnt2[R393L]$ and $\Delta ldnt2[D389E]$, respectively (data not shown). The lack of transport by $\Delta ldnt2[D389N]$ cells obviously precluded an accurate K_m determination.

Cell surface targeting of GFP-LdNT2 and GFP-ldnt2 - Since the ligand affinities of the mutant transporters were apparently not altered in comparison to the wild type transporter, to determine whether the impaired transport capacity of the *ldnt2* transfectants affected proper targeting or expression of the transporter both wild type and all of the mutant transporters were tagged with GFP at the NH_2 -terminus and the corresponding genes transfected into the $\Delta ldnt2$ background. The wild type transfectant, $\Delta ldnt2[\text{GFP-LdNT2}]$, exhibited an EC_{50} value of $7.9 \pm 0.8 \text{ nM}$ for FoB, a value virtually identical to that observed for $\Delta ldnt2[LdNT2]$ (Table I). Moreover, $\Delta ldnt2[\text{GFP-LdNT2}]$ parasites also displayed robust [³H]inosine uptake with a K_m value of $1.3 \pm 0.6 \mu\text{M}$ ($n=3$) (Fig. 2-3 and Table II), an inosine affinity slightly less than that observed with the

Chapter 2: MANUSCRIPT 1

Δldnt2[LdNT2] transfectant described above. Localization studies using direct GFP fluorescence and deconvolution microscopy demonstrated that GFP-LdNT2 was robustly synthesized and targeted to both the plasma membrane and flagellum (Fig. 2-4, Panel A). A diffuse and relatively weak cytosolic GFP fluorescence was observed with *Δldnt2* parasites transfected with the empty pXG-GFP+2' vector alone (Fig. 2-4, Panel B).

The transport capabilities of the GFP-tagged wild type and mutant transporters were similar to those observed for the untagged transporters. The *Δldnt2*[GFP-R393K], *Δldnt2*[GFP-R393L], and *Δldnt2*[GFP-D389E] lines transported [³H]inosine at 21%, 6%, and 6% of the rate of *Δldnt2*[GFP-LdNT2] parasites, respectively (values based upon the observed V_{\max} reported in Table II), whereas the *Δldnt2*[GFP-D389N] transfectant showed no [³H]inosine uptake capability (Table II). K_m values for [³H]inosine transport were equivalent among all the transport-competent transfectants (Fig. 2-3 and Table II). All of the mutant Ldnt2 transporters localized to the parasite plasma membrane, except GFP-R393L, which predominantly localized to the flagellar membrane (Fig. 4, Panels C-F). Additionally, a rod-like formation was observed in the *Δldnt2*[GFP-R393L] mutant (Fig. 2-4, Panel D). A similar structure, a novel multivesicular tubular compartment, was previously described in *Leishmania* parasites where the cell surface trafficking of membrane proteins was impaired (22,23).

Although GFP fluorescence data suggested that nearly all of the mutant transporters (with the exception of GFP-R393L) are produced and targeted to the cell surface, similar to GFP-LdNT2, the relative level of cell surface protein expression could not be assessed by this approach. Thus, to ascertain the amount of LdNT2 protein at the cell surface the GFP-tagged transporters were quantitated using a membrane-impermeable biotin probe (Fig. 2-5). Significant levels of LdNT2 were detected at the cell surface in all lines except $\Delta Idnt2$ [GFP-R393L] in which Idnt2 protein at the cell surface was ~7 % of the LdNT2 levels observed in the $\Delta Idnt2$ [GFP-LdNT2] line. As expected, no cell surface biotinylation was observed for $\Delta Idnt2$ [GFP] parasites which contained no GFP-tagged transporter (Fig. 2-5). The results of the biotinylation experiments were bolstered by parallel analyses of fractionated integral membrane proteins from each of the GFP transfectants probed with a GFP antibody (Fig. 2-5). These analyses confirmed the reduced level of Idnt2 expression in the $\Delta Idnt2$ [GFP-R393L] cells. Equal loading of the integral membrane fractions was verified by probing with an independent antibody to the leishmanial MIT (19).

The overall transport capacities of the mutant nucleoside transporters could, therefore, be readjusted based on the relative levels of LdNT2/Idnt2 at the cell surface in each of the transfectants (Table II). The adjusted specific activities of the Arg³⁹³ mutants, Idnt2-R393K and Idnt2-R393L, were, therefore, 36% and

Chapter 2: MANUSCRIPT 1

79% of that of LdNT2, whereas the two Asp³⁸⁹ mutants, Idnt2-D389E and Idnt2-D389N, were severely crippled in their permease function.

Mutational analysis of Asp³⁸⁹ and Arg³⁹³ interactions - The location and proximity of Asp³⁸⁹ and Arg³⁹³ within the predicted helical TM8 structure implies that these charged residues are likely situated on the same side of the helix and conceivably interact. Therefore, a series of mutants was generated in which either Asp³⁸⁹ or Arg³⁹³ were substituted for the opposite residue. Thus, D389R and R393D single mutations and a D389R/R393D double mutation were constructed within the pXG-GFP+2'-LdNT2 plasmid and each construct transfected into the Δ Idnt2 cell line. Growth curves in the presence of increasing concentrations of FoB revealed that Δ Idnt2 cells expressing each of these mutations were at least 3 orders of magnitude less sensitive to FoB compared to Δ Idnt2[GFP-LdNT2] parasites (Table I). Furthermore, inosine and guanosine transport measurements indicated that Δ Idnt2[GFP-D389R], Δ Idnt2[GFP-R393D], and Δ Idnt2[GFP-D389R/R393D] cells were all transport incompetent, equivalent to Δ Idnt2 cells producing GFP alone, whereas Δ Idnt2[GFP-LdNT2] cells expressing GFP-tagged LdNT2 exhibited robust transport capability of both 6-oxypurine nucleosides (Fig. 2-6, panel A). To assess whether the severely impaired transport capability of the mutants could be ascribed to transporter mislocalization, total integral membrane proteins from each of the transfectants were isolated and subjected to western blotting using a GFP monoclonal antibody for detection. As

revealed in Fig. 2-6B, *ldnt2* was found within the membrane fraction of $\Delta ldnt2$ [GFP-D389R/R393D] parasites but not in $\Delta ldnt2$ [GFP-D389R] or $\Delta ldnt2$ [GFP-R393D] cells. Direct fluorescence of GFP using deconvolution microscopy confirmed the plasma membrane localization of *ldnt2* in $\Delta ldnt2$ [GFP-D389R/R393D] cells, whereas minimal diffuse fluorescence was observed for the $\Delta ldnt2$ [GFP-D389R] and $\Delta ldnt2$ [GFP-R393D] transfectants (Fig. 2-6, panel C).

Subsequently, two additional double mutants were created in which both Asp³⁸⁹ and Arg³⁹³ were replaced with either a polar (Asn) or hydrophobic (Leu) residue within the pXG-GFP+2'-*LdNT2* vector. Only the $\Delta ldnt2$ [GFP-D389N/R393N] transfectant was expressed and localized to the parasite plasma membrane (Fig. 2-6, panels B and C), however, as expected, both the $\Delta ldnt2$ [GFP-D389N/R393N] and $\Delta ldnt2$ [GFP-D389L/R393L] transfectants were functionally impaired, similar to the $\Delta ldnt2$ cell line (Table I and Figure 6, panel A).

Orientation of the NH₂-Terminus of LdNT2 – The ability to express a functional GFP-tagged *LdNT2* also provided a vehicle to solve the NH₂-terminal topology of the transporter. Indirect immunofluorescence analysis of $\Delta ldnt2$ [GFP-*LdNT2*] using a GFP antibody with permeabilized and non-permeabilized parasites indicated that the NH₂-terminus of GFP-*LdNT2* is located on the cytoplasmic face of the parasite membrane (Fig. 2-7). Non-permeabilized parasites did not react with the GFP antibody or with control tubulin antisera,

Chapter 2: MANUSCRIPT 1

whereas both GFP and tubulin could be detected with their respective antibodies after permeabilization. This cytoplasmic orientation of the NH₂-terminus of LdNT2 is consistent with the recently solved gross topology determined for the human hENT1 (24), a protein with which LdNT2 shares ~25% sequence identity (2,5).

2.5 DISCUSSION

Multisequence alignments of all functionally characterized ENTs from phylogenetically disparate eukaryotes, from protozoa to human, reveal the presence of a 'signature' motif comprised of two charged amino acids separated by 3 nonconserved residues within predicted TM8 (Fig. 2-1 and Ref. 5). Specifically, this motif, D-x-x-x-R, is found in both nucleoside transporters of *L. donovani* and all mammalian and parasite ENTs characterized to date. It should be noted, however, that a number of ENT sequences containing the 'signature' motif D-x-x-x-K have recently emerged from various genome sequencing databases (6), but these proteins have yet to be functionally characterized. To dissect the functional roles of these charged residues in a model transporter, site-directed mutants were generated in Asp³⁸⁹ and Arg³⁹³ of LdNT2, a *L. donovani* ENT that exhibits a strict and unusual ligand specificity for 6-oxypurine nucleosides. The

data demonstrate that even conservative mutations introduced at Asp³⁸⁹ crippled LdNT2 inosine and guanosine transport activity (Fig. 2-2 and Table II). However, this diminished transport capacity cannot be ascribed to decreased ligand affinity (where it can be measured, i.e., for the D389E mutant) or to a reduced amount of protein at the parasite plasma membrane (Table II and Fig. 2-4). Thus, it appears that Asp³⁸⁹ is a key residue within the translocation process. Negatively charged residues in TM domains of several different transporters are known to play a direct role in ligand recognition, particularly for positively charged ligands such as choline or protons (25). However, since the D389E mutant exhibited wild type affinity for inosine, it is unlikely that Asp³⁸⁹ functions primarily to bind to the uncharged nucleoside ligand. Moreover, these residues are conserved among all functionally characterized ENT family members, which display a wide variation in ligand specificities (nucleoside and/or nucleobase) and affinities (5). Thus, Asp³⁸⁹ must play another role in the translocation mechanism, likely by inducing or stabilizing a conformation of the transporter that is vital to the permeation mechanism. Although these studies are too preliminary to speculate further on the role of this conserved residue in the permeation mechanism, positive genetic screens to select for second site suppressors of the D389N mutation may reveal a plausible mechanism by which Asp³⁸⁹ participates in transport.

Chapter 2: MANUSCRIPT 1

Conversely, biochemical characterization of the Arg³⁹³ mutants has suggested that this positively charged residue is important for the stability and localization of the transporter rather than being central to ligand translocation or recognition. The introduction of a Lys at Arg³⁹³ results in a functional transporter with properties similar to the wild type transporter (Fig. 2-2 and Table II). It is intriguing that ENT-like sequences from several eukaryotes have been deposited in GenBank (6) that possess a Lys at this position, although it should be noted that their ability to translocate nucleosides and nucleobases has not been experimentally demonstrated. The introduction of a Leu, however, at Arg³⁹³ drastically reduces transport capability to a level similar to that observed with the D389E mutant (Fig. 2-2). Unlike the D389E mutant, however, the low transport capacity of the R393L mutant can be imputed to dramatically reduced amounts of transporter at the cell surface (Fig. 2-4 and Table II). Accounting for the observation that GFP-R393L cell surface levels in Δ *ldnt2*[GFP-R393L] parasites were only ~7% of the LdNT2 amounts in the Δ *ldnt2*[GFP-LdNT2] transfectant, adjustment of the kinetic parameters revealed that the R393L Ldnt2 mutant possessed kinetic properties similar to those of the wild type LdNT2 protein (Table II). Intriguingly, most of the GFP-R393L Ldnt2 that is produced in the Δ *ldnt2*[GFP-R393L] transfectants is targeted to the parasite flagellar membrane (Fig. 2-4), as well as to the flagellar pocket and possibly the multivesicular tubule (22,23). In contrast, GFP-LdNT2 and GFP-R393K are found chiefly at the parasite plasma

membrane and flagellar pocket (Fig. 2-4). Such differences in localization were unexpected and are, as yet, inexplicable. Currently, the mechanisms of protein segregation between the flagellar and plasma membranes are unknown. Regardless, the limited amount of mutant transporter in the $\Delta Idnt2[R393L]$ strain favors the flagellar compartment, and whether this is due to altered interactions with protein sorting machinery or to the distinct (or unique) composition of the flagellar compartment (26,27) remains to be determined.

Given the proximity of Asp³⁸⁹ and Arg³⁹³ within TM8 and that helical wheel predictions suggest that both residues lie on the same side of the helix (D-x-x-x-R), it seemed plausible that these two residues participate in either a charge stabilizing or hydrogen bond interaction. To test this conjecture, both Asp³⁸⁹ and Arg³⁹³ were mutated to the opposite charge to destabilize these potential interactions. As demonstrated in Fig. 2-6, neither GFP-D389R nor GFP-R393D could be detected by immunoblotting of the integral membrane fraction and only diffuse cytosolic staining equivalent to that observed with GFP alone could be detected by direct fluorescence (Fig. 2-6). Surprisingly, the D389R/R389D double mutant appeared to be synthesized and present in normal amounts in $\Delta Idnt2[GFP-D389R/R393D]$ transfectants. Furthermore, the D389R/R389D protein was appropriately targeted to the plasma membrane (Fig. 2-6). The D389R/R393D Idnt2 protein, as expected from the Asp³⁸⁹ alteration, was nonfunctional (Fig. 2-6). These data reinforce the concept that Asp³⁸⁹ is

Chapter 2: MANUSCRIPT 1

absolutely critical for proficient transporter function but also signify a possible interaction between Asp³⁸⁹ and Arg³⁹³ in the maintenance of LdNT2 structural integrity and membrane targeting. It is not known whether the nature of this interaction is in the form of an intrahelical salt bridge, as found for the *E. coli* glucose-6-phosphate carrier (28), and the melibiose carrier (29), or a hydrogen bond interaction between the Asp³⁸⁹ and Arg³⁹³. Support for a hydrogen bond interaction is bolstered by the fact that a D389N/R393N double mutant, although transport incompetent, is expressed and targeted to the plasma membrane, whereas a D389L/R393L double mutant is neither stably produced nor properly targeted (Fig. 2-7). Since the double Asn mutant has the propensity to form hydrogen bonds, whereas the double Leu mutant is unable to form such an interaction yet would be expected to favor the formation of an alpha helix (30), this suggests that an interaction between these two charged residues maybe key for the stable production and proper localization of LdNT2.

In addition to providing evidence for the role of conserved, charged TM residues in the translocation mechanism, these studies demonstrate for the first time that GFP-tagged LdNT2 is localized to both the flagellar and pellicular plasma membranes, as well as to the flagellar pocket (Fig. 2-4A) and displays a cytoplasmic NH₂-terminal topology (Fig. 2-8) consistent with that observed for the human hENT1 (24). The only other parasite nucleoside transporters that have been localized are LdNT1 (31) and PfNT1 (32), the *Plasmodium falciparum*

nucleoside transporter. Although the location of LdNT2 still needs to be confirmed using antisera against LdNT2 protein to demonstrate conclusively that the cellular environment of the transporter is not influenced by the presence of a large fluorescent tag, it is noteworthy that LdNT1 does not show flagellar targeting when a similar GFP targeting construct is used to monitor its overproduction and localization (31).

In conclusion, these studies support a role for Asp³⁸⁹ and Arg³⁹³ in LdNT2 function, cellular maintenance, and targeting. Previous studies using chimeras between the human hENT1 and hENT2 implicate TM-spanning domains 3-6 in inhibitor binding, and mutational dissection of hENT1 (7,8,33) and LdNT1 signify a role for TMs 5 and 7 in ligand translocation and specificity (31). Our results with LdNT2 suggest that conserved residues within TM8 also contribute to the ENT translocation mechanism. Moreover, they establish genetically that intrahelical interactions within TM8 are important determinants of transporter stability. Finally, the conservation of these amino acids within the ENT family suggests that these residues are likely crucial in a generalized ENT translocation mechanism.

Acknowledgements - This work was supported in part by grants RO1 AI23682 and RO1 AI44138 from the National Institutes of Health (B.U.) and a

Chapter 2: MANUSCRIPT 1

grant 0360022Z from the American Heart Association (N.S.C.). S.A. has received financial support from the N.L.Tartar Research Fellowship from the Oregon Health & Science University. We would like to thank Aurelie Snyder of the Molecular Microbiology and Immunology Department of the Oregon Health & Science University for her technical assistance with the deconvolution microscopy. The authors are grateful to Dr. Scott Landfear and Dr. Cassandra S. Arendt for helpful comments during the preparation of the manuscript.

2.6 FIGURES

FIG. 2.1. Multiple sequence alignment of predicted TM8 of ENT family members.

hENT1 (AAF02777), hENT2 (Q14542), hENT3 (AAK00958), LdNT1 (AAC32597), LdNT2 (AAF74264), LmaNT3 (CAC33972), TbAT1 (AAD45278), TbNT2 (AAF04490), PfNT1 (CAD52595), and TgAT (AAF03247), were aligned by the method of Feng and Doolittle (34). Amino acids identical among all aligned TM8 domains are *shaded black*, and highly conserved amino acids are *shaded gray*.

Chapter 2: MANUSCRIPT 1

FIG. 1

hENT1	323 . T	. ERYFIPVSCFLT	IFDWLGRSLTA.	349
hENT2	323 . K	. SQFFNPICCFLL	IMDWLGRSLTS.	349
hENT3	341 . .	TTKFFIPLTTFLL	FADLCGRQLTA.	367
LdNT1	361 . .	. FSTIAVFI	VFDVLGRFSPSLKL.	385
LdNT2	375 . G	. YMTIIVTL	AGDFVARVLL.	396
LmaNT3	377 FATIAI.LL	CGDATGRWLSS.	398
TbAT1	337 . G	. YLTIAAAL	LGDFLSRLCL.	358
TbNT2	337 . F	. YFPVAIAM	LGDFLSRLVL.	358
PfNT1	273 . D	. NVTIIVGM	VFDFLSR	YPPN..LTHIK.	300
TgAT	332 . V	. NHFIIMFG	LG DVTGR	FFPDLSQFSPK.	362

FIG. 2.2. Functional characterization of Asp³⁸⁹ and Arg³⁹³ Idnt2 mutants.

Panels A and B, *Δldnt2* parasites expressing *Δldnt2*[LdNT2] (●) *Δldnt2*[R393K] (■), *Δldnt2*[R393L] (□), *Δldnt2*[D389E] (▲), *Δldnt2*[D389N] (△) were tested for uptake of 10 μM [³H]inosine or 10 μM [³H]guanosine over 4 min. The *Δldnt2* cell line (○) served as a negative control. Panels C and D, These experiments were performed essentially as Panels A and B with the exception that the initial rate of uptake was measured over 10 s. Results are expressed as mean ± standard deviation (*n* = 2).

FIG. 2

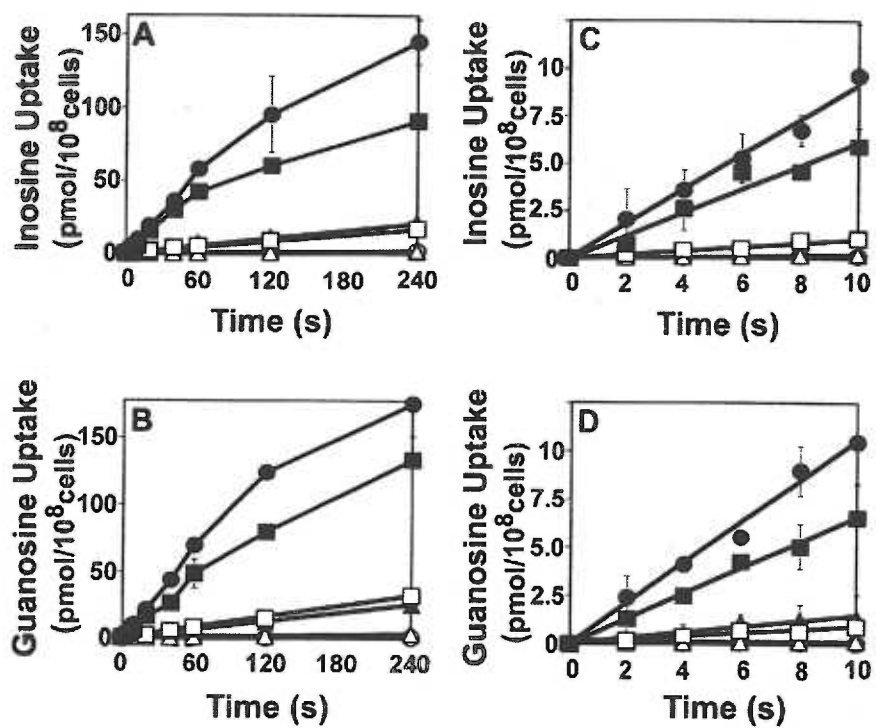


FIG. 2.3. Asp³⁸⁹ and Arg³⁹³ mutant transporter kinetics.

Uptake of [³H]inosine by Δ *dnt2* cells expressing Δ *dnt2*[GFP-LdNT2] (●), Δ *dnt2*[GFP-R393K] (■), Δ *dnt2*[GFP-R393L] (□), Δ *dnt2*[GFP-D389E] (▲) was determined over 10 s for GFP-LdNT2 and GFP-R393K or over 1 min for GFP-R393L and GFP-D389E. The experiments were performed at a range of [³H]inosine concentrations (0.3 - 10 μ M) and the rate of uptake was determined for each concentration by linear regression analysis. The results represented as a Hanes analysis (16) are expressed as inosine(μ M)/rate of uptake (pmol/s/10⁸ cells) as a function of inosine (μ M). The calculated kinetic parameters are reported in Table II.

FIG. 3

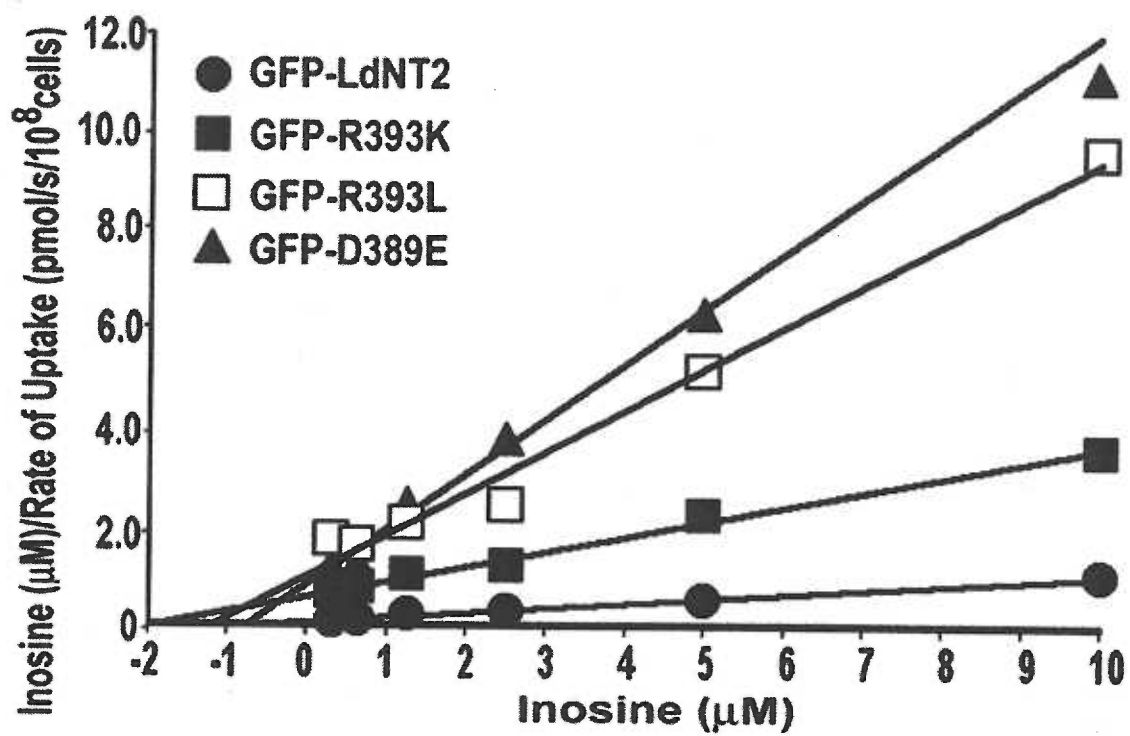


FIG. 2.4. Deconvolution microscopy of *Δldnt2* transfectants.

Live parasites were prepared for deconvolution microscopy as described in the Experimental Procedures. Deconvolved fluorescent images of *Δldnt2* parasites overexpressing GFP-LdNT2 (Panel A), GFP (Panel B), GFP-R393K (Panel C), GFP-R393L (Panel D), GFP-D389E (Panel E), GFP-D389N (Panel F). Each fluorescent image is accompanied by a phase contrast of the field of view shown for the respective GFP illumination

FIG. 4

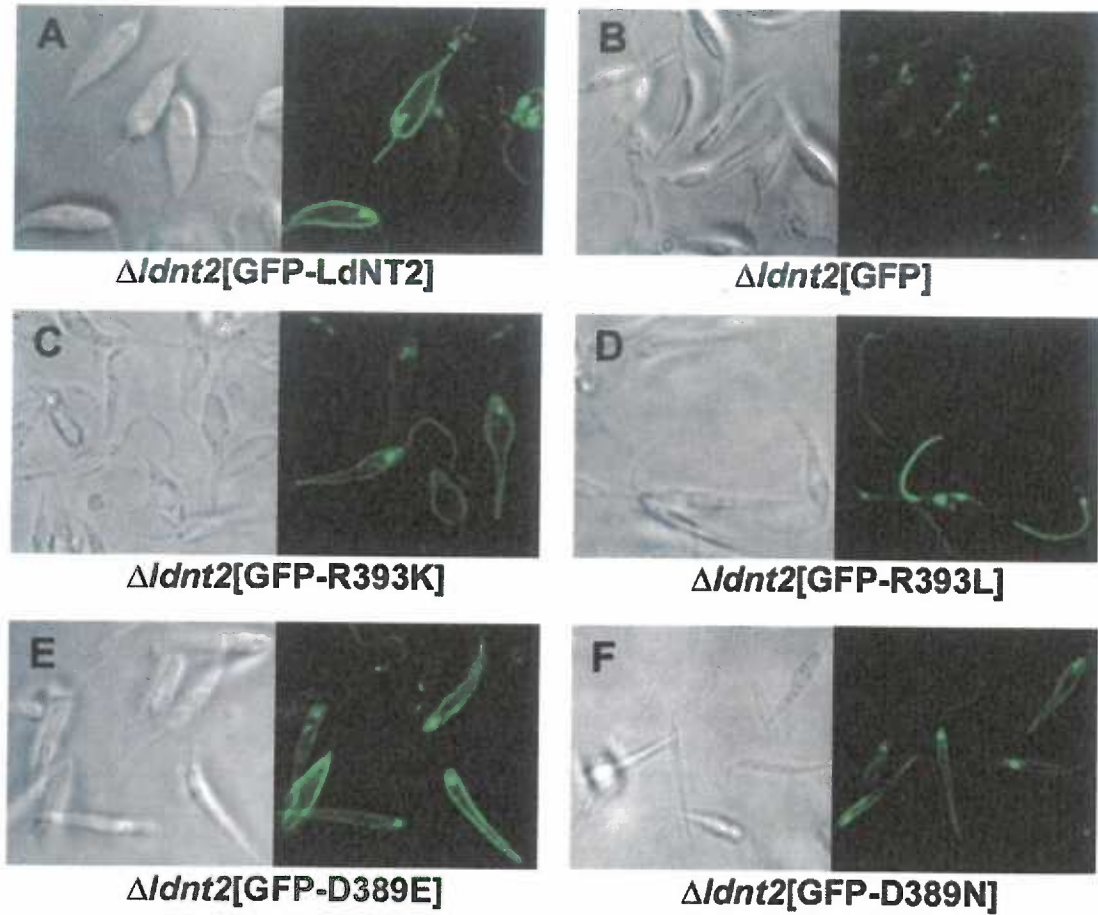


FIG. 2.5. Cell surface expression of wild type and mutant *Idnt2* in $\Delta Idnt2$ transfectants.

Panel A, Live parasites were subjected to cell surface biotinylation, lysis, immunoprecipitation, and Western analysis using a GFP antibody as described in the Experimental Procedures. Panel B, Detection of GFP in integral membrane protein fractions prepared from GFP-*LdNT2* and GFP-*Idnt2* mutants using a GFP antibody. Panel C, Detection of an endogenous transporter, MIT, used as a control to demonstrate equal loading of lanes in the integral membrane western analysis.

FIG. 5

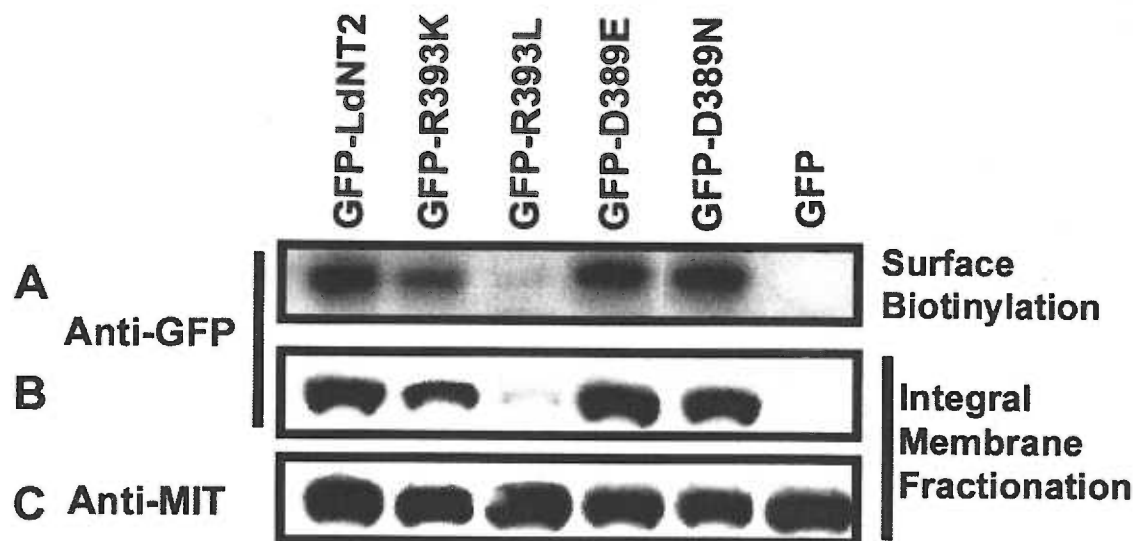


FIG. 2.6. Characterization of D389R/R³⁹³, D³⁸⁹/R393D, D389R/R393D GFP-*ldnt2* mutants.

Panel A, Uptake of 10 μ M [³H]inosine (*shaded black*) and 10 μ M [³H]guanosine (*shaded gray*) by GFP-*LdNT2* and GFP-*ldnt2* mutants over a 1 min interval.

Results are expressed as mean \pm standard deviation ($n = 3$). Panel B, Detection of GFP in integral membrane protein fractions using a GFP antibody. A MIT antibody was used as a control for equal loading of lanes. Panel C, Deconvolution microscopy of GFP-D389R, GFP-R393D, and GFP-D389R/R393D as described in the Experimental Procedures. I, Δ *ldnt2*[GFP-*LdNT2*]; II, Δ *ldnt2*[GFP-D389R]; III, Δ *ldnt2*[GFP-R393D]; IV, Δ *ldnt2*[GFP-D389R/R393D]; V, Δ *ldnt2*[GFP-D389N/R393N]; VI, Δ *ldnt2*[GFP-D389L/R393L]; VII, Δ *ldnt2*[GFP].

FIG. 6

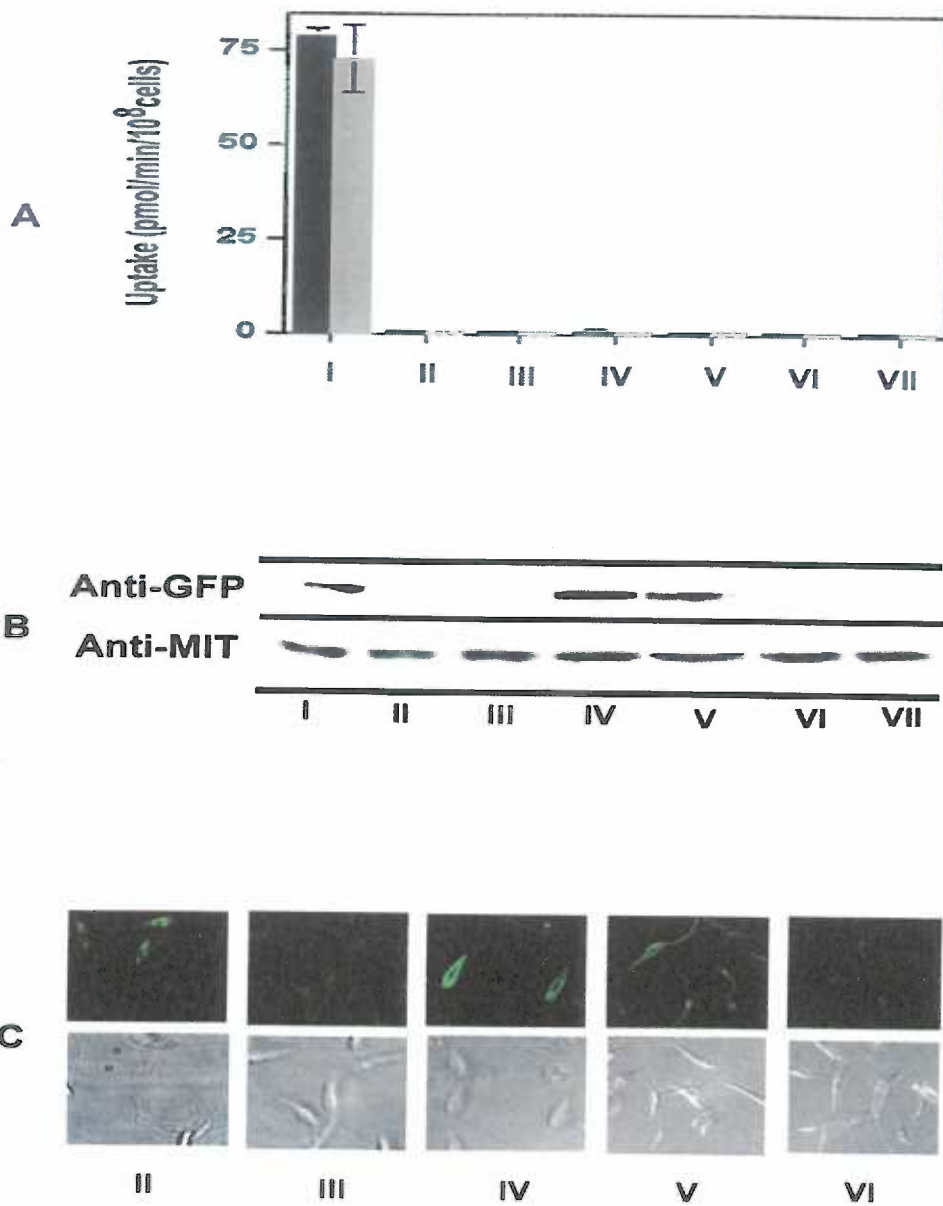
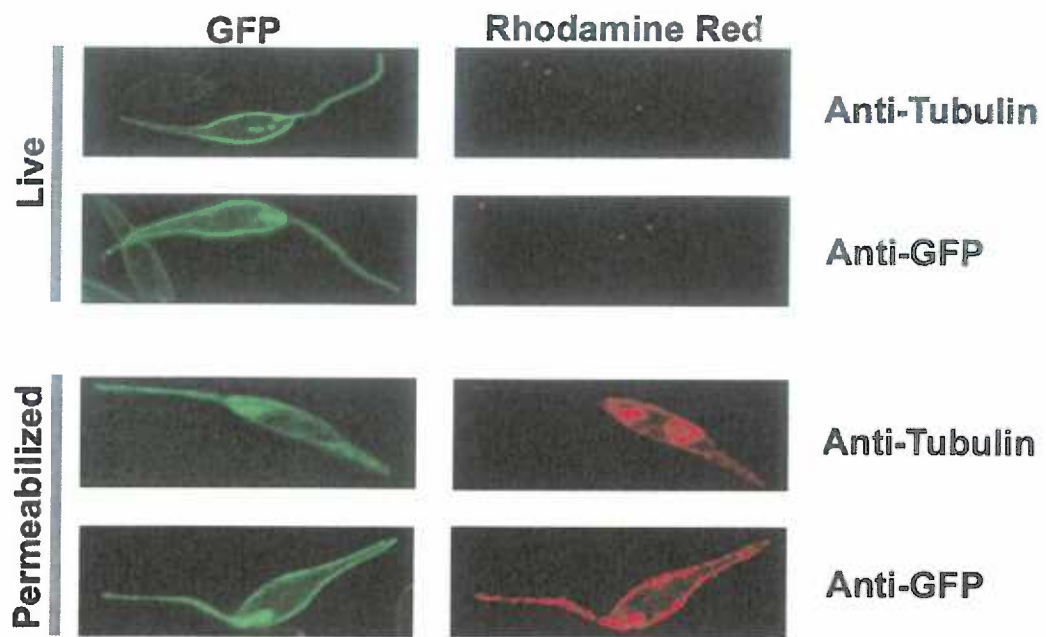


FIG. 2.7. Topology of the NH₂-Terminus of GFP-LdNT2.

Direct and indirect fluorescence deconvolution microscopy in both membrane-intact and permeabilized parasites. GFP direct fluorescence is shown in the left hand panels, whereas indirect immunofluorescence with tubulin and GFP antibodies is depicted in the right hand panels. Methods are according to the Experimental Procedures.

FIG. 7



2.7 TABLES

TABLE I

Sensitivity to Formycin B

Δldnt2 and its transfectants were incubated with varying concentrations of FoB and the parasites enumerated after 6 days to determine the EC₅₀ value, which is the effective concentration of drug that inhibits parasite growth by 50%. All analyses were performed three times or more with the exception of *Δldnt2*[GFP-D389N/R393N] and *Δldnt2*[GFP-D389L/R393L].

Cell Line	EC ₅₀ (μM)
<i>Δldnt2</i>	8.3 ± 0.9
<i>Δldnt2</i> [LdNT2]	0.0073 ± 0.0017
<i>Δldnt2</i> [R393K]	0.19 ± 0.04
<i>Δldnt2</i> [R393L]	0.6 ± 0.1
<i>Δldnt2</i> [D389E]	0.71 ± 0.15
<i>Δldnt2</i> [D389N]	5.7 ± 1.4
<i>Δldnt2</i> [D389R]	5.7 ± 0.9
<i>Δldnt2</i> [R393D]	7.3 ± 0.9
<i>Δldnt2</i> [D389R/R393D]	6.3 ± 1.3
<i>Δldnt2</i> [GFP-LdNT2]	0.0079 ± 0.0008
<i>Δldnt2</i> [GFP-D389N/R393N]	6.0
<i>Δldnt2</i> [GFP-D389L/R393L]	7.5

TABLE II

Kinetic parameters of GFP-LdNT2 and Asp³⁸⁹ and Arg³⁹³ GFP-Ldnt2 mutants.

The kinetic parameters, V_{\max} and K_m , were calculated according to the Hanes method (16). The relative expression was determined by densitometry on data obtained from western analysis of the cell surface biotinylation experiments detailed under Experimental Procedures. The results are expressed as mean \pm standard deviation ($n = 3$).

Cell Line	V_{\max} (pmol/min/ 10^8 cells)	% Expression	Adjusted V_{\max}	K_m (μ M)
Δ ldnt2[GFP-LdNT2]	14 \pm 5.3	100	14	1.3 \pm 0.6
Δ ldnt2[GFP-R393K]	3 \pm 0.8	67 \pm 25	5	1.7 \pm 0.3
Δ ldnt2[GFP-R393L]	0.8 \pm 0.3	7.1 \pm 0.7	11	1.6 \pm 0.4
Δ ldnt2[GFP-D389E]	0.8 \pm 0.4	120 \pm 37	0.7	1.1 \pm 0.5
Δ ldnt2[GFP-D389N]	N.D.*	140 \pm 20	N.D.*	N.D.*

*N.D., not detectable.

2.8 REFERENCES

1. Carter, N.S., Rager, N., Ullman, B. (2003) in *Molecular Medical Parasitology* (J. Joseph Marr, T. W. N., Richard W. Komuniecki, ed), pp. 197-223, Elsevier Science Ltd., London
2. Carter, N. S., Drew, M. E., Sanchez, M., Vasudevan, G., Landfear, S. M., and Ullman, B. (2000) *J Biol Chem* **275**, 20935-20941
3. Vasudevan, G., Carter, N. S., Drew, M. E., Beverley, S. M., Sanchez, M. A., Seyfang, A., Ullman, B., and Landfear, S. M. (1998) *Proc Natl Acad Sci U S A* **95**, 9873-9878
4. Griffiths, M., Beaumont, N., Yao, S. Y., Sundaram, M., Boumah, C. E., Davies, A., Kwong, F. Y., Coe, I., Cass, C. E., Young, J. D., and Baldwin, S. A. (1997) *Nat Med* **3**, 89-93
5. Carter, N. S., Landfear, S. M., and Ullman, B. (2001) *Trends Parasitol* **17**, 142-145
6. Acimovic, Y., and Coe, I. R. (2002) *Mol Biol Evol* **19**, 2199-2210

Chapter 2: MANUSCRIPT 1

7. SenGupta, D. J., Lum, P. Y., Lai, Y., Shubochkina, E., Bakken, A. H., Schneider, G., and Unadkat, J. D. (2002) *Biochemistry* **41**, 1512-1519
8. Sundaram, M., Yao, S. Y., Ng, A. M., Griffiths, M., Cass, C. E., Baldwin, S. A., and Young, J. D. (1998) *J Biol Chem* **273**, 21519-21525
9. Visser, F., Vickers, M. F., Ng, A. M., Baldwin, S. A., Young, J. D., and Cass, C. E. (2002) *J Biol Chem* **277**, 395-401
10. Iovannisci, D. M., and Ullman, B. (1983) *J Parasitol* **69**, 633-636
11. Laban, A., Tobin, J. F., Curotto de Lafaille, M. A., and Wirth, D. F. (1990) *Nature* **343**, 572-574
12. Ha, D. S., Schwarz, J. K., Turco, S. J., and Beverley, S. M. (1996) *Mol Biochem Parasitol* **77**, 57-64
13. Kapler, G. M., Coburn, C. M., and Beverley, S. M. (1990) *Mol Cell Biol* **10**, 1084-1094

Section: 2.8 REFERENCES

14. Robinson, N., Kaur, K., Emmett, K., Iovannisci, D. M., and Ullman, B. (1984) *J Biol Chem* **259**, 7637-7643
15. Aronow, B., Kaur, K., McCartan, K., and Ullman, B. (1987) *Mol Biochem Parasitol* **22**, 29-37
16. Hanes, C. S. (1932) *Biochem J* **26**, 1406
17. Laemmli, U. K. (1970) *Nature* **227**, 680-685
18. Towbin, H., Staehelin, T., and Gordon, J. (1979) *Proc. Natl. Acad. Sci. U. S. A.* **76**, 4350-4354
19. Drew, M. E., Langford, C. K., Klamo, E. M., Russell, D. G., Kavanaugh, M. P., and Landfear, S. M. (1995) *Mol Cell Biol* **15**, 5508-5515
20. Agard, D. A., Hiraoka, Y., Shaw, P., and Sedat, J. W. (1989) *Methods Cell Biol* **30**, 353-377
21. Tuszny, G. E., and Simon, I. (1998) *J Mol Biol* **283**, 489-506

Chapter 2: MANUSCRIPT 1

22. Mullin, K. A., Foth, B. J., Ilgoutz, S. C., Callaghan, J. M., Zawadzki, J. L., McFadden, G. I., and McConville, M. J. (2001) *Mol Biol Cell* **12**, 2364-2377
23. Ghedin, E., Debrabant, A., Engel, J. C., and Dwyer, D. M. (2001) *Traffic* **2**, 175-188
24. Sundaram, M., Yao, S. Y., Ingram, J. C., Berry, Z. A., Abidi, F., Cass, C. E., Baldwin, S. A., and Young, J. D. (2001) *J Biol Chem* **276**, 45270-45275
25. Putman, M., van Veen, H. W., and Konings, W. N. (2000) *Microbiol Mol Biol Rev* **64**, 672-693
26. Landfear, S. M., and Ignatushchenko, M. (2001) *Mol Biochem Parasitol* **115**, 1-17
27. da Cunha e Silva, N. L., Hasson-Voloch, A., and de Souza, W. (1989) *Mol Biochem Parasitol* **37**, 129-136
28. Hall, J. A., Fann, M. C., and Maloney, P. C. (1999) *J Biol Chem* **274**, 6148-6153

Section: 2.8 REFERENCES

29. Franco, P. J., and Wilson, T. H. (1999) *J Bacteriol* **181**, 6377-6386
30. Ulmschneider, M. B., and Sansom, M. S. (2001) *Biochim Biophys Acta* **1512**, 1-14
31. Vasudevan, G., Ullman, B., and Landfear, S. M. (2001) *Proc Natl Acad Sci U S A* **98**, 6092-6097
32. Rager, N., Mamoun, C. B., Carter, N. S., Goldberg, D. E., and Ullman, B. (2001) *J Biol Chem* **276**, 41095-41099
33. Yao, S. Y., Sundaram, M., Chomey, E. G., Cass, C. E., Baldwin, S. A., and Young, J. D. (2001) *Biochem J* **353**, 387-393
34. Feng, D. F., and Doolittle, R. F. (1987) *J Mol Evol* **25**, 351-360

Chapter 3

MANUSCRIPT 2

Second-Site Suppression of a Non-functional Mutation within the *Leishmania donovani* Inosine-Guanosine Transporter

**Shirin Arastu-Kapur, Cassandra S. Arendt, Tina Purnat, Nicola S. Carter, &
Buddy Ullman**

*From the Department of Biochemistry and Molecular Biology, Oregon Health &
Science University, Portland, OR 97239*

3.1 ABSTRACT

LdNT2 from *Leishmania donovani* is a member of the equilibrative nucleoside transporter (ENT) family, which contains 19 conserved residues located mainly in membrane-spanning domains. One of these conserved residues, Asp³⁸⁹ within LdNT2, was previously shown to be important for transporter function without affecting ligand affinity or plasma membrane targeting. To further delineate the role of Asp³⁸⁹ in LdNT2 function, second-site suppressors of the *ldnt2*-D389N mutation were selected in a strain of *Saccharomyces cerevisiae*, which is deficient in purine nucleoside transport and purine biosynthesis. A library of random mutants within the *ldnt2*-D389N background was screened in yeast for restoration of growth on inosine. Twelve independent clones were obtained, each containing secondary site mutations throughout the transporter sequence and capable of inosine transport. One mutation, N175I, was prevalent in the clones obtained and significantly augmented inosine transport capability compared to LdNT2 in yeast. N175I was subsequently introduced into a *ldnt2*-D389N construct tagged at the NH₂-terminus with green fluorescent protein and transfected into a Δ *ldnt1*/ Δ *ldnt2* *L. donovani* knockout. GFP-N175I/D389N significantly suppressed the D389N phenotype in the knockout and targeted properly to the plasma membrane and flagellum. Interestingly, N175I decreased inosine affinity by 10-fold within the D389N background relative to wild type GFP-LdNT2.

Chapter 3: MANUSCRIPT 2

Additional substitutions at Asn¹⁷⁵ established that only large, nonpolar amino acids were capable of suppressing the D389N phenotype, suggesting that the suppression at D389N has a specific size and charge requirement at position 175. Furthermore, since multiple second-site suppressor mutations were uncovered that alleviate the constraint imparted by the D389N mutation, these data suggest that Asp³⁸⁹ is a conformationally sensitive residue. To impart spatial orientation to the clustering of second-site mutations, a 3-dimensional model was based on members of the major facilitator superfamily using threading analysis. The model is consistent with previous genetic and biochemical data on ENTs, and indicates that Asn¹⁷⁵ and Asp³⁸⁹ lie in close proximity, and that all of the second-site suppressor mutations cluster to one region of the transporter, supporting the idea that these mutations act to alleviate the conformational constraint imposed by the crippling D389N mutation.

3.2 INTRODUCTION

Leishmania donovani is a protozoan parasite that is the causative agent of visceral leishmaniasis, a disease that is invariably fatal if untreated. The genus is digenetic, existing as the extracellular promastigote in the phlebotomine sandfly vector and as the intracellular amastigote within the phagolysosome of macro-

phages in the infected mammalian host. The current arsenal of drugs employed to treat leishmaniasis is far from ideal and is compromised by both toxicity and therapeutic failure. The need for additional drugs is acute, and rational approaches to drug development dictate exploitation of novel targets within the parasite. Perhaps the most striking metabolic disparity between protozoan parasites and their mammalian hosts is the inability of the former to synthesize purine nucleotides *de novo* (1). Thus, purine salvage is an indispensable nutritional function for all protozoan parasites, and many unique purine salvage enzymes have been identified and characterized (1). The initial component of purine acquisition from the host involves the translocation of purines into the parasite, a process that is mediated by nucleoside and nucleobase transporters.

Nucleoside permeation into *L. donovani* is mediated by two high affinity transporters with non-overlapping ligand specificity, LdNT1 and LdNT2, both of which are members of the equilibrative nucleoside transporter¹ (ENT) family. LdNT1 transports adenosine and pyrimidine nucleosides, whereas LdNT2 is selective for inosine and guanosine (2,3). Essentially nothing is known about the permeation mechanism of the ENTs, and only a few amino acids that govern

¹ The abbreviations used are: ENT, equilibrative nucleoside transporter; TM, transmembrane; MFS, major facilitator superfamily; GFP, green fluorescent protein; LiOAc, lithium acetate; OD₆₀₀, optical density at 600 nm; YPD, yeast rich media; SC, yeast minimal media; MIT, *myo*-inositol transporter; PCR, polymerase chain reaction

Chapter 3: MANUSCRIPT 2

ligand recognition have been identified. Conserved Gly residues within transmembrane (TM) 5 and 4 of hENT1 and TM5 of LdNT1 have been shown to be critical for transport function and ligand selectivity (4,5), and a Leu within TM2 of hENT1 has also been revealed as a ligand specificity determinant (6). Additional studies have supported the role for hENT1 TMs 3-6 in the binding of 4-nitrobenzylthioinosine (7), and Met³³ within hENT1 TM1 in the binding of dipyridamole and dilazep (8). 4-nitrobenzylthioinosine, dipyridamole and dilazep are all potent inhibitors of hENT1 but do not significantly affect parasite nucleoside transporters (9).

Multisequence alignments of ENT family members reveal 19 conserved or “signature” residues, located predominantly in predicted TM regions (10). The most striking among these signatures are two charged residues, an Asp and an Arg, that are located within TM8. The preservation of these residues and secondary topological prediction implies their participation in the translocation mechanism. Site-directed mutagenesis revealed that Asp³⁸⁹ of LdNT2 is essential for both inosine and guanosine permeation and implied a structural role for both Asp³⁸⁹ and Arg³⁹³ in transporter function (11).

To further elucidate the role of Asp³⁸⁹ in the translocation mechanism of LdNT2, a screen for second-site suppressors was implemented using the non-functional *ldnt2-D389N* mutant. The screen was performed with *ade2* mutant *Saccharomyces cerevisiae* which are deficient in purine nucleoside transport and

purine biosynthesis (6). A number of second-site suppressor mutations were identified, and a frequently occurring N175I mutation was further characterized and shown to significantly suppress the D389N phenotype in yeast and *Leishmania*. The distribution of mutations throughout the TMs 1 – 8 underscore the premise that Asp³⁸⁹ is a conformationally sensitive residue, since these diverse mutations appear to alleviate the conformational constraints imparted by the D389N mutation. Finally, a tertiary topology prediction is presented, which is supported by previously published biochemical and genetic data and suggests that the second-site suppressor mutations cluster and Asn¹⁷⁵ is perhaps proximal to the Asp³⁸⁹.

3.3 EXPERIMENTAL PROCEDURES

Strains and Culture Methods – The *S. cerevisiae* strain YPH499 (a *ura3-52 lys2-801 ade2-101 trp1-Δ63 his3-Δ200 leu2Δ1*) was constructed by Sikorski and Heiter (12). Rich (YPD) and minimal (SC) medium plates were prepared as described, and standard methods were used for genetic manipulation of yeast (13). All *E. coli* transformations were performed in the DH5α strain (Invitrogen Life Technologies, Carlsbad, CA) using usual methodologies (14). *L. donovani* promastigotes were cultured at 26 °C in DME-L medium (Invitrogen) as described

Chapter 3: MANUSCRIPT 2

(15). The construction and phenotypic characterization of the $\Delta ldnt1/\Delta ldnt2$ *L. donovani* null mutant in which both copies of *LdNT1* and *LdNT2* were eliminated by targeted gene replacement followed by loss-of-heterozygosity will be described elsewhere. The $\Delta ldnt1/\Delta ldnt2$ strain was cultured continuously in 50 $\mu\text{g/ml}$ hygromycin (Roche Pharmaceuticals, Nutley, NJ) and 50 $\mu\text{g/ml}$ phleomycin (Research Products International, Mount Prospect, IL) for which the selective markers hygromycin phosphotransferase and phleomycin binding protein used in the gene replacement strategy confer resistance. Cell lines generated by transfection of $\Delta ldnt1/\Delta ldnt2$ with pXG-GFP+2' (16) were selected and maintained in 25 $\mu\text{g/ml}$ Geneticin (BioWhittaker, Inc., Walkersville, MD), as well as 50 $\mu\text{g/ml}$ hygromycin and 50 $\mu\text{g/ml}$ phleomycin.

Generation of pRS424-Cu-ldnt2-D389N for the Second Site Suppressor Screen – *LdNT2* was subcloned into the *pRS424-Cu* yeast-*E. coli* shuttle vector (17). This vector contains the *TRP1* gene for selection in yeast, an ampicillin resistance gene for selection in *E. coli*, and a polylinker flanked by the copper-inducible promoter *CUP1* and transcriptional terminator *CYC1*. *LdNT2* was amplified by the polymerase chain reaction (PCR) using primers that introduced a BamHI site immediately upstream of the translational start site, a His₆ tag immediately downstream of the translational start site, and an EcoRI site downstream of the stop codon. The PCR product was then ligated into the *pCRII-TOPO* vector (Invitrogen). *LdNT2* was subsequently excised with BamHI/EcoRI

Section: 3.3 EXPERIMENTAL PROCEDURES

from the *pCRII-TOPO* construct and subcloned into *pRS424-Cu* to generate *pRS424-Cu-LdNT2*. The D389N mutation was generated within the *pRS424-Cu-LdNT2* construct by site-directed mutagenesis to generate *pRS424-Cu-ldnt2-D389N* using the QuikChange® site-directed mutagenesis protocol (Stratagene, La Jolla, CA) as described (11).

Mutagenic Library Construction for Second Site Suppressor Screen - A library of mutant *ldnt2* constructs within *pRS424-Cu-ldnt2-D389N* was prepared by mutagenic PCR of *pXG-GFP+2'-ldnt2-D389N* (11), followed by *in vivo* reconstitution of the yeast expression vector encompassing the PCR amplicons in the YPH499 *S. cerevisiae* (18). The open reading frame of *ldnt2-D389N* was initially amplified from *pXG-GFP+2'-ldnt2-D389N*, a leishmanial expression construct, to provide a PCR template devoid of yeast sequences. Mutagenic PCR was conducted using the Diversify PCR Random Mutagenesis Kit (BD Biosciences, Palo Alto, CA) and *pXG-GFP+2'-ldnt2-D389N* as template conditions that were expected to produce ~2.0 base changes per open reading frame. Two independent PCR reactions were pooled, fractionated on agarose gels and the PCR amplicons isolated.

To construct the mutagenic library in the yeast shuttle vector, two unique restriction sites were engineered into *pRS424-Cu-ldnt2-D389N*. Silent mutations were introduced at Pro¹⁶ and Trp¹⁷ to generate an NcoI site and Arg⁴⁷⁰ and Ser⁴⁷¹ to generate a BglII site. The engineered construct was subsequently digested

Chapter 3: MANUSCRIPT 2

with NcoI and BglII and the resulting linearized DNA, designated *pRS424-Cu-ldnt2-D389N*Δ1200bp, containing only 45 bp of 5' and 60 bp of 3' *LdNT2* coding sequence, was gel purified. DNA isolation was performed with a QIAquick Gel Extraction Kit (QIAGEN Sciences, MD) and the concentration of DNA determined on a DU® 640 Spectrophotometer (Beckman Instruments, Inc. Seattle, WA).

Second Site Suppressor Screen in Yeast - To screen the library of random mutants by *in vivo* recombination in yeast, YPH499 cells were transformed with 0.25-1.0 μg of the PCR-mutagenized *pXG-GFP+2'-ldnt2-D389N* and 1 μg *RS424-Cu-ldnt2-D389N*Δ1200bp using the TRAF0 method (19). Transformants were plated on SC *trp-* *ade-* + 100 μM inosine + 100 μM CuSO₄ media. An aliquot of cells was plated on SC *trp-* to allow quantitation of the transformation efficiency. The plates were incubated at 30 °C for 3-5 days and colonies capable of growing in inosine isolated. Colonies were restreaked on SC *trp-* *ade-* + 100 μM inosine + 100 μM CuSO₄ media to verify colony phenotype.

Confirmation and Sequencing of Candidate Plasmids – Plasmids containing mutant *ldnt2* were recovered from yeast colonies that grew on SC *trp+* + 100μM inosine + 100 μM CuSO₄ plates by the smash and grab method (14). The recovered DNA was electroporated into ElectroMAX™ DH5α-E™ Cells (Invitrogen) in 0.2 cm cuvettes with a BIO-RAD Gene Pulser™ (Bio-Rad Laboratories, Inc., Hercules, CA) with electroporation parameters of 1.8 KV, 25 μF, and 200 Ω. The amplified plasmids in *E. coli* were harvested and retransformed into

Section: 3.3 EXPERIMENTAL PROCEDURES

YPH499 cells using the lithium acetate method. Transformants were plated on SC ade- trp- plates containing 100 μ M inosine and 100 μ M CuSO₄ to confirm the contribution of the plasmid to the transport phenotype. The plasmids were sequenced in both directions at the Vollum Institute sequencing core facility at the Oregon Health & Science University. All transport data reported in yeast were obtained with retransformed strains.

Transport Capabilities of the Second-Site Suppressor Clones - Nucleoside transport measurements in yeast were performed by a previously described oil-stop method with some modifications (20). YPH499 transformants were grown overnight in SC trp- media after which they were diluted to an optical density at 600 nm (OD₆₀₀) of 0.25 per ml. CuSO₄ to a concentration of 100 μ M was added to induce transporter expression and cells were grown to mid-log phase (OD₆₀₀ ~ 1). 5.0 ml of culture at an OD₆₀₀ ~ 1 were used per time point and transport capability assessed at 10 μ M [³H]inosine (0.2 Ci/mmol) (Moravek Biochemicals, Inc., Brea, CA).

Nucleoside transport measurements in *L. donovani* promastigotes were performed by the previously described oil-stop method (20). Transport was measured using 10 μ M [³H]inosine (0.2 Ci/mmol) and 10 μ M [³H]guanosine (0.15 Ci/mmol), and kinetic data were obtained by measuring rates of inosine transport at concentrations between 0.2 μ M and 15 μ M for the N175I mutant and 1 μ M and 50 μ M for the N175I/D389N mutant. [³H]inosine (19.5 Ci/mmol) and

Chapter 3: MANUSCRIPT 2

[³H]guanosine (15 Ci/mmol) were purchased from Moravsek Biochemicals, Inc. Transport rates were calculated by linear regression analysis and kinetic parameters determined by the method of Hanes (21).

Introduction of Site-Directed Mutations into Idnt2 - Mutations within *LdNT2* and *D389N-Idnt2* were introduced by the QuikChange® method described above. Mutations were inserted within the *LdNT2* open reading frame in the previously described pXG-GFP+2'-*LdNT2* vector (11), confirmed by nucleotide sequencing, and the wild type and mutant constructs were then transfected into the $\Delta Idnt1/\Delta Idnt2$ cell line using standard electroporation conditions (22).

Integral Membrane Protein Preparations – Crude membrane fractions were prepared as previously conveyed (11). The pattern of expression of mutant *Idnt2* proteins in *L. donovani* was determined by immunoblotting (11).

Cell Surface Labeling – Cell surface biotinylation was performed as described (11), but the beads were ImmunoPure® Immobilized Streptavidin beads (Pierce Biotechnology Inc., Rockford, IL). For analysis, all samples were fractionated on a 10% sodium dodecyl sulphate gel by electrophoresis and biotinylated GFP-tagged *LdNT2* protein detected by immunoblotting as described (11). To determine the relative amount of GFP-tagged *LdNT2/Idnt2* at the cell surface, signals from the immunoblots were scanned using an Epson Perfection 3200 Photo Scanner (Epson America, Inc., Long Beach, CA) and the intensity of each band corresponding to GFP-tagged transporter assessed by the *UN-SCAN-*

Section: 3.3 EXPERIMENTAL PROCEDURES

*IT gel*_{TM} version 4.3 (Silk Scientific, Inc., Orem, UT). The percentage of relative cell surface expression for each mutant GFP-tagged *Ldnt2* transporter to wild type GFP-tagged *LdNT2* was determined as described (11). Equal loading in each lane was ensured using the leishmanial *myo*-inositol transporter (MIT) as reported (11). MIT was a generous gift from Dr. Scott M. Landfear of The Oregon Health & Science University (26).

Fluorescence Microscopy – *Leishmania* cells expressing transporter tagged with GFP were prepared and affixed to slides for microscopy by a method related previously (11). Images were acquired on a Zeiss Axiovert 200 inverted microscope and deconvolution carried out using Axiovision 3.1 software (Carl Zeiss Optical, Chesterfield, VA, USA).

Threading Analyses and Tertiary Topology Prediction – Threading analyses were undertaken by submitting the *LdNT2* protein sequence to the web based software mGenThreader (<http://bioinf.cs.ucl.ac.uk/psipred/>) and 3DPSSM (www.sbg.bio.ic.ac.uk/~3dpssm/). A tertiary topology prediction was generated by submitting the first 48 hits from the query of *LdNT2* in PSI-BLAST (<http://www.ncbi.nlm.nih.gov/BLAST/>) to ModWeb (<http://alto.compbio.ucsf.edu/modweb-cgi/main.cgi>), a web adapted version of the MODELLER software developed for protein modeling by Sali et al (23) and available as freeware through the University of California, San Francisco.

3.4 RESULTS

Isolation of Suppressor Mutants – Previous data has shown that the D389N mutation in LdNT2 abolishes both inosine and guanosine transport in parasites and imply that this residue is part of a generalized ENT translocation mechanism (11). To further examine the role of Asp³⁸⁹ in LdNT2 function, a screen for second-site suppressor mutations was developed for *ldnt2*-D389N. This screen was implemented in the YPH499 strain of *S. cerevisiae*, which is incapable of both purine biosynthesis and purine nucleoside transport. In initial experiments, YPH499 cells transformed with *pRS424-Cu-LdNT2* were shown to be capable of forming colonies on plates containing 100 μ M inosine as the sole purine source, whereas YPH499 cells transformed with *pRS424-Cu-ldnt2-D389N* did not grow even after 7 days of incubation (data not shown). A library of random mutants within *ldnt2*-D389N was generated as described in *Experimental Procedures*, and a total of 5×10^5 transformants were screened for growth on inosine. A total of 24 colonies were obtained after 5 days incubation on the inosine plates, however plasmids from only 16 clones restored the ability of growth on inosine following retransformation in YPH499 cells.

Sequence of the Second-Site Suppressor Mutations – Sequence analysis of the 16 clones revealed that 2 had reverted back to Asp³⁸⁹ from the D389N mutation, and three were identical containing the single N175I second-site

mutation. Of the 12 remaining independent clones, 3 harbored single mutations that suppressed the D389N phenotype (S50T, Y213C, and N175I), whereas the remaining 9 contained either two or three secondary mutations, as well as the starting D389N alteration. These "suppressor" mutations spanned TMs 1 – 8, excluding TM5 (Fig. 3-1 and Table I).

Transport Capability of the Second-Site Suppressor Clones – To verify the transport phenotype of each YPH499 transformant that grew on inosine, transport measurements were conducted at 10 μ M [3 H]inosine at 60 second time points (Fig. 3-2). As shown in Fig. 2, all 12 clones that suppressed the D389N growth phenotype were capable of transporting inosine, and 6 (*shaded gray* in Fig. 3-2) exhibited a transport capacity significantly greater than YPH499 cells transformed with wild type *LdNT2*. Because of the frequency of N175I within the 12 clones and the robust transport capacity that it conferred to the transformants, it was chosen for further investigation.

*Creation and Evaluation of *ldnt2* Mutants in *Leishmania** - To ensure that the suppression of the D389N mutation could be reproduced in other expression systems, the N175I mutation was inserted into both *pXG-GFP2+'-ldnt2-D389N* and *pXG-GFP2+'-LdNT2* and the resulting constructs transfected into the nucleoside transport deficient cell line, $\Delta ldnt1/\Delta ldnt2$ *L. donovani*. These lines were designated $\Delta ldnt1/\Delta ldnt2$ [GFP-N175I/D389N] and $\Delta ldnt1/\Delta ldnt2$ [GFP-N175I]. $\Delta ldnt1/\Delta ldnt2$ [GFP-*LdNT2*] and $\Delta ldnt1/\Delta ldnt2$ [GFP] were also generated as

Chapter 3: MANUSCRIPT 2

controls. To verify the function of the selected second-site suppressor mutations in intact parasites, each transfectant was evaluated for both 10 μM [^3H]inosine and 10 μM [^3H]guanosine uptake, ligand concentrations which were previously determined to be saturating for LdNT2 transport (2). Whereas $\Delta\text{ldnt1}/\Delta\text{ldnt2}[\text{GFP-N175I/D389N}]$ cells incorporated both inosine and guanosine at rates comparable to the $\Delta\text{ldnt1}/\Delta\text{ldnt2}[\text{GFP-LdNT2}]$ transfectant, the capacity of the $\Delta\text{ldnt1}/\Delta\text{ldnt2}[\text{GFP-Y213C/D389N}]$ line to take up both ligands was only ~20% of the wild type transfectant (Fig. 3-3A). $\Delta\text{ldnt1}/\Delta\text{ldnt2}[\text{GFP-N175I/D389N}]$ and $\Delta\text{ldnt1}/\Delta\text{ldnt2}[\text{GFP-N175I}]$ parasites transported 10 μM [^3H]inosine at a rate equivalent to the $\Delta\text{ldnt1}/\Delta\text{ldnt2}[\text{GFP-LdNT2}]$ transfectant, whereas, as expected, the $\Delta\text{ldnt1}/\Delta\text{ldnt2}[\text{GFP}]$ did not take up the nucleoside (Fig. 3-3B).

Substitutions at Asn¹⁷⁵ – To assess the range of secondary mutations at Asn¹⁷⁵ that would suppress the D389N phenotype, a series of mutations were created at Asn¹⁷⁵ within *pRS424-Cu-ldnt2-D389N*, and the mutant alleles were transformed into yeast and screened for growth on 100 μM inosine. Of the substitutions introduced (Gly, Ala, Ser, Thr, Gln, Asp, Lys, Phe, Val or Leu) at Asn¹⁷⁵, only the large branched chain aliphatic residues Ile, Val and Leu, enabled growth on inosine plates (Table II).

Cell surface targeting of GFP-ldnt2 - To determine whether the mutant ldnt2 proteins expressed and targeted properly in the knockout *L. donovani*, GFP fluorescence was monitored in the $\Delta\text{ldnt1}/\Delta\text{ldnt2}[\text{GFP-LdNT2}]$,

Δldnt1/Δldnt2[GFP-N175I], *Δldnt1/Δldnt2*[GFP-N175I/D389N], and *Δldnt1/Δldnt2*[GFP-D389N] transfectants. The data exhibited in Fig. 4 indicate that the wild type LdNT2 and mutant Idnt2-N175I, Idnt2-N175I/D389N, and Idnt2-D389N alleles are all robustly expressed and localize to the parasite plasma membrane and flagellum in the *Δldnt1/Δldnt2* null mutant (Fig. 3-4). However, the relative amount of transporter on the cell surface could not be directly assessed by this approach.

To ascertain the comparative quantities of LdNT2/Idnt2 protein at the plasma membrane and flagellum of the 4 *L. donovani* transfectants, the GFP on the cell surface was quantitated using a membrane-impermeable biotin probe (Fig. 3-5). Equal loading of the cell surface biotinylation membrane fractions was verified by probing with an independent antibody to MIT. Comparable amounts of GFP-LdNT2/GFP-Idnt2 were detected at the cell surface in all transfectants except *Δldnt1/Δldnt2*[GFP-N175I] in which surface membrane-attached Idnt2 protein was ~50% of the LdNT2 level observed in the *Δldnt1/Δldnt2* [GFP-LdNT2] line. As expected, no cell surface biotinylation was observed in *Δldnt1/Δldnt2* [GFP] parasites (Fig. 3-5). The results of the biotinylation experiments were mirrored by parallel analyses of fractionated integral membrane proteins from each of the GFP transfectants (Fig. 3-5). These analyses confirmed the reduced level of Idnt2 expression in the *Δldnt1/Δldnt2* [GFP-N175I] parasites.

Chapter 3: MANUSCRIPT 2

Kinetics of the Asn¹⁷⁵ Mutants – To determine whether the mutation at Asn¹⁷⁵ affected the transport kinetics of Ldnt2, the rates of inosine transport were measured in the $\Delta ldnt1/\Delta ldnt2$ [GFP-N175I] and $\Delta ldnt1/\Delta ldnt2$ [GFP-N175I/D389N] transformants at a range of ligand concentrations. The K_m values for [³H]inosine transport in $\Delta ldnt1/\Delta ldnt2$ [GFP-N175I] cells was calculated by Hanes analysis to be $0.4 \pm 0.2 \mu\text{M}$ for GFP-Ldnt2-N175I, comparable to the $1.3 \pm 0.6 \mu\text{M}$ value previously determined for wild type GFP-LdNT2 (Fig. 3-6 and Table III). Interestingly, the K_m value of the GFP-Ldnt2-N175I/D389N second-site suppressor mutant was significantly higher, $11 \mu\text{M} \pm 3.6 \mu\text{M}$.

Threading Analyses and Tertiary Topology Prediction – To spatially orient the second-site suppressor mutants, a tertiary topology model of LdNT2 was constructed. A suitable template for constructing the ENT model was ascertained by threading analyses, which exploit web-based algorithms to identify existing macromolecular crystal structures that exhibit similarity at the secondary structure level to secondary topology profile of the ENTs without the caveat of necessitating significant sequence identity (24). Three independent threading algorithms described in the *Experimental Methods* elected to generate a three-dimensional model based upon the major facilitator superfamily (MFS). The three-dimensional model predicted by ModWeb was the most consistent with the secondary topology of the ENTs. Specifically, ModWeb identified the crystal structure of the *E. coli* glycerol-3-phosphate transporter, an MFS member, with a

good expected value of $1e^{-56}$. In this structure, the helix packing for LdNT2 was similar to that of MFS members, excluding, of course, TM12 of the latter (Fig. 3-8A). Furthermore, all the residues that have been identified through biochemical and genetic data for the ENTs to be either solvent accessible or important ligand selectivity determinants do point into the putative ligand binding pore (Fig. 3-8A). Finally, the majority of the second-site mutations obtained for D389N do appear to cluster on the tertiary topology model (Fig. 3-8B).

3.5 DISCUSSION

Forward genetic approaches have been implemented in this investigation to further dissect the role of a critical Asp residue within predicted TM8 of LdNT2 in the translocation mechanism. A conserved D-X-X-X-R pentapeptide within TM 8 is an unusual charged signature motif found in all ENT family members that have been functionally characterized (1). Site-directed mutants of Asp³⁸⁹ within LdNT2 are known to cripple transport capability without affecting ligand affinity or protein expression or targeting to the parasite plasma membrane and flagellum (11). Thus, Asp³⁸⁹ is inferred to be an important component of the LdNT2 translocation mechanism, although it may not directly bind nucleoside. Because structural information on ENTs is limited, a forward genetic strategy was ex-

Chapter 3: MANUSCRIPT 2

exploited to select for second-site suppressor mutations within LdNT2 that would further our understanding of Asp³⁸⁹ in the translocation mechanism. Second-site suppression strategies have proven extremely useful in the unveiling of the functional role of cryptic first-site mutations within a variety of membrane proteins, revealing information about tertiary structure, as well as identifying critical functional domains (25-27). In this study, second-site mutations that suppress the D389N null-transport phenotype were selected in *S. cerevisiae* auxotrophic for purines by virtue of their ability to confer growth on inosine. A diverse number of mutations, that occurred throughout the first 8 TMs (except TM5) and their interconnecting loops of *ldnt2* were identified (Fig. 3-1). Of the 24 clones selected, 2 were genuine revertants to the wild type allele. The ability to obtain revertants substantiates our previous observations that Asp³⁸⁹ is a key signature residue for ENTs that plays an important role in the permeation mechanism.

The diversity of second-site mutations obtained in the screen implied that the D389N mutation likely confers a structural constraint that is alleviated by other mutations within the *ldnt2* structure. The second-site mutations grouped to TMs 1, 3, 6 and at the COOH cusp of the large intracellular loop between TMs 6 and 7 (Fig. 3-1). Mutations within the second cluster were uncovered in almost 50% of the suppressor mutants. The clustering in the highly divergent TM 6 – TM 7 intracellular loop suggests that this loop may contribute to the conformational changes that accompany translocation (Fig. 3-1). Clustering of second-

site suppressor mutations were also obtained with the *E. coli* lactose permease, which revealed potential interactions between residues identified in the screen and were later confirmed when the lactose permease crystal structure was solved (27,28). In the absence of a crystal structure, the significance of the clustering of the second-site suppressor mutants obtained for the D389N Ldnt2 null mutant cannot be established.

To develop a structural framework to understand the significance of the suppressor mutations, a tertiary structural prediction of LdNT2 was computationally generated by threading analyses, which have become much more feasible because the accuracy of algorithmic secondary structure predictions is approaching 80% (24). Baldwin *et al.* hypothesized that the overall tertiary topology of ENTs would be similar to that of the human glucose transporters, which are members of the MFS. Crystal structures of MFS members encompass 12 TMs with cytosolic NH₂- and COOH-termini and a large intracellular loop between TMs 6 – 7, while ENTs are similar in predicted membrane topology but conjectured to have 11 TMs with an extracellular COOH-terminus (29). As reported in the results, the tertiary topology prediction was constructed by the ModWeb algorithm, which elected to use the MFS member glycerol-3-phosphate transporter with a good expected value of $1e^{-56}$. The expected value indicates that the glycerol-3-phosphate transporter is a good template for constructing the ENT family tertiary model. However, due to low sequence identity (<14%) between

Chapter 3: MANUSCRIPT 2

the MFS and ENT, the exclusion of TM12 of the MFS in the ENT model, and the inherent difficulty in modeling loops, the structural prediction requires extensive computational refinement and experimental validation to evolve as a model. Although, the drastic exclusion of TM12 in the ENT prediction from the MFS template is of concern, an extensive mutagenesis study of lactose permease TM12 suggests that these residues do not participate in ligand binding or translocation (33). Furthermore, key residues in TMs 1, 2, 4, and 5 reported in the literature to be solvent accessible and critical for ligand selectivity map towards the putative aqueous pore of the transporter (Fig. 3-8A) (4-6,8,30-32).

Significantly, when the second-site suppressor mutations are mapped onto a cross-sectional schematic of the tertiary prediction generated for ENTs, a distinct clustering of TMs 1, 3, and 6 is observed, suggesting that alterations in the tertiary structure in this part of the protein are able to suppress the deleterious effects of the D389N mutation (Fig. 3-8B). However, since no independent charge neutralizations were unveiled in the second-site suppressor screen between TMs 1, 3, and 6, it is unlikely that these TMs directly interact with TM 8 during the translocation process indicating that the critical role of Asp³⁸⁹ in the translocation mechanism is not through an interhelical salt bridge. If Asp³⁸⁹ was involved in a charge-charge interaction, a second-site suppressor screen should have selected for the neutralization of a positive charge since this strategy has been successfully employed to identify a charge pair in various transporters (34-

39). However, with the exception of R393Q that only appeared as a triple mutant with Y213C and D389N (clone 6 in Table I), no other charged residues were mutated in this second-site suppressor screen. Although an R393Q mutation was selected in the context of two other mutations, our previous data suggest that it is unlikely that an intrahelical salt bridge between Asp³⁸⁹ and Arg³⁹³ exists, since previously constructed site-directed mutants D389N/R393N or D389L/R393L are both non-functional (11). Thus, it is more likely that the second-site mutations either compensate for D389N or enhance the overall function of LdNT2. One possibility that does remain is that the charge partner of Asp³⁸⁹ is an irreplaceable residue. If this were the case, then the mutations obtained in the second-site suppressor screen are likely to compensate for the irreplaceable residue.

A detailed kinetic characterization of the most prevalent second-site mutation, N175I, in *Leishmania* revealed some further insights into the suppression of D389N. Although, it is possible that in the PCR based methodology to generate the random mutant library, N175I was an original mutant that propagated through the reaction, its ability to allow growth on inosine plates does indicate that it is an important second-site suppressor of D389N. N175I in the context of D389N does not alter protein expression, targeting, but it does alter ligand affinity (Fig. 3- 2 and 4 and Table III). Whereas, N175I by itself does not alter targeting and ligand affinity, but it does alter protein expression (Fig. 3- 2 and 4 and Table III). The

Chapter 3: MANUSCRIPT 2

decrease in ligand affinity for the $\Delta dnt1/\Delta dnt2$ [N175I/D389N] ($11 \pm 3.6 \mu\text{M}$ for inosine (Table III) relative to $1.3 \pm 0.6 \mu\text{M}$ (11) for GFP-LdNT2) suggests that the N175I second-site suppressor mutation is a bypass suppressor which does not completely reverse the incapacitating structural constraints imposed by the D389N mutation. Although a shift in ligand affinity for inosine was observed for the GFP-N175I/D389N mutant was observed, no uptake was detected with [H^3]adenosine and [H^3]uridine, suggesting that the ligand selectivity of LdNT2 may not be altered. (data not shown). Furthermore, since the N175I mutation by itself did not appear to significantly alter ligand affinity relative to LdNT2, it may suggest that original D389N mutation could have affected the ligand affinity. Unfortunately, binding experiments of inosine with GFP-D389N in whole cells was technically challenging. Taken together, these data suggest that the N175I mutation may be altering the conformation of the transporter during the translocation process. Interestingly, the tertiary topology predicted places TM5 adjacent to TM8 (Fig. 8). These data are intriguing since TM5 was recently shown to be a critical component of the ligand binding pore through site-directed mutagenesis and Cys-modification studies (4,5,31). Perhaps, the significance of TM 5 in the putative role of ligand selectivity excluded any mutants clustering within this critical domain.

Furthermore, the only amino acid substitutions at Asn¹⁷⁵ able to suppress the D389N phenotype were large nonpolar residues, Ile, Val and Leu (Table II).

Since small nonpolar residues such as Ala and Gly were not able to suppress the D389N phenotype, perhaps the requirement of the large nonpolar residues suggests a local volume compensation that could be shifting the position of TM5 relative to TM8. Interestingly, the isoleucine substitution at Asn¹⁷⁵ is predicted to shift the local secondary structure probability from loop to helix according to the Protein Sequence Analysis server (bmerc-www.bu.edu/psa/), suggesting that perhaps the N175I mutation causes an extension of one helical turn in TM5. Both, Val and Leu are also predicted to favor helix formation. No secondary structure shifts were predicted for the D389N.

Finally, Asn¹⁷⁵ is predicted to be located in the TM4-TM5 loop proximal to TM5 (Fig. 3-1). Although Asn¹⁷⁵ is not a conserved residue (Fig. 7), it is located in an evolutionarily conserved region of the ENTs, which are TM1, TM4 to TM5, TM8, and TM9 to TM10 (40), suggesting that Asn¹⁷⁵ and Asp³⁸⁹ may be part of an evolutionarily conserved network of amino acid. Interacting residues within proteins represent structural motifs for cooperativity within the protein as described by Ranganathan *et al* for the G-protein coupled receptors (41). These studies are statistical analyses done by evaluating the variance of a amino acid position in relation to a conserved position through evolution. Although a statistical analysis may be interesting to undertake for the conserved aspartate residue in the ENTs, the reliability of the study could be compromised due to the fact that

Chapter 3: MANUSCRIPT 2

the ENTs only have ~50 members identified compared to the approximate thousand members of the G-protein coupled receptor family.

We have developed a second-site suppressor screen for an ENT family member in yeast. This technique, which has been instrumental in probing the mechanism of the lactose permease, will be a useful tool for future structure/function studies of the ENT family. The second-site suppressor data bolster the role of Asp³⁸⁹ as a conformationally sensitive residue in the LdNT2 translocation mechanism. Furthermore, we have generated a crude tertiary prediction for the ENT family. While this remains to be challenged through experimental data, it is a first step towards an understanding the protein structure of this family.

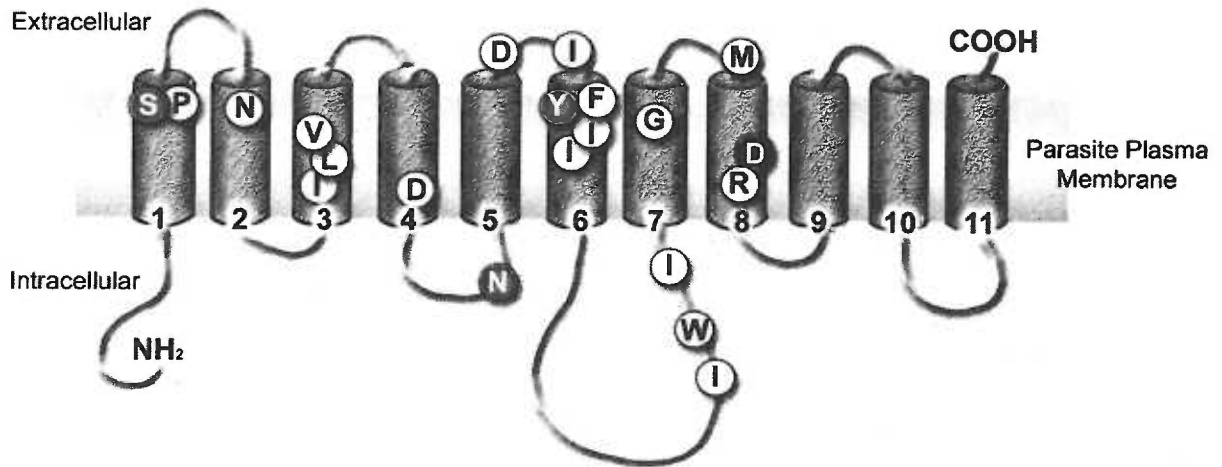
Acknowledgements - We thank Nicolle Rager for the original artwork for the secondary topology of the ENTs in Fig. 1. This work was supported in part by grants RO1 AI23682 and RO1 AI44138 from the National Institutes of Health (B.U.) and a grant 0360022Z from the American Heart Association (N.S.C.). S.A. has received financial support from the N.L.Tartar Research Fellowship from the

Oregon Health & Science University. C.S.A. was supported by a postdoctoral fellowship grant PF-02-097-01-CSM from the American Cancer Society.

3.6 FIGURES

FIG. 3.1. Distribution of residues mutated in the second-site suppressor clones.

Asp³⁸⁹, the position of the original null mutant D389N, is shaded in *black*. Asn¹⁷⁵, Tyr²¹³, and Ser⁵⁰, mutations that were singly able to suppress the D389N mutation, are shaded in *gray*.

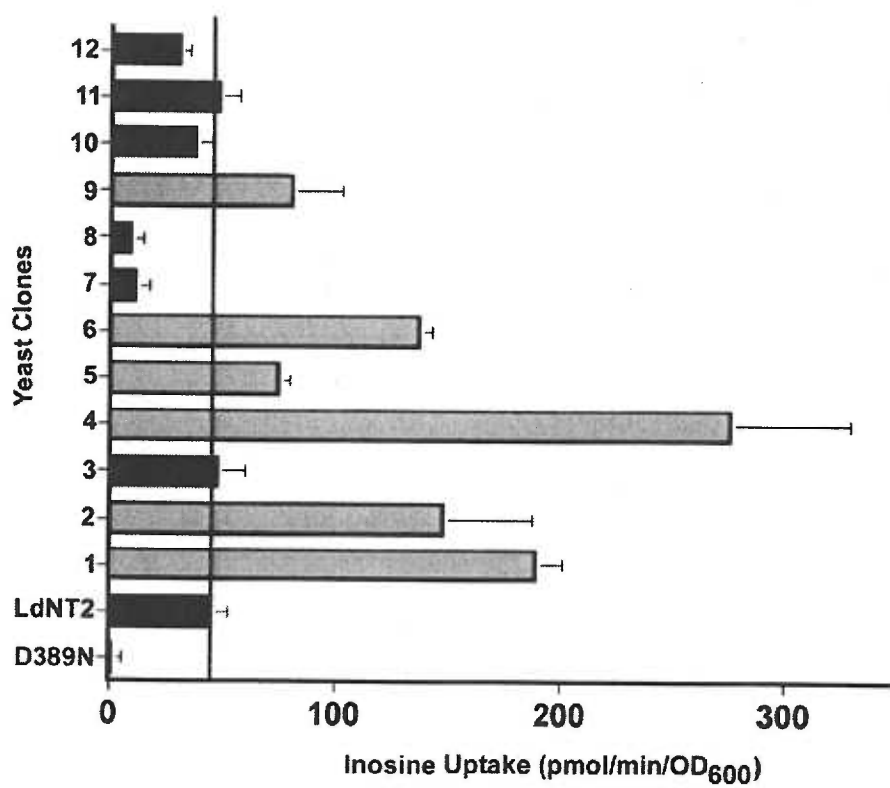


Chapter 3: MANUSCRIPT 2

FIG. 3.2. Functional characterization of second-site suppressor clones.

Yeast were grown to an OD₆₀₀ of 1 and then evaluated for uptake of 10 μ M [³H]inosine at 60s. Results are expressed as mean \pm standard deviation ($n = 6$).

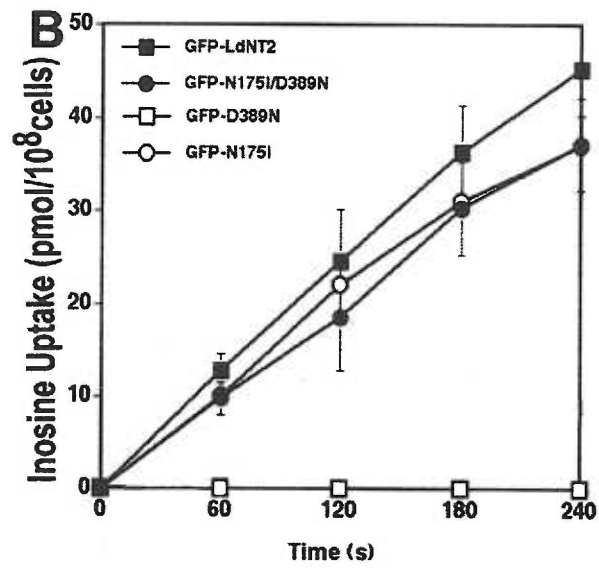
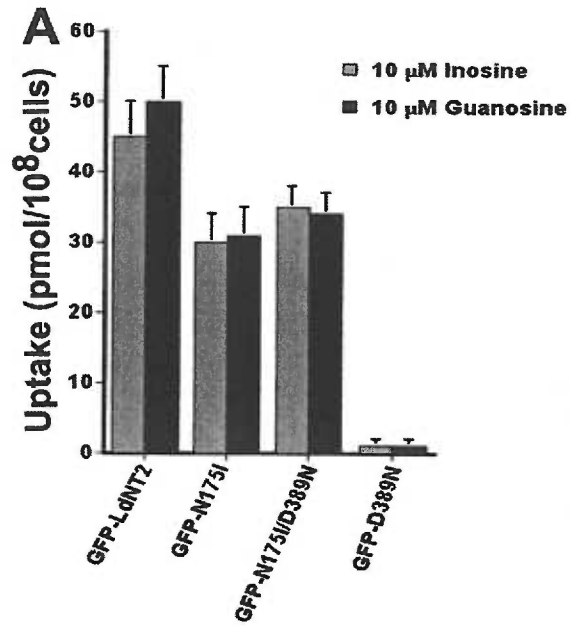
Section: 3.6 FIGURES



Chapter 3: MANUSCRIPT 2

FIG. 3.3. Functional characterization of Asn¹⁷⁵ Idnt2 mutants.

Panel A, $\Delta Idnt1 / \Delta Idnt2$ parasites expressing GFP-LdNT2, GFP-N175I, GFP-N175I/D389N, and GFP-D389N were tested for uptake of 10 μM [³H]inosine (*shaded gray*) or 10 μM [³H]guanosine (*shaded black*) over 4 min. Results are expressed as mean \pm standard deviation ($n = 2$). Panel B, $\Delta Idnt1 / \Delta Idnt2$ parasites expressing GFP-LdNT2 (■), GFP-N175I (○), GFP-N175I/D389N (●), GFP-D389N (□) were tested for uptake of 10 μM [³H]inosine over 4 min. Results are expressed as mean \pm standard deviation ($n = 2$).

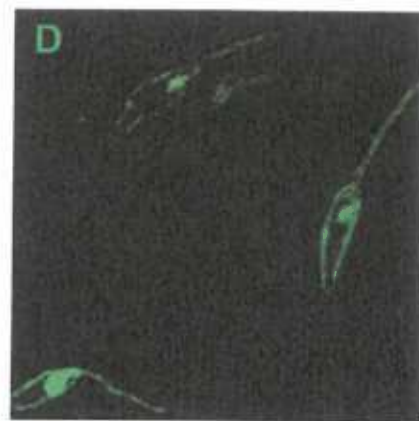
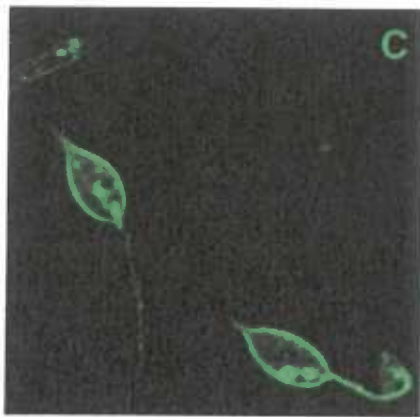
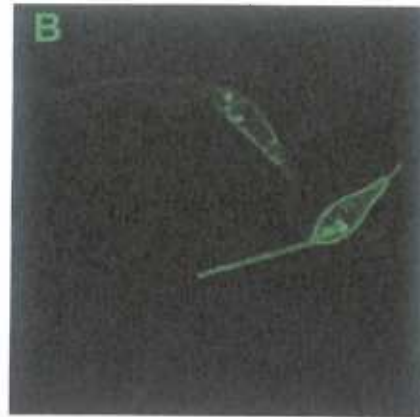
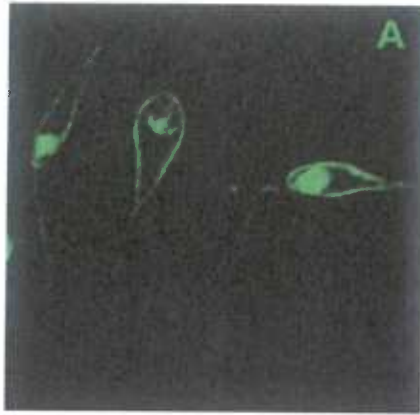


Chapter 3: MANUSCRIPT 2

FIG. 3.4. Deconvolution microscopy of Δ ldnt1/ Δ ldnt2 transfectants.

Live parasites were prepared for deconvolution microscopy as described in the Experimental Procedures. Deconvolved fluorescent images of Δ ldnt1 / Δ ldnt2 parasites overexpressing GFP-LdNT2 (Panel A), GFP-N175I (Panel B), GFP-N175I/D389N (Panel C), GFP-D389N (Panel D).

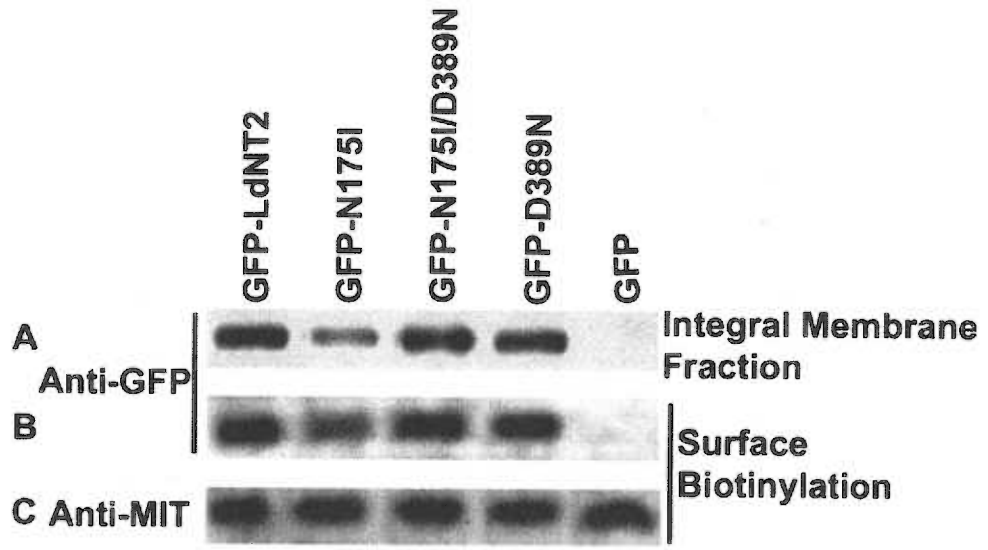
Section: 3.6 FIGURES



Chapter 3: MANUSCRIPT 2

FIG. 3.5. Cell surface expression of wild type and mutant *ldnt2* in $\Delta ldnt2$ transfectants.

Panel A, Detection of GFP in integral membrane protein fractions prepared from GFP-*LdNT2* and GFP-*ldnt2* mutants using a anti-GFP antibody. Panel B, Live parasites were subjected to cell surface biotinylation, lysis, immunoprecipitation, and Western analysis using a GFP antibody as described in the Experimental Procedures. Panel C, Detection of an endogenous transporter, MIT, used as a control to demonstrate equal loading of lanes in the cell surface biotinylation western analysis.

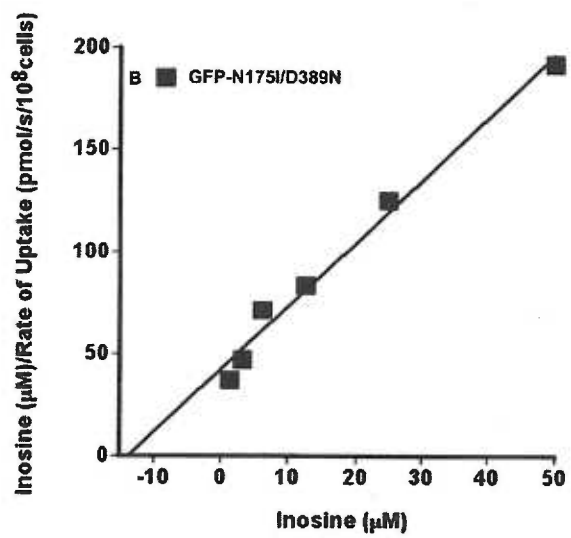
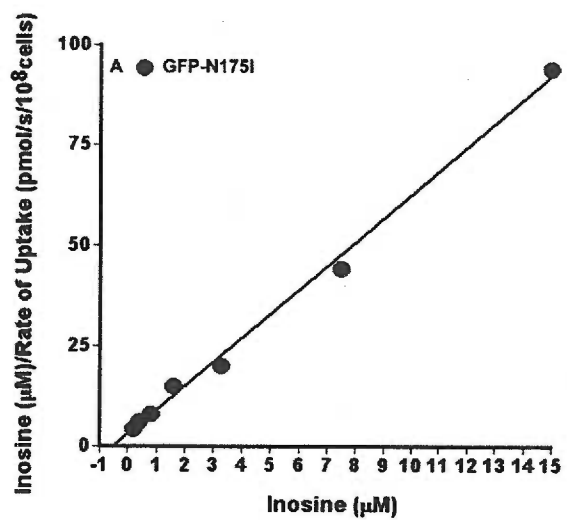


Chapter 3: MANUSCRIPT 2

FIG. 3.6. Asn¹⁷⁵ mutant transporter kinetics.

Uptake of [³H]inosine by $\Delta dnt1/\Delta dnt2$ cells expressing GFP-N175I (●) and GFP-N175I/D389N (■) was determined over 60s. The experiments were performed at a range of [³H]inosine concentrations (0.2 – 15 μ M for GFP-N175I and 1.3 – 50 μ M for GFP-N175I/D389N) and the rate of uptake was determined for each concentration by linear regression analysis. The results represented as a Hanes analysis (24) are expressed as inosine(μ M)/rate of uptake (pmol/s/ 10^8 cells) as a function of inosine (μ M). The calculated kinetic parameters are reported in Table III.

Section: 3.6 FIGURES



Chapter 3: MANUSCRIPT 2

FIG. 3.7. Multiple sequence alignment of predicted TM4 – TM5 region of ENT family members.

hENT1 (AAF02777), hENT2 (Q14542), TbAT1 (AAD45278), TbNT2 (AAF04490), LdNT1 (AAC32597), and LdNT2 (AAF74264), were aligned by Vector NTI® (Boston, MA). Amino acids identical among all aligned domains are *shaded black*, and highly conserved amino acids are *shaded gray*. The column of Asn¹⁷⁵ of LdNT2 is shaded dark gray and denoted by an arrowhead.

Section: 3.6 FIGURES

```

hENT1 146 ...KIVLINSFGAT L QGSLF LA LL PAS T A P IMS G Q L A G F F A V A M C A I ...
hENT2 133 ...SVCFINFSFAV L QGSLF QL TMP T S T L FLS G Q L A G F F A A A M S M ...
TbAT1 128 ...IAIAN VAMT L C D A G N A L I P P K Y S V V W G I A V C G V T F F S V I K T ...
TbNT2 130 ...VAFVC ISMT L C D S S N A L A P P K Y G A T V W G L A V S G I M T F L A V I Q ...
LdNT1 145 ...TGFIG FGK S F E S T T Y M F C A P S T S T M M G G V M S G V L T S E L Q I V K ...
LdNT2 147 ...VAMMG LSKA L C D S C T N A L V P P K M N G A Q W G L T V I A L F M S E I Q I I Q V ...

```

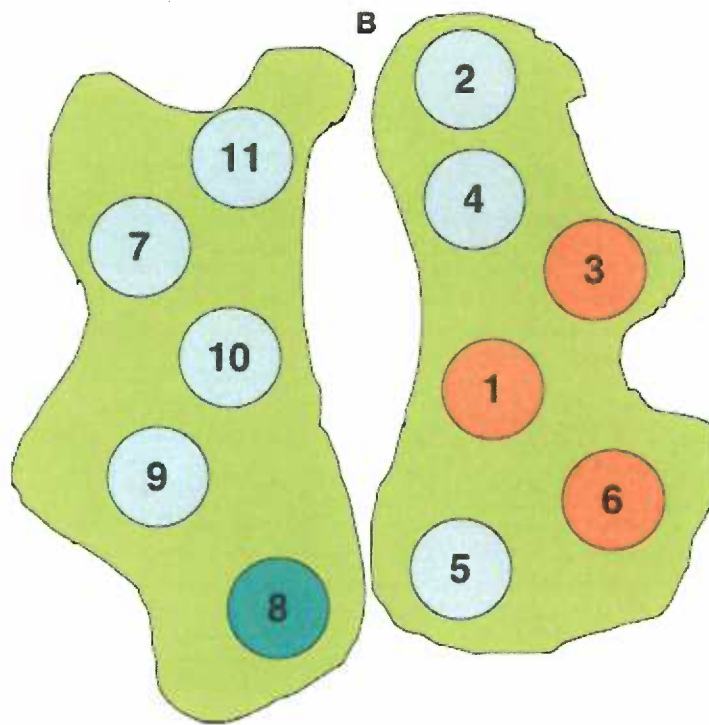
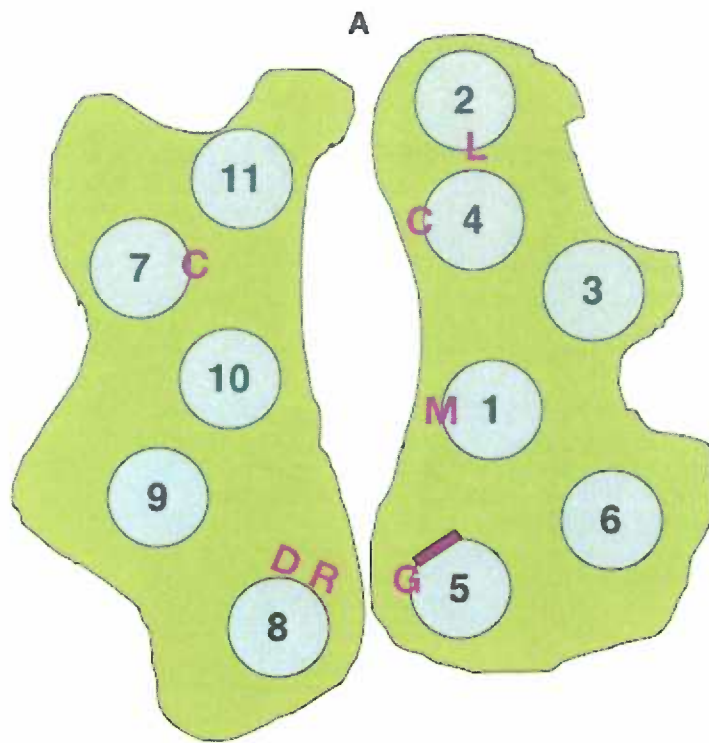
▲

TM 4
TM 5

Chapter 3: MANUSCRIPT 2

FIG. 3.8. Tertiary topology prediction.

Panel A, The schematic of the predicted helical arrangement is shown with the residues that have been found to be critical in ligand binding as described in chapter 1 are highlighted in *dark purple*. The *dark purple* rectangle on TM5 denotes the face of TM5 that was found to be solvent accessible as described in chapter 1. Panel B, The schematic depicts the clustering of the helixes accommodating the majority of the second-site suppressors as shown in *orange*, TM8 is shown in *teal*.



3.7 TABLES

TABLE I
Second-Site Suppressor Clones of D389N-Icnt2

Clone number	Suppressor Mutations
1	N175I
2	N175I, I345V
3	N175I, L123Q
4	N175I, D205G, W339R
5	Y213C
6	Y213C, R393Q
7	D159N, I220T
8	P52H, I209V
9	V124G, I218T, W339R
10	N84S, I118P, F214C
11	S50T
12	I327T, G365V, M378T

TABLE II
*Various Substitutions at Asn¹⁷⁵ within D389N-Idnt2 were Evaluated for
Yeast Growth on Inosine.*

<i>Substitution at Asn¹⁷⁵</i>	<i>Yeast growth phenotype</i>
Gly	-
Ala	-
Ser	-
Thr	-
Glu	-
Asp	-
Lys	-
Phe	-
Val	+
Leu	+

TABLE III

Kinetic parameters of Asn¹⁷⁵ GFP-Ldnt2 mutants.

The kinetic parameters, V_{\max} and K_m , were calculated according to the Hanes method (24). The relative expression was determined by densitometry on data obtained from western analysis of the cell surface biotinylation experiments where [GFP-LdNT2] expression was set to 100%. The results are expressed as mean \pm standard deviation ($n = 3$). The published kinetic parameters for GFP-LdNT2 are $V_{\max} = 14 \pm 5.3$ pmol/min/ 10^8 cells and $K_m = 1.3 \pm 0.6$ μ M (11).

Cell Line	V_{\max} (pmol/min/ 10^8 cells)	% Expression	Adjusted V_{\max}	K_m (μ M)
Δ ldnt1/ Δ ldnt2[GFP -N175I]	9.0 ± 1.8	51 ± 2.8	18	0.4 ± 0.2
Δ ldnt1/ Δ ldnt2[GFP -N175I/D389N]	16 ± 4.8	91 ± 13	18	11 ± 3.6

3.8 REFERENCES

1. Carter, N. S., Rager, N. & Ullman, B. (2003) in *Molecular Medical Parasitology* (Marr, J. J., Nilsen, T.W. and Komuniecki, R.W., ed), Academic Press, San Diego, CA
2. Carter, N. S., Drew, M. E., Sanchez, M., Vasudevan, G., Landfear, S. M., and Ullman, B. (2000) *J Biol Chem* **275**, 20935-20941
3. Vasudevan, G., Carter, N. S., Drew, M. E., Beverley, S. M., Sanchez, M. A., Seyfang, A., Ullman, B., and Landfear, S. M. (1998) *Proc Natl Acad Sci U S A* **95**, 9873-9878
4. Vasudevan, G., Ullman, B., and Landfear, S. M. (2001) *Proc Natl Acad Sci U S A* **98**, 6092-6097
5. SenGupta, D. J., Lum, P. Y., Lai, Y., Shubochkina, E., Bakken, A. H., Schneider, G., and Unadkat, J. D. (2002) *Biochemistry* **41**, 1512-1519

Chapter 3: MANUSCRIPT 2

6. Endres, C. J., SenGupta, D. J., and Unadkat, J. D. (2004) *Biochem J Pt*
7. Sundaram, M., Yao, S. Y., Ng, A. M., Griffiths, M., Cass, C. E., Baldwin, S. A., and Young, J. D. (1998) *J Biol Chem* **273**, 21519-21525
8. Visser, F., Vickers, M. F., Ng, A. M., Baldwin, S. A., Young, J. D., and Cass, C. E. (2002) *J Biol Chem* **277**, 395-401
9. Baldwin, S. A., Beal, P. R., Yao, S. Y., King, A. E., Cass, C. E., and Young, J. D. (2004) *Pflugers Arch* **447**, 735-743
10. Carter, N. S., Landfear, S. M., and Ullman, B. (2001) *Trends Parasitol* **17**, 142-145
11. Arastu-Kapur, S., Ford, E., Ullman, B., and Carter, N. S. (2003) *J Biol Chem* **278**, 33327-33333
12. Vickers, M. F., Mani, R. S., Sundaram, M., Hogue, D. L., Young, J. D., Baldwin, S. A., and Cass, C. E. (1999) *Biochem J* **339 (Pt 1)**, 21-32

Section: 3.8 REFERENCES

13. De Koning, H. P., Al-Salabi, M. I., Cohen, A. M., Coombs, G. H., and Wastling, J. M. (2003) *Int J Parasitol* **33**, 821-831
14. Sikorski, R. S., and Hieter, P. (1989) *Genetics* **122**, 19-27
15. Guthrie, C. F., G.R. (1991) *Guide to Yeast Genetics and Molecular Biology*, Academic Press, San Diego, CA
16. Sambrook, J., Fritsch, E.F., & Maniatis, T. (1989) *Molecular Cloning: A laboratory Manual*, Second Ed. (Nolan, C., Ed.), Cold Spring Harbor Laboratory Press, Cold Spring Harbor
17. Iovannisci, D. M., and Ullman, B. (1983) *J Parasitol* **69**, 633-636
18. Ha, D. S., Schwarz, J. K., Turco, S. J., and Beverley, S. M. (1996) *Mol Biochem Parasitol* **77**, 57-64
19. Labbe, S., and Thiele, D. J. (1999) *Methods Enzymol* **306**, 145-153
20. Colon, M., and Walworth, N. C. (2004) *Methods Mol Biol* **241**, 175-187

Chapter 3: MANUSCRIPT 2

21. Agatep, R., Kirkpatrick, R.D., Parchaliuk, D.L., Woods, R.A., & Gietz, R.D. (1998) *Technical Tips Online*, <http://tto.trends.com>
22. Aronow, B., Kaur, K., McCartan, K., and Ullman, B. (1987) *Mol Biochem Parasitol* **22**, 29-37
23. Kapler, G. M., Coburn, C. M., and Beverley, S. M. (1990) *Mol Cell Biol* **10**, 1084-1094
24. Hanes, C. S. (1932) *Biochem J* **26**, 1406
25. Baker, D., and Sali, A. (2001) *Science* **294**, 93-96
26. Drew, M. E., Langford, C. K., Klamo, E. M., Russell, D. G., Kavanaugh, M. P., and Landfear, S. M. (1995) *Mol Cell Biol* **15**, 5508-5515
27. Sundaram, M., Yao, S. Y., Ingram, J. C., Berry, Z. A., Abidi, F., Cass, C. E., Baldwin, S. A., and Young, J. D. (2001) *J Biol Chem* **276**, 45270-45275
28. Orengo, C. A., Bray, J. E., Hubbard, T., LoConte, L., and Sillitoe, I. (1999) *Proteins Suppl* **3**, 149-170

Section: 3.8 REFERENCES

29. He, M. M., Voss, J., Hubbell, W. L., and Kaback, H. R. (1995) *Biochemistry* **34**, 15667-15670
30. Green, A. L., Hrodey, H. A., and Brooker, R. J. (2003) *Biochemistry* **42**, 11226-11233
31. Cain, S. M., Matzke, E. A., and Brooker, R. J. (2000) *J Membr Biol* **176**, 159-168
32. Abramson, J., Smirnova, I., Kasho, V., Verner, G., Kaback, H. R., and Iwata, S. (2003) *Science* **301**, 610-615
33. Palczewski, K., Kumasaka, T., Hori, T., Behnke, C. A., Motoshima, H., Fox, B. A., Le Trong, I., Teller, D. C., Okada, T., Stenkamp, R. E., Yamamoto, M., and Miyano, M. (2000) *Science* **289**, 739-745
34. Meltzer, J. C., Sanders, V., Grimm, P. C., Stern, E., Rivier, C., Lee, S., Rennie, S. L., Gietz, R. D., Hole, A. K., Watson, P. H., Greenberg, A. H., and Nance, D. M. (1998) *Brain Res Brain Res Protoc* **2**, 339-351

Chapter 3: MANUSCRIPT 2

35. Veenhoff, L. M., Geertsma, E. R., Knol, J., and Poolman, B. (2000) *J Biol Chem* **275**, 23834-23840
36. Amillis, S., Koukaki, M., and Diallinas, G. (2001) *J Mol Biol* **313**, 765-774
37. Dogovski, C., Pi, J., and Pittard, A. J. (2003) *J Bacteriol* **185**, 6225-6232
38. Hall, J. A., Fann, M. C., and Maloney, P. C. (1999) *J Biol Chem* **274**, 6148-6153
39. Johnson, J. L., and Brooker, R. J. (2003) *Biochemistry* **42**, 1095-1100
40. Yao, S. Y., Ng, A. M., Sundaram, M., Cass, C. E., Baldwin, S. A., and Young, J. D. (2001) *Mol Membr Biol* **18**, 161-167
41. Yao, S. Y., Ng, A. M., Vickers, M. F., Sundaram, M., Cass, C. E., Baldwin, S. A., and Young, J. D. (2002) *J Biol Chem* **277**, 24938-24948
42. Valdes, R., Vasudevan, G., Conklin, D., Landfear, S.M. (2004) *Biochemistry* manuscript in press.

Section: 3.8 REFERENCES

43. SenGupta, D. J., and Unadkat, J. D. (2004) *Biochem Pharmacol* **67**, 453-458
44. Yao, S. Y., Sundaram, M., Chomey, E. G., Cass, C. E., Baldwin, S. A., and Young, J. D. (2001) *Biochem J* **353**, 387-393
45. Stewart, C., Bailey, J., and Manoil, C. (1998) *J Biol Chem* **273**, 28078-28084
46. Acimovic, Y., and Coe, I. R. (2002) *Mol Biol Evol* **19**, 2199-2210
47. Suel, G. M., Lockless, S. W., Wall, M. A., and Ranganathan, R. (2003) *Nat Struct Biol* **10**, 59-69

Chapter 4

MANUSCRIPT 3

Characterization of a Truncated *Leishmania donovani* Inosine-Guanosine Transporter

Shirin Arastu-Kapur, Nicola S. Carter, & Buddy Ullman

Department of Biochemistry and Molecular Biology

Oregon Health & Science University, Portland, OR 97239

4.1 ABSTRACT

LdNT2 from *Leishmania donovani* is a member of the equilibrative nucleoside transporter family, a group of membrane proteins that possess 19 conserved residues located mostly in predicted membrane-spanning domains. One of these conserved residues, Trp³⁷⁶ in TM8 was shown to be mutated to a STOP codon in clonal isolates of a chemically mutagenized wild-type *L. donovani* selected for resistance to formycin B, a toxic inosine analog. Furthermore, an occurrence of this mutation in *LdNT2* upon a subsequent chemical mutagenesis of *L. donovani*, suggested that either the Trp³⁷⁶ residue is prone to mutation or the wild-type *L. donovani* has a STOP codon on one of the *LdNT2* copies. Restriction fragment length polymorphism at the Trp³⁷⁶ locus indicates that the wild-type *L. donovani* has two functional copies of *LdNT2*. Expression of a W376X *ldnt2* mutant with an amino terminus green fluorescent tag in a $\Delta ldnt1/\Delta ldnt2$ *L. donovani* knockout cell line revealed that although the truncation mutant is expressed, it mislocalizes to the endoplasmic reticulum and a faint appearance at the plasma membrane is observed. The truncation mutant is not functional. These data demonstrate that TMs 8 - 11 are critical for the proper localization and function of LdNT2.

4.2 INTRODUCTION

Leishmania donovani is the causative agent of visceral leishmaniasis, a disease that is invariably fatal if untreated. Nucleoside permeation into *L. donovani* is mediated by two high affinity transporters with non-overlapping ligand specificity, LdNT1 and LdNT2. LdNT1 transports adenosine and pyrimidine nucleosides, whereas LdNT2 is selective for inosine and guanosine (1,2). Based on their primary structures and predicted membrane topologies, LdNT1 and LdNT2 belong to the equilibrative nucleoside transporter (ENT) family first described in mammals (3).

LdNT1 and LdNT2 were first described in chemically mutagenized cell lines of wild-type *Leishmania donovani*, DI700, which were isolated for their resistance to growth inhibition by cytotoxic nucleoside analogs were isolated (4). DI700 resistant to the inosine analog formycin B (FBD5 cell line) abolished LdNT2 transport capability; while, DI700 resistant to the adenosine analog tubercidin (TUBA5 cell line) abolished LdNT1 transport capability (4). Recently, sequencing of the *ldnt1* alleles in TUBA5 revealed two point mutations, C337Y in TM7 and G183D in TM5 (5). Interestingly, Gly¹⁸³ was found to be a ligand selectivity determinant in LdNT1 (5). A similar sequencing study of the *ldnt2*

Section: 4.3 EXPERIMENTAL PROCEDURES

alleles in FBD5 to determine the point mutations that confer formycin B resistance revealed two point mutations, S189T in TM 5 and W376X (stop) on the extracellular edge of TM 8 (Galazka *et al*, unpublished). Interestingly, when the same chemical mutagenesis was repeated recently on DI700 cells, the same W376X mutation reoccurred (Galazka *et al*, unpublished) on one of the *ldnt2* alleles. This suggested that Trp³⁷⁶, a conserved residue, is either prone to mutagenesis or one of the *LdNT2* alleles in DI700 harbors a STOP codon at position 376 (Fig. 2-1). Through restriction fragment length polymorphism studies we show in the present report that Trp³⁷⁶ is likely a locus prone to mutagenesis. The W376X mutant was expressed with an amino terminus green fluorescent protein (GFP) tag to determine if it targets properly. The data suggest that TMs 8 – 11 are required for proper and robust localization although, some fluorescence can be observed at the plasma membrane. As indicated by the selection of W376X mutant for formycin B resistance, TMs 8 – 11 are essential for inosine transport.

4.3 EXPERIMENTAL PROCEDURES

Culture Methods –*L. donovani* promastigotes were cultured at 26 °C in DME-L medium (Invitrogen) as described (6). DI700 and FBD5 strains were

Chapter 4: MANUSCRIPT 3

propagated as described (4). The $\Delta Idnt1/\Delta Idnt2$ strain (7) and the $\Delta Idnt2$ strain (8) were propagated as described. The *LdNT2* heterozygote cell line, *LdNT2^{+/hyg}*, was propagated similar to the $\Delta Idnt2$ strain. Transfectants of $\Delta Idnt1/\Delta Idnt2$ with pXG-GFP+2' (7) were propagated as described (8).

Restriction Fragment Length Mapping of LdNT2 alleles at the Trp³⁷⁶ locus

– The W376X mutation causes a loss of an *Rsa I* restriction site into the mutant *Idnt2* gene. Genomic DNA was isolated from $\Delta Idnt2$, *LdNT2^{+/hyg}*, FBD5, and DI700 cell lines according to established methods (10). The genomic DNA served as a template for amplifying a 700 base pair fragment of *LdNT2* with the Advantage®-HF 2 PCR Kit (BD Biosciences, Palo Alto, CA). The sense primer used was 5'-ATCGCTGAGTTCCGTGCTGCTGCGCTGCGCCG-3' and the antisense primer was 5'-AAGGATCCTCTAGATTAGTAGGTCAGGGTTATGGC-3'. The products were digested with *Rsa I* and fractionated on a 3% agarose gel.

Introduction of Trp mutant into Idnt2 - Mutations in *LdNT2* were generated, confirmed, and transfected as described (8).

Transport Assays - Nucleoside transport measurements in *L. donovani* promastigotes were performed by a previously described oil-stop method (11). Time courses were generated using 10 μ M [³H]inosine (0.2 Ci/mmol). [³H]inosine (19.5 Ci/mmol) was purchased from Moravек Biochemicals, Inc. (Brea, CA).

Integral Membrane Protein Preparations and Immunoblotting – Crude membrane fractions were prepared as described (8). The expression of the

truncated mutant *ldnt2* gene in *L. donovani* was determined by immunoblotting as described (8).

Fluorescence Microscopy – *Leishmania* cells expressing the transporter tagged with GFP were prepared, affixed on slides, and imaged as described (7).

4.4 RESULTS

Restriction Fragment Length Mapping of LdNT2 at the Trp³⁷⁶ locus – 700 bp fragments were obtained from PCR reactions on the genomic DNA of *LdNT2+/hyg*, DI700, and FBD5 cell lines (Fig. 4-1, lanes 3,5,7). There was no product amplified from the $\Delta ldnt2$ knockout cell line. *Rsa I* digest of DI700 and *LdNT2+/hyg* were similar; while, FBD5 had an extra 500 bp band resulting from the loss of *Rsa I* site on one of its *LdNT2* gene copies.

Creation and Evaluation of ldnt2 Mutants in Leishmania – The W376STOP mutation was inserted into *LdNT2* within the expression construct *pXG-GFP2+/-LdNT2*. The mutant constructs were transfected into $\Delta ldnt1/\Delta ldnt2$ *L. donovani* to create $\Delta ldnt1/\Delta ldnt2[W376X]$, $\Delta ldnt1/\Delta ldnt2$ harboring wild-type *LdNT2* or GFP alone were created as controls. In the $\Delta ldnt1/\Delta ldnt2$ cell line both *LdNT1* and *LdNT2* genes have been deleted and these cells are consequently, deficient in purine nucleoside transport. To verify the function of $\Delta ldnt1/\Delta ldnt2[W376X]$, the

Chapter 4: MANUSCRIPT 3

transfectant was evaluated at 10 μM [^3H]inosine, ligand concentrations which previously were shown to be saturating for LdNT2 transport (1).

$\Delta\text{ldnt1}/\Delta\text{ldnt2}[\text{W376X}]$ exhibited no detectable transport capability, which is similar to the level of the $\Delta\text{ldnt1}/\Delta\text{ldnt2}$ cell line (Fig. 4-3).

Cell surface targeting of GFP-Ldnt2 - To determine whether the W376X mutation affected proper targeting or expression of the transporter the mutant transporters were tagged with GFP at the NH_2 -terminus and the corresponding genes transfected into the $\Delta\text{ldnt1}/\Delta\text{ldnt2}$ background. Previous studies established that the NH_2 -terminal GFP tag does not significantly affect the ligand affinity of LdNT2 (8). Also, localization studies done previously using direct GFP fluorescence and deconvolution microscopy demonstrated that GFP-LdNT2 was robustly synthesized and targeted to both the plasma membrane and flagellum, while a diffuse and relatively weak cytosolic GFP fluorescence was observed with parasites transfected with the empty pXG-GFP+2' vector alone (8). W376X-Ldnt2 appears to accumulate in the endoplasmic reticulum and faint staining at the plasma membrane can be detected (Fig. 4-4). However, there is no staining at the flagellum or flagellar pocket (Fig. 4-4). Furthermore, integral membrane western analysis revealed that the truncated W376X-Ldnt2 protein is expressed at significant levels (Fig. 4-4).

4.5 DISCUSSION

The W376X mutation occurred in two separate chemical mutagenesis studies suggesting that Trp³⁷⁶ is either prone to mutagenesis or one of the *LdNT2* copies in DI700 carries the W376X mutation. The data show that Trp³⁷⁶ is likely to be prone to mutagenesis (Fig. 4-2). Furthermore, the truncation mutant expressed with an amino terminal GFP tag is expressed and detectable by an integral membrane immunoblot, but does not target properly and is nonfunctional (Fig. 4-3 & 4). The faint staining at the plasma membrane could be protein that has escaped the endoplasmic reticulum, however, it is interesting that no flagellar pocket staining is observed since it is thought to be the station for sorting of membrane proteins (12). Cell surface biotinylation studies will have to be performed to confirm the presence of W376X *Ldnt2* mutant at the plasma membrane. Furthermore, the deletion of an evolutionarily conserved region TM8 - TM10 (13), likely hinders the proper insertion of *LdNT2* into the membrane. Recently, a W258X mutation of TM 6 – TM 7 loop of the human uric acid transporter, a member of the major facilitator superfamily, was found to reoccur in patients with Japanese renal hypouricemia, and upon microinjections of the transporter cRNA in *Xenopus* oocytes it was not expressed (14,15). If the MFS and the ENTs are similar in their global translocation mechanism, then perhaps the W258X truncation of the uric acid transporter is analogous to the W376X *Ldnt2* truncation

Chapter 4: MANUSCRIPT 3

(Chapter 3). Furthermore, since a truncation mutant consisting of the last 5 TMs out of 12 TMs of the human Na⁺/glucose cotransporter, a member of the MFS, was purified from *E. coli* and determined to be functional, it may be interesting to express TMs 8 – 11 of the ENTs on their own (16).

Trp that are critical for transporter function play a role in ligand stacking such as the sugar ring stacking with the Trp aromatic within the binding pocket of lactose permease, a paradigm transporter from *E. coli* (17). Conversely, Trp that are critical in transporter expression mediate lipid-protein interactions such as the role of Trp in the shaker potassium channel (18). Trp³⁷⁶ may be critical in anchoring since it is highly conserved and is predicted to be located at the cusp on the extracellular edge of TM8 (Fig. 2-1). Further site-directed mutagenesis have been initiated at Trp³⁷⁶ to Ala, Phe, and Tyr, which may lead to insights into the role of this conserved residue.

Acknowledgements - This work was supported in part by grants RO1 AI23682 and RO1 AI44138 from the National Institutes of Health (B.U.). S.A. has received financial support from the N.L.Tartar Research Fellowship from the Oregon Health & Science University.

4.6 FIGURES

FIG. 4.1. Restriction Fragment Length Polymorphism at Trp^{376} locus.

The *Rsa* I digested 700 bp amplified products from genomic DNA of Δldnt2 , $\text{LdNT2}^{+/hyg}$, DI700, and FBD5 were fractionated on a 3% agarose gel. The odd numbered lanes show the 700 bp uncut fragment of *LdNT2* amplified from genomic DNA of Δldnt2 , $\text{LdNT2}^{+/hyg}$, DI700, and FBD5 cell lines. The even numbered lanes show an *Rsa* I digest pattern of the 700 bp amplified fragment.

Chapter 4: MANUSCRIPT 3

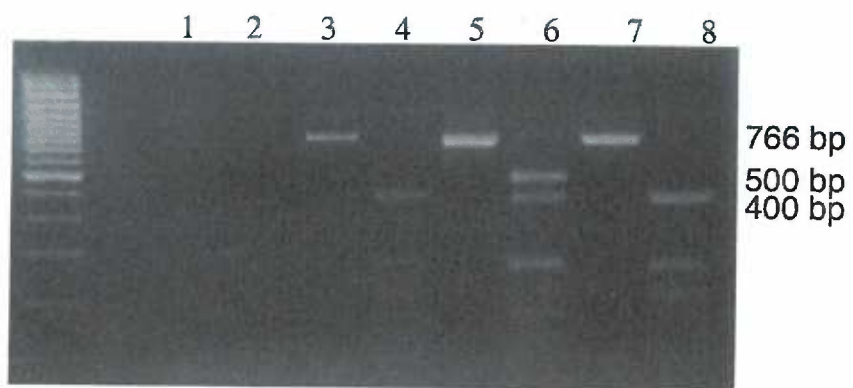


FIG. 4.2. Functional characterization of W376X-Ldnt2 mutant.

Δldnt1 /Δldnt2 parasites expressing *Δldnt1 /Δldnt2*[LdNT2] (■) *Δldnt1 /Δldnt2*[W376X] (●), *Δldnt1 /Δldnt2* (▲) were tested for uptake of 10 μM [³H]inosine over 4 min. Results are expressed as mean ± standard deviation (*n* = 2).

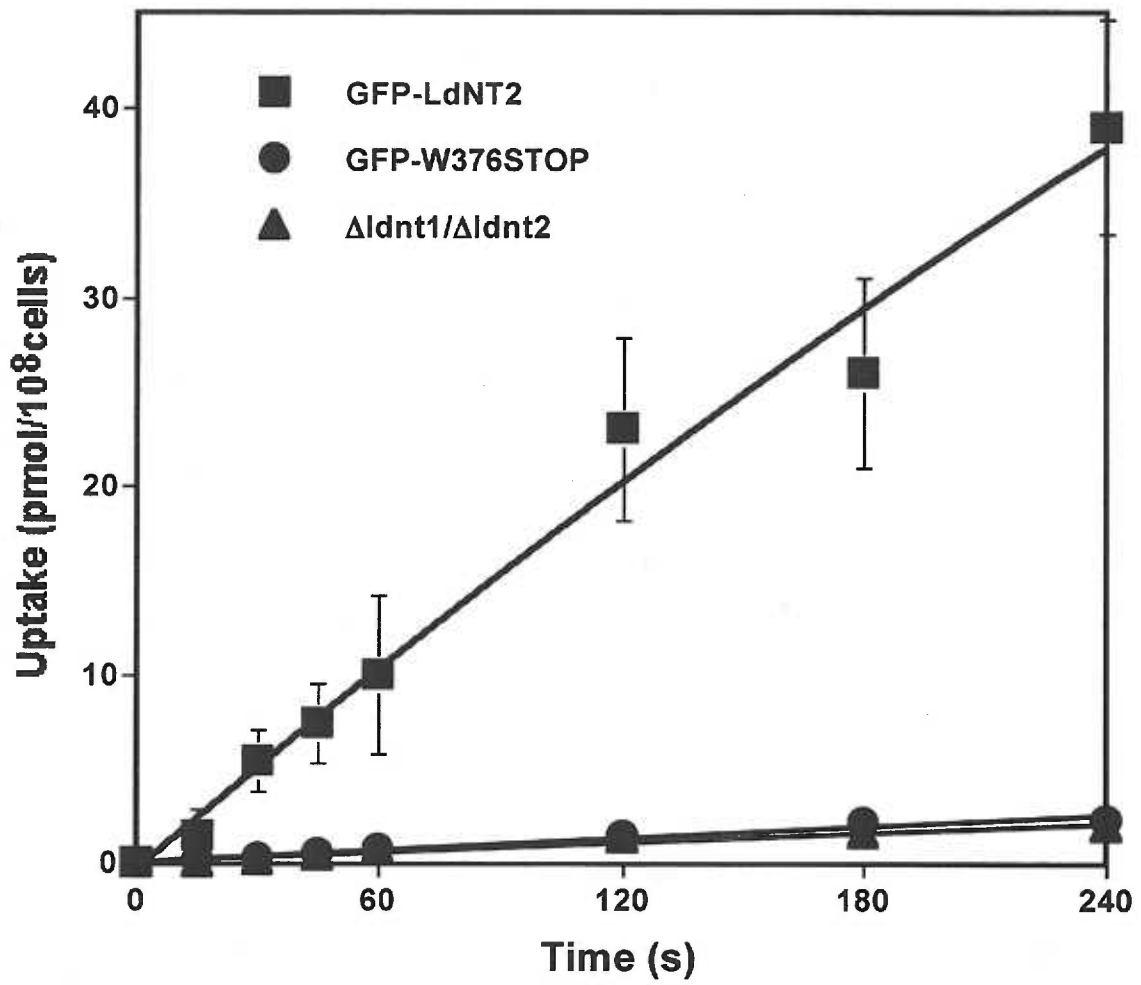
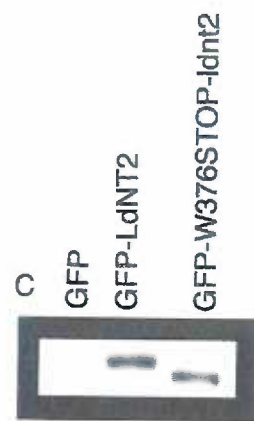
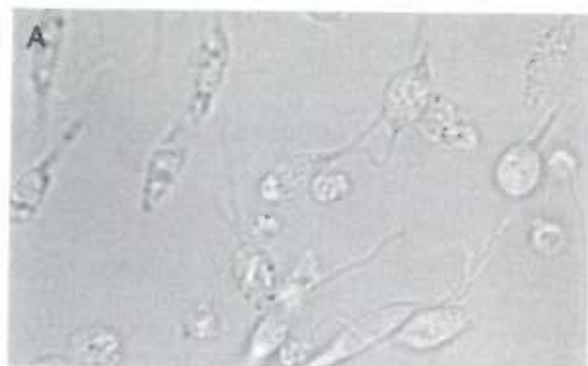


FIG. 4.3. Expression of W376X-Ldnt2 in Δ ldnt1 / Δ ldnt2 transfectants.

Live parasites were prepared for deconvolution microscopy as described in the Experimental Procedures. Panel A, Phase images of Δ ldnt1 / Δ ldnt2 parasites overexpressing GFP-W376X. Panel B, Deconvolved fluorescent image of. Panel C, Detection of GFP in integral membrane protein fractions prepared from GFP-LdNT2 and GFP-W376X-Ldnt2 mutants using a GFP antibody.

Chapter 4: MANUSCRIPT 3



4.7 REFERENCES

1. Carter, N. S., Drew, M. E., Sanchez, M., Vasudevan, G., Landfear, S. M., and Ullman, B. (2000) *J Biol Chem* **275**, 20935-20941
2. Vasudevan, G., Carter, N. S., Drew, M. E., Beverley, S. M., Sanchez, M. A., Seyfang, A., Ullman, B., and Landfear, S. M. (1998) *Proc Natl Acad Sci U S A* **95**, 9873-9878
3. Griffiths, M., Beaumont, N., Yao, S. Y., Sundaram, M., Boumah, C. E., Davies, A., Kwong, F. Y., Coe, I., Cass, C. E., Young, J. D., and Baldwin, S. A. (1997) *Nat Med* **3**, 89-93
4. Iovannisci, D. M., Kaur, K., Young, L., and Ullman, B. (1984) *Mol Cell Biol* **4**, 1013-1019
5. Vasudevan, G., Ullman, B., and Landfear, S. M. (2001) *Proc Natl Acad Sci U S A* **98**, 6092-6097

Chapter 4: MANUSCRIPT 3

6. Iovannisci, D. M., and Ullman, B. (1983) *J Parasitol* **69**, 633-636
7. Arastu-Kapur, S., Arendt, C. S., Purnat, T., Carter, N. S., & Ullman, B. (2004) *J Biol Chem* manuscript in preparation
8. Arastu-Kapur, S., Ford, E., Ullman, B., and Carter, N. S. (2003) *J Biol Chem* **278**, 33327-33333
9. Ha, D. S., Schwarz, J. K., Turco, S. J., and Beverley, S. M. (1996) *Mol Biochem Parasitol* **77**, 57-64
10. Sambrook, J., Fritsch, E.F., & Maniatis, T. (1989) *Molecular Cloning: A laboratory Manual*, Second Ed. (Nolan, C., Ed.), Cold Spring Harbor Laboratory Press, Cold Spring Harbor
11. Aronow, B., Kaur, K., McCartan, K., and Ullman, B. (1987) *Mol Biochem Parasitol* **22**, 29-37
12. Landfear, S. M., and Ignatushchenko, M. (2001) *Mol Biochem Parasitol* **115**, 1-17

Section: 4.7 REFERENCES

13. Acimovic, Y., and Coe, I. R. (2002) *Mol Biol Evol* **19**, 2199-2210
14. Komoda, F., Sekine, T., Inatomi, J., Enomoto, A., Endou, H., Ota, T., Matsuyama, T., Ogata, T., Ikeda, M., Awazu, M., Muroya, K., Kamimaki, I., and Igarashi, T. (2004) *Pediatr Nephrol*
15. Enomoto, A., Kimura, H., Chairoungdua, A., Shigeta, Y., Jutabha, P., Cha, S. H., Hosoyamada, M., Takeda, M., Sekine, T., Igarashi, T., Matsuo, H., Kikuchi, Y., Oda, T., Ichida, K., Hosoya, T., Shimokata, K., Niwa, T., Kanai, Y., and Endou, H. (2002) *Nature* **417**, 447-452
16. Panayotova-Heiermann, M., Leung, D. W., Hirayama, B. A., and Wright, E. M. (1999) *FEBS Lett* **459**, 386-390
17. Vazquez-Ibar, J. L., Guan, L., Svrakic, M., and Kaback, H. R. (2003) *Proc Natl Acad Sci U S A* **100**, 12706-12711
18. Hong, K. H., and Miller, C. (2000) *J Gen Physiol* **115**, 51-58

Chapter 5

DISCUSSION

5.1 Asp³⁸⁹: Insights into function of LdNT2

Asp³⁸⁹ is likely involved in a network of electrostatic interactions that could be mediated by solvent molecules or hydrogen bonding. The complexity of electrostatic interaction networks that are crucial for transporter function were predicted in previous mutagenesis studies of lactose permease, member of the major facilitator superfamily (MFS), and have been recently confirmed through its crystal structures (1,2). In lactose permease of *E. coli*, there are four irreplaceable charged residues within transmembrane (TM) domains that play essential roles in proton translocation and coupling. One of these residues is Glu³²⁵ of lactose permease that reduces the transport capability when mutated to an Asp

(2). This is similar to what is observed for the highly conserved Asp³⁸⁹ of LdNT2 in chapter 2. In lactose permease, Glu³²⁵ was known to interact with Arg³⁰² in an adjacent helix (2). The E325D mutant of lactose permease was rescued by introducing conformational flexibility in the loop between the two helices by Gly scanning mutagenesis (2). In LdNT2, a candidate for charge-charge interaction with Asp³⁸⁹ is a conserved Arg⁴¹⁵ in TM9, which is the only other positively conserved charged residue besides Arg³⁹³ (Fig. 1-8). Arg⁴¹⁵ may not have been neutralized in the second-site suppressor screen because it may be an irreplaceable residue. A switch mutant between Asp³⁸⁹ and Arg⁴¹⁵ to determine if further studies are required has been initiated. Another reason Arg⁴¹⁵ or any other charged residue was not neutralized in the second-site suppressor screen is that the D389N mutant could retain its ability to maintain an electrostatic interaction since Asn have a propensity to hydrogen bond. Asn may lock the protein into a nonfunctional conformation due to hydrogen bonding rather than a functionally preferred charge-charge interaction. It would be interesting to repeat this study with another Asp³⁸⁹ mutant that will not participate in electrostatic interactions and is expressed but nonfunctional, such as a D389A mutant. Finally, the second-site suppressors that were obtained to suppress D389N phenotype are likely introducing conformational flexibility into a rigid D389N-Ldnt2 protein.

The second-site suppressor screen revealed Asn¹⁷⁵ as a residue that could suppress the D389N phenotype. It enhanced the transport capability of

Chapter 5: DISCUSSION

D389N-Icnt2 in yeast relative to LdNT2 and was significantly able to suppress the D389N phenotype in *Leishmania* (Fig. 3-2 and 3-3). Asn¹⁷⁵ is located at the cusp of TM 4 – TM 5 loop and the cytoplasmic face of TM 5 suggesting that this residue may be shifting the position of TM 5 (Fig. 3-1). This speculation was supported by the fact that the Protein Sequence Analysis server (bmerc-www.bu.edu/psa/) indicates that the N175I mutant obtained shifts the probability of loop to helix at the 175 position. An elongation of the TM 5 helix may affect its positioning within the lipid bilayer. Furthermore, it is intriguing that only large nonpolar substitutions (Ile, Leu, Val) work at Asn¹⁷⁵ to suppress the D389N phenotype. This suggests that it is a specific interaction that is being altered perhaps by volume compensation or the interaction of the position 175 with the lipid bilayer that could result in a shift of TM 5 relative to TM 8 (Table 3-II). It may be interesting to investigate whether Asn¹⁷⁵ can provide the conformational flexibility to increase the activity of D389E-Icnt2, a mutant that has ten fold lower activity than LdNT2 (Fig. 2-2).

Taken together, the studies on Asp³⁸⁹ indicate that it is a conformationally sensitive residue. It is likely to be involved in a critical electrostatic network that may be irreplaceable and thus could not be identified in the second-site suppressor screen. Or, it may be a residue that only transiently interacts with another charged residue to attain an intermediate translocation conformational state and thus, could be compensated for by an array of mutations.

5.2 Arg³⁹³: Insights into function and targeting of LdNT2

Arg residues play two important roles in TM domains. The first is to stabilize the structure by participating in a membrane-embedded electrostatic network (1). An example is Arg¹³⁵ of rhodopsin, which is involved in interactions that hold rhodopsin TMs 3 and 6 in close proximity (3). A R135L mutation found in the disease retinitis pigmentosa results in the loss of interactions and leads to structure destabilization (4). The second is that most of the membrane-buried Arg residues are located at the extremities of the membrane helices (1). This observation perhaps suggests the role of Arg residues in anchoring of TM domains to the membrane. For example, mutations of conserved arginines in the glucose transporter (GLUT1) impairs the proper TM topology (5).

R393L mutation in LdNT2 does not target properly to the plasma membrane (Fig. 2-4). However, the 7% of the protein that does target to the flagellum functions similar to LdNT2 (Table 2-II and Fig. 2-4, Panel D). The rest of the protein appears to be mistargeted to an organelle similar to the multivesicular tubular compartment, a terminal lysosome, which is indicative of an unstable or misfolded membrane protein (6,7). The small amount of R393L-Ldnt2 that does

Chapter 5: DISCUSSION

escape the endoplasmic reticulum quality control targets to the flagellar pocket and seems to either stay there or traffic to the flagellum (Fig. 2-4, Panel D). These data are similar to the R135L mutation phenotype in rhodopsin and perhaps indicate that Arg³⁹³ of LdNT2 is involved in electrostatic interactions important for the helix packing of the transporter (1). However, data with a series of double and switch discussed in chapter 2, support the hypothesis that Arg³⁹³ may be involved in critical membrane embedded electrostatic interactions. Only the substitutions that could retain the ability to maintain electrostatic interactions were even expressed. However, since the R393L mutant mainly targets to the flagellum, the data may also suggest that the fluidity of the plasma membrane is unable to trap the R393L-Ldnt2 in a stable conformation whereas, the rigidity of the flagellum (sterol rich) is able to trap the R393L-Ldnt2 in a functional conformation (8,9). Perhaps, Arg³⁹³ is a membrane anchor for LdNT2. Since Trp scanning mutagenesis has been employed to identify regions that may be associated with or interact with lipids within the membrane for the shaker potassium channel, a R393W mutation in LdNT2 could be useful to implicate the conserved Arg³⁹³ as a membrane anchor for the ENTs (10).

Unfortunately, little is known about membrane protein targeting and even less about flagellar targeting in kinetoplastids (Chapter 1). Thus, before the targeting of R393L-Ldnt2 to the flagellum can be investigated, it is critical to understand why GFP-LdNT2 targets to the flagellum. The direct fluorescence

Section: 5.2 Arg393: Insights into function and targeting of LdNT2

and immunofluorescence localization studies in chapter 2 were the first data to establish that LdNT2 localizes to the flagellum, plasma membrane, and flagellar pocket (Fig. 2-4 and 2-7). The flagellar pocket is thought to be a station for sorting of membrane proteins in kinetoplastids and thus fluorescence in this organelle was always observed with LdNT2/lmnt2 transporters tagged with GFP (Fig. 2-4 and 3-4). It is possible that overexpression on the GFP vector causes an overflow of the protein into the flagellum; however, LdNT1 tagged with GFP does not localize to the flagellum (11). There is evidence that membrane proteins move into the flagellum via lateral translocation from the flagellar pocket (12). Lipid rafts have been implicated in membrane lateral diffusion and consequently in the targeting of a variety of membrane proteins, such as the potassium channel (13). Lipid rafts are 50 nm wide sphingolipid and cholesterol rich microdomains found in biological membranes. The rafts have been implicated in cell signaling and membrane protein trafficking (13). Peripheral membrane proteins and monotopic membrane proteins associate with lipid rafts by post-translational modification moieties such as acylation, palmitoylation, and myristoylation (10,14,15). Recently, the localization of a 24 kDa flagellum calcium binding protein from *Trypanosoma cruzi* was shown to occur through the association of its acyl moieties with lipid rafts (16). *Trypanosoma cruzi* is a member of the *trypanosomatidae* family and the causative agent of chagas disease (17). Interestingly, according to ProSite analysis (<http://au.expasy.org/prosite/>) LdNT2

Chapter 5: DISCUSSION

has two myristoylation sites at the amino terminus, while LdNT1, which does not localize to the flagellum, does not have the myristoylation sites at the amino terminus. Gly³ starts the first predicted myristoylation site of LdNT2 with the motif GQSAAV and Gly¹⁰ starts the next predicted site with the motif GSNSAL. Also, since the ENTs have a very short carboxy terminus, it is likely that the targeting information is contained in the amino terminus or large loops. To investigate the role of lipid rafts in the targeting of LdNT2 to the flagellum, it will first be necessary to establish by fractionation and localization studies that LdNT2 does associate with the lipid rafts. Subsequent site-directed mutagenesis of the myristoylation sites will perhaps be able to establish the role of lipid rafts in plasma membrane targeting. Finally, since LdNT2 targets to the plasma membrane and flagellum, perhaps the question raised by Ldnt2-R393L is why does it not target to the plasma membrane. Once again, there is very little known on the targeting of membrane proteins to the parasite surface in *Leishmania*. Perhaps an initial experiment is to do an immunoprecipitation of metabolically labeled cells expressing LdNT2 and Ldnt2-R393L. Unfortunately, similar immunoprecipitation experiments were unsuccessful on the *Leishmania* glucose transporter isoforms, which exhibit differential targeting to either the plasma membrane (Iso I) or the flagellum exclusively (Iso II) (18).

5.3 Tertiary Topology Model

In the absence of a clear ligand affinity or specificity shift, mutational analyses without a three-dimensional prediction mainly result in a hypothesis that is corroborated by subsequent mutational studies. Threading analyses were undertaken to obtain a global view of the ENTs. Threading analysis is the identification of proteins that are similar at the secondary structural level rather than the primary structural level. These analyses have identified the MFS to be similar to the ENTs in their helix packing (Chapter 3). In fact, the helix packing is exactly alike between the two transporter families, except the loss of TM12 in the ENTs. Investigations with TM12 of lactose permease have shown that the majority of mutations in TM12 do not affect transporter function, however, a few do affect transporter expression and cause cell toxicity, suggesting a gross misfolding (19). The identification that ENTs are conformationally similar to the MFS by threading analyses demonstrates the conservation of structural determinants through evolutionarily distinct protein families. Furthermore, the known data for ligand selectivity and solvent accessible residues (reviewed in Chapter 1: Met³³ of TM1 hENT1, Leu⁹² of TM2 hENT1, Cys¹⁴⁰ of TM4 rENT1, Gly¹⁸³ of TM5 LdNT1, Met¹⁷⁶, Thr¹⁸⁶, Ser¹⁸⁷, Gln¹⁹⁰, Val¹⁹³, and Lys¹⁹⁴ of TM5 LdNT1) logically mapped onto the three-dimensional prediction with these residues facing the predicted pore, suggesting that the hydrophilic face of the helices are oriented

Chapter 5: DISCUSSION

correctly. Indeed, the helices predicted to be in the ligand pore by mutagenesis studies, TMs 1, 2, 4, and 5, are predicted to form the core in the three-dimensional model. Unfortunately, there is no interhelical interaction data for the ENTs to be able to corroborate the model. However, the model for the helix packing of ENTs does support the second-site suppressor data of chapter 3. The second-site suppressor mutations that seem to occur in four distinct clusters across the ENT secondary topology (Fig. 3-1), do cluster to one region on the three-dimensional model (Fig. 3-8). Furthermore, Asn¹⁷⁵ and Asp³⁸⁹ are in proximity on the model.

Future experiments that can be pursued to validate the model would likely be based on the established methods employed for lactose permease: engineering divalent metal-binding sites within the permease (20-22), site-directed chemical cleavage (23), site-directed spin labeling and chemical crosslinking (24), and disulfide bond formation between paired Cys residues (25). Site-directed spin labeling, crosslinking, and disulfide bond formation require a Cys-less mutant, which has been difficult to generate. LdNT2 has seven Cys that are mainly located within TM domains. There are four Cys found in two pairs with the motif CXXC; one pair is at the TM 4 cytoplasmic cusp and the second pair is at the cytoplasmic cusp of TM 10. Interestingly, substitutions to Ser of all the unpaired Cys, positions 351, 425, and 486, did not affect transporter function, expression and localization (26). The Cys in pairs, 158 & 161 and 455 & 458, did

not tolerate Ser substitutions. However, these Cys are likely not involved in disulfide bonds within the pairs since a subsequent attempt at generating a Cys-less Ldnt2, which was successful in removing two more Cys one from each pair with the following mutations, C158L and C455A (Arendt *et al*, unpublished). On the other hand, a Cys-less LdNT1 does exist which should be amenable to these studies (27).

Furthermore, The techniques established to understand helix packing of a transporter mentioned above require the purification and reconstitution of the transporter, which could prove to be another challenge. However, *in vivo* approaches have also been recently established. The first *in vivo* approach is to express two halves of the protein, each containing a single Cys and then assay for crosslinking efficiency and transport activity. This technique could be done in *Leishmania*, the host environment of LdNT1, however, it would first have to be determined whether the two halves of the wild-type LdNT1 can complement each other *in vivo*. This technique has been successfully developed and employed for the lactose permease by Wu *et al* (28). The second *in vivo* approach is to employ repeated second-site suppressor screens with various first site mutations to observe a pattern of mutations, which can then be placed in proximity to each other. This method has been successfully developed and employed for the lactose permease by Brooker *et al* (29-31). Furthermore, this method has already been developed and established for LdNT2 in chapter 3 of this thesis.

5.4 Concluding Remarks

Less than decade ago, the first of the ENTs were cloned and characterized. The translocation mechanism of the ENTs is slowly, but steadily being unveiled through mutagenesis. The ENTs not only serve an important physiological function, but are also a significant therapeutic target since they are the mode of entry for efficacious anticancer and antiviral agents such as cytarabine and zalcitabine respectively (32). Furthermore, they are excellent targets for anti-parasitic agents, since all protozoan parasites known to date are incapable of *de novo* purine biosynthesis and must rely on their host for these essential nutrients. Thus, the delivery of a toxic compound through the ENTs is a plausible antiparasitic drug strategy since pyrimidine analogs such as allopurinol are taken up through the ENTs (12). Understanding the general mechanism of the ENTs is imperative before the nuances between different members of the family can be exploited to develop better therapeutic agents. In this thesis, the generalized mechanism was explored through forward and reverse genetics. The study began with site-directed mutagenesis of two conserved charged residues of the ENTs, Asp³⁸⁹ and Arg³⁹³ of LdNT2. Asp³⁸⁹ was critical in transporter function, while Arg³⁹³ was key for protein expression and targeting (Chapter 2). A subse-

quent second-site suppressor screen bolstered Asp³⁸⁹ as a conformationally sensitive residue in the translocation mechanism of the ENTs (Chapter 3). However, to understand the array of second-site suppressor mutants obtained a tertiary topology prediction was sought through the emerging bioinformatics tools, specifically, threading analysis. Although this is a prediction and not yet confirmed, this three-dimensional prediction provides an important global view of the ENTs. It is a significant advance enabling key residues previously identified through mutagenesis studies to be located onto a three dimensional ENT template. It will also serve as a model for future mutagenesis studies to identify key residues in TMs predicted to form the ligand binding pocket by the three-dimensional model, namely TMs 1, 2, 4, 5, 8, 10, and 11. Interestingly, mutagenesis data already predict TMs 1, 2, 4, and 5 to line the ligand pore. Finally, the three-dimensional prediction was built on the MFS as a template, suggesting the conservation of structural determinants to define a general functional phenomenon (transport) through evolutionarily diverse proteins (Chapter 3).

Chapter 5: DISCUSSION

5.5 References

1. Partridge, A. W., Therien, A. G., and Deber, C. M. (2004) *Proteins* **54**, 648-656
2. Weinglass, A. B., Smirnova, I. N., and Kaback, H. R. (2001) *Biochemistry* **40**, 769-776
3. Palczewski, K., Kumasaka, T., Hori, T., Behnke, C. A., Motoshima, H., Fox, B. A., Le Trong, I., Teller, D. C., Okada, T., Stenkamp, R. E., Yamamoto, M., and Miyano, M. (2000) *Science* **289**, 739-745
4. <http://www.hgmd.org>.
5. Sato, M., and Mueckler, M. (1999) *J Biol Chem* **274**, 24721-24725
6. Ghedin, E., Debrabant, A., Engel, J. C., and Dwyer, D. M. (2001) *Traffic* **2**, 175-188

Section: 5.5 References

7. Mullin, K. A., Foth, B. J., Ilgoutz, S. C., Callaghan, J. M., Zawadzki, J. L., McFadden, G. I., and McConville, M. J. (2001) *Mol Biol Cell* **12**, 2364-2377
8. da Cunha e Silva, N. L., Hasson-Voloch, A., and de Souza, W. (1989) *Mol Biochem Parasitol* **37**, 129-136
9. Landfear, S. M., and Ignatushchenko, M. (2001) *Mol Biochem Parasitol* **115**, 1-17
10. Monks, S. A., Needleman, D. J., and Miller, C. (1999) *J Gen Physiol* **113**, 415-423
11. Vasudevan, G., Ullman, B., and Landfear, S. M. (2001) *Proc Natl Acad Sci U S A* **98**, 6092-6097
12. Vasudevan, G. (2001) in *Biochemistry and Molecular Biology*, Oregon Health and Science University, Portland
13. Martens, J. R., O'Connell, K., and Tamkun, M. (2004) *Trends Pharmacol Sci* **25**, 16-21

Chapter 5: DISCUSSION

14. Melkonian, K. A., Ostermeyer, A. G., Chen, J. Z., Roth, M. G., and Brown, D. A. (1999) *J Biol Chem* **274**, 3910-3917
15. Zhang, W., Tribble, R. P., and Samelson, L. E. (1998) *Immunity* **9**, 239-246
16. Qiao, X., Lee, P. & Lee, M.G. (2002) in *Molecular Parasitology Meeting XIV*, Woods Hole, MA
17. Bogtish, B. J. a. C., T.C. (1998) *Human Parasitology*, Second Ed., Academic Press, San Diego, CA
18. Landfear, S. M., personal communication, OHSU
19. Stewart, C., Bailey, J., and Manoil, C. (1998) *J Biol Chem* **273**, 28078-28084
20. He, M. M., Voss, J., Hubbell, W. L., and Kaback, H. R. (1995) *Biochemistry* **34**, 15667-15670
21. Jung, K., Voss, J., He, M., Hubbell, W. L., and Kaback, H. R. (1995) *Biochemistry* **34**, 6272-6277

Section: 5.5 References

22. He, M. M., Voss, J., Hubbell, W. L., and Kaback, H. R. (1995) *Biochemistry* **34**, 15661-15666
23. Wu, J., Perrin, D. M., Sigman, D. S., and Kaback, H. R. (1995) *Proc Natl Acad Sci U S A* **92**, 9186-9190
24. Wu, J., Voss, J., Hubbell, W. L., and Kaback, H. R. (1996) *Proc Natl Acad Sci U S A* **93**, 10123-10127
25. Yu, H., Kono, M., McKee, T. D., and Oprian, D. D. (1995) *Biochemistry* **34**, 14963-14969
26. Beklouche, S., personal communication, OHSU
27. Valdes, R., Vasudevan, G., Conklin, D., Landfear, S.M. (2004) *Biochemistry* manuscript in press.
28. Wu, J., and Kaback, H. R. (1996) *Proc Natl Acad Sci U S A* **93**, 14498-14502
29. Johnson, J. L., and Brooker, R. J. (2003) *Biochemistry* **42**, 1095-1100

Chapter 5: DISCUSSION

30. Cain, S. M., Matzke, E. A., and Brooker, R. J. (2000) *J Membr Biol* **176**, 159-168
31. Green, A. L., Hrodey, H. A., and Brooker, R. J. (2003) *Biochemistry* **42**, 11226-11233
32. Baldwin, S. A., Beal, P. R., Yao, S. Y., King, A. E., Cass, C. E., and Young, J. D. (2004) *Pflugers Arch* **447**, 735-743